Mechanisms of near-surface current and upwelling variability in the Tropical Atlantic

Dissertation
zur Erlangung des Doktorgrades
der Mathematisch-Naturwissenschaftlichen Fakultät
der Christian-Albrechts-Universität
zu Kiel

vorgelegt von
Sabine Hüttl

Kiel
2006

Referent:	Prof. Dr. C. W. Böning
Korreferent:	Prof. Dr. F. Schott
Tag der mündlichen Prüfung:	12.12.2006
Zum Druck genehmigt:	Kiel, 12.12.2006

Der Dekan

Zusammenfassung

Einen wichtigen Teil der oberflächennahen äquatorialen Zirkulation bilden die Auftriebsgebiete im östlichen tropischen Atlantik. Der in ihnen stattfindende Vertikaltransport kalter Wassermassen beeinflusst einerseits lokal die biologische Aktivität im Hinblick auf Sauerstoff- und Nährstoffkonzentrationen und hat andererseits über die Ozeanoberflächentemperaturen (SSTs) Auswirkungen auf die darüberliegende atmosphärische Zirkulation. Allerdings ist, unter Ausnahme des äquatorialen Auftriebs, bisher wenig über die Herkunft des Auftriebswassers bekannt. Ein erster Schwerpunkt dieser Arbeit liegt daher auf einer Analyse der mittleren Versorgungspfade des Auftriebs im Guinea und Angola Dom. Basierend auf einem sehr hoch auflösenden (1/12°) Modell des Atlantiks werden die zahlreichen äquatorialen Strombänder und deren Rolle für den Auftrieb untersucht. Die längerfristige Variabilität der tropischen Strömungen und deren potentielle Auswirkungen auf den äquatorialen Auftrieb werden in einem zweiten Schwerpunkt der vorliegenden Arbeit untersucht.

Im ersten Teil der Arbeit werden mit Hilfe von Trajektorienanalysen die Quellen der äquatorialen Zonalströmungen erkundet. Es hat sich herausgestellt, dass diese ausschließlich auf der Südhemisphäre liegen und dass darüberhinaus starke Austauschprozesse zwischen den einzelnen äquatorialen Strombändern stattfinden. Als Ursache dieses Austauschs konnten tropische Instabilitätswellen identifiziert werden, aus denen sich Wirbel ablösen, deren Transport einen Massentransfer über die Grenzen der zonalen Strombänder hinweg verursacht. Diese Wirbeltransporte führen zu Zick-Zack-Pfaden des Wassers durch die verschiedenen Strömungen und stellen den einzigen Versorgungsweg des südlichen äquatorialen Unterstroms (SEUC) dar. Zudem werden wesentliche Beiträge zum ostwärtigen Transport des nördlichen äquatorialen Unterstroms (NEUC) über diese Verbindung gewährleistet. Die Analyse der Wassermassenpfade zwischen NEUC, SEUC und den Auftriebsregionen ergab, dass der NEUC den Guinea Dom, Teile des äquatorialen Auftriebs (durch Rezirkulation in den äquatorialen Unterstrom (EUC)) sowie den Auftrieb entlang der afrikanischen Küste speist, während der SEUC fast ausschließlich zwischen den Zonalströmungen rezirkuliert.

Der zweite Teil dieser Arbeit befasst sich mit längerfristigen Änderungen der äquatorialen Strömungen durch Schwankungen der Subtropisch-Tropischen Zelle (STC) und durch Anomalien der Conveyor-Belt-Zirkulation (MOC). Um deren mögliche Effekte auf die tropische Zirkulation leichter zu verstehen, wurden verschiedene Sensitivitätsexperimente mit gröber auflösenden Ozeanmodellen durchgeführt (FLAME 1/3°, ORCA 1/2°). Die Resultate beider Modelle stimmen gut überein und zeigen, dass keine kohärente Schwankung der atlantischen STCs festzustellen ist. Vielmehr hat sich gezeigt, dass die STCs vom lokalen Wind angetrieben werden, der auch den Auftrieb am Äquator bestimmt. Neben den dominierenden windgetriebenen Strömungsschwankungen auf zwischenjährlicher Zeitskala konnten aber auch dekadische Schwankungen festgestellt werden. Deren Ursache liegt in Änderungen des MOC-Transports über den Äquator hinweg, die von der Variabilität in der Bildung von Labradorseewasser bestimmt werden. Die MOC-Anomalien zeigen eine beckenweite Struktur, haben aber nur im Bereich des Tiefen- und Zwischenwassers starke Amplituden und besitzen daher keine Bedeutung für die SSTs oder den Auftrieb.

Abstract

In the eastern equatorial oceans upwelling regions are found. The cold upwelling waters not only interact with the atmospheric circulation via changing the sea surface temperatures (SSTs) but also influence the biological activity via affecting the nutrient and oxygen contents. However, the sources of the upwelling waters are well known only for the sources of the equatorial upwelling but remained unclear for the off-equatorial upwelling regions. A main aspect of this work is to contribute to the understanding of the mean pathways into the Guinea and Angola Dome. The analysis bases on a high resolution model (1/12°) of the Atlantic and will focus on a discussion of the role of the various zonal current bands in supplying the off-equatorial upwelling. Longer term variability of the equatorial currents and their possible influence on the equatorial upwelling will be discussed in a second part of this work.

In the first part of the work trajectory calculations were used to investigate the sources of the equatorial zonal currents. It could be shown that they belong almost exclusively to the southern hemisphere and additionally, strong interaction between the different zonal currents has been found. This interaction is caused by tropical instability waves which are created by the shear between the zonal currents. The waves produce also eddies which cause a watermass transfer between the different currents. It was shown, that this eddy-transport is the main watermass pathway supplying the southern equatorial undercurrent (SEUC) and it was also found to play a major role for the sources of the northern equatorial undercurrent (NEUC). The analysis of the pathways between NEUC, SEUC and the eastern upwelling regions revealed that the NEUC feds into the Guinea Dome, into the equatorial upwelling (via retroflection into the equatorial undercurrent (EUC)) as well as into the upwelling along the African coast, while most of the SEUC waters recirculate in the equatorial zonal currents.

The second part of this work focused on interannual to decadal variability of the equatorial currents related to fluctuations of the subtropical-tropical cell (STC) and the conveyor belt (MOC) return flow. For the discussion of these phenomena different sensitivity experiments have been performed using lower resolution models as a FLAME 1/3° Atlantic model and the 1/2° global ORCA configuration. The results from both models were found to be very similar and showed that the STC is not varying coherently, thus there is no obvious interaction between subtropical and tropical variability. In fact, the STCs are driven mainly by the local zonal wind stress. Despite the overriding importance of the wind-forced variability on interannual timescales, all model results showed also decadal variability signals. They were found to belong to variations of the deep water export across equator which is influenced by the formation rate of Labrador Sea Water. These MOC anomalies revealed a basin-wide structure and were found to modulate the shallow transports in the tropical Atlantic on decadal timescales. However, the main signal of the MOC anomalies was found to be confined to the deep and intermediate waters and the amplitudes in vicinity of the surface are negligible.

Contents

1 Introduction

The upwelling regions of the eastern tropical oceans are areas of strong interaction between the different components of the climate system. The cold upwelling waters not only influence the heat contents of the atmosphere and ocean but also are essential for the biological activity by providing recently ventilated waters, enriched in oxygen and nutrients. There are two processes determining the watermass properties in the upwelling regions which will be in the focus of this study: first the watermass pathways feeding the upwelling regions by advection of subtropical waters and second the near-surface current variability which is mainly driven by the wind but might also involve thermohaline fluctuations.

The main pathways connecting the subtropics and tropics have been studied earlier by analyzing salinities (METCALF & STALCUP (1967)) and tracers (TSUCHIYA (1986)) in the tropical Atlantic region. An asymmetry of the source regions for the upwelling waters was observed, manifested in a prevailing southern hemispheric origin of the watermasses in the tropical Atlantic. The detailed watermass pathways towards the equator are complicated as the tropics reveal a complex current system with a regime of small bands of alternating east- and westward currents in and above the thermocline from about 10°N to approximately 6°S. This zonal current system is fed by a meridional circulation which is significantly influenced by the conveyor belt circulation (MOC), transferring cold waters southward in depth and warm water northward in the upper 1000m.

A comprehension of the meridional circulation is essential to understand why the sources of the various zonal currents are expected to be on the southern hemisphere. Modeling results related the asymmetry of the watermass origins to the existence of the northward MOC return flow which is is found to block a northern hemispheric subtropical-tropical watermass exchange (FRATANTONI ET AL. (2000), JOCHUM & MALANOTTE-RIZZOLI (2001)). The transfer of subtropical waters into the tropics is understood as a shallow meridional cell (STC) connecting the subtropics via geostrophic flow to the inner tropics where the waters upwell and flow back via surface Ekman transport to the subtropics (MCCREARY & LU (1994)). Thus, the meridional circulation in the Atlantic is a combination of deep and shallow circulation, each associated with different variability mechanisms and time scales.

The Equatorial Undercurrent (EUC), flowing eastward along the equator, is regarded to be the upwelling branch of the above mentioned STC and is the only one of the zonal currents that has been shown to feed the equatorial upwelling (Tsuchiya (1986)). Modeling studies by Philander & Pacanowski (1986) revealed the direct link between the EUC variability, the thermocline depth and the strength of the zonal wind stress and eludicated the main physical mechanisms creating variability of the undercurrent.

As a source of the off-equatorial upwelling regions in the tropical Atlantic the eastward flows centered around 4°N/S (the North/South Equatorial Undercurrent (NEUC/SEUC)) are under discussion. An early description of such a link between the Guinea Dome (10°N-18°N, 30°W-20°W) and the NEUC as well as between the Angola Gyre (5°S-15°S, 5°W-5°E) and the SEUC was suggested by Voituriez (1981) relying on analogies between the tropical eastern Atlantic and the eastern equatorial Pacific. For the Pacific eastern upwelling Tsuchiya (1975) stated such a connection to the off-equatorial undercurrents from watermass analyses. However, there were only sparse measurements in the doming regions and along the undercurrents and ocean models failed in resolving such narrow features of the zonal currents system as the off-equatorial undercurrents. During the last years the NEUC and SEUC received more attention in the observations and several sections along 23°W and 29°W (Brandt et al. (2006)) and 10°W and 5°E (Bourles et al. (2002)) have been carried out showing the small meridional scales of the equatorial flow. However, concerning the connection of the NEUC and SEUC to the doming circulations and the upwelling in the east, still not much more is known than from the works of Tsuchiya (1986) and Voituriez (1981).

An understanding of the dynamics and pathways of the subtropical-tropical exchange is complicated by the presence of intense variability associated with the equatorial waveguide. Equatorial waves are strongest in amplitude on subseasonal to annual time scales and influence not only the current strengths but also the stratification in the tropical oceans. The meridional shear between the zonal currents creates tropical instability waves (TIWs, Weisberg & Weingartner (1988)) which occur mainly in the summer months, are confined to the central and western tropical Atlantic and show periods between 30 and 60 days. These waves are known to disturb also the meridional heat transports and hence play also a role in the equatorial heat budget. The dynamical role of this high-frequency variability for the pathways received little attention in the past but a study by Jochum et al. (2004a) linked these waves to the generation of the South Equatorial Undercurrent.

Summarizing, the main aspects of the subtropical-tropical exchange are understood but mainly focused on the role of the meridional flow in supplying the EUC. The small-scale features of the zonal current system and their possible connections to the upwelling areas away from the equator have received increasing attention during the last years both in observations and modeling. However, the role and dynamics of the off-equatorial currents (OEUCs) remained controversial and pathways into the currents have not been studied within the framework of ocean models. Hence, in this work first a description of the OEUCs and their variability from monthly to interannual scales will be given. Afterwards a discussion of the pathways into the OEUCs will reveal if and how strong these depend on the high-frequency variability associated with the Tropical Instability Waves and what the nature of this interac-

tion is. The connection of the OEUCs to the off-equatorial upwelling areas will be described last.

A second mechanism influencing the watermass properties in the upwelling regions was associated with fluctuations of the near-surface circulation. For annual and longer term fluctuations equatorial Rossby waves play an important role for the variability. Partly they are directly wind-driven, partly they result from the reflection of equatorial Kelvin waves which are forced by sudden wind changes. The effect of the annual and semi-annual wind-driven Rossby waves on the current variability along the equator has been discussed in detail by THIERRY ET AL. (2004) and BÖNING & KRÖGER (2005); the fastest baroclinic modes were found to introduce a lag of several months between wind fluctuations in the central and eastern tropics and current variability in the western tropical Atlantic. The reflection of the equatorial Kelvin wave initiates also higher mode waves with longer periods and a larger meridional extent. Hence, these waves might modulate equatorial variability on interannual to decadal timescales.

Associated with the wave disturbances in the equatorial current system are changes in upwelling transports and, consequently, other parameters like sea surface temperature and ocean heat content which have a significant influence on the ocean-atmosphere interaction in the inner tropics. There, the ocean provides a huge heat reservoir which drives the atmospheric circulation in the tropics: strong convection occurs over the regions of warmest SSTs and forms the upward branch of the atmospheric Hadley cell. The warm air is transported poleward and sinks around 30° latitude. The cell is closed by the trade winds. Since, in turn, changes in the trade wind regime are able to create equatorial variability and shifts in the SST patterns, the tropics should be understood to as a region of strongly coupled ocean-atmosphere processes.

Interannual to decadal changes in the trade winds have been found to be connected to variation of the North Atlantic Oscillation (NAO, XIE & TANIMOTO (1998)) but there are also suggestions of remote effects of the El Nino-Southern Oscillation (ENSO, ENFIELD & MAYER (1997)). Both mechanisms influence the trade winds mostly in winter and spring (SUTTON ET AL. (2000)). In addition, an oceanic inter-annual El-Nino-like mode has been suggested in the tropical Atlantic ("equatorial mode", RIUZ-BARRADAS ET AL. (2000)) which appears most pronounced in boreal summer where a strong correlation between SST and thermocline depths exists in the eastern tropical Atlantic. Another SST variability mode, occurring mainly on decadal timescales, is referred as the "meridional gradient mode" (RIUZ-BARRADAS ET AL. (2000)), sometimes called also the "Atlantic dipole mode". It is not clear whether this mode really represents a dipole because statistical analyses by ENFIELD & MAYER (1997) reveal two independently varying centers north and south of the equator. An analysis by DOMMENGET & LATIF (2000) strengthens this interpretation by showing that the dipole found in the observations is an artifact of the statistical analysis technique used.

While all decadal SST-modes appear to be forced by the variability of the atmospheric circulation, the dipole mode has also been related to changes in the MOC. YANG (1999) stated a link between variability of the Labrador Sea Water (LSW) formation and the variations of the SST dipole at the equator five years later in observed, but relatively short, timeseries of the LSW formation and SST, which

could be reproduced in an idealized model. The underlying mechanism is a fast communication of subarctic signals by the basinwide circulation: MOC variability driven by LSW changes and propagating by boundary waves processes to the equator would lead to an enhanced/diminished southward deep water transport which has to be compensated by a corresponding increase/decrease in the northward return flow in the upper 1000m of the tropics. Going along with the strength of meridional overturning is the amount of heat transferred from the southern to the northern hemisphere. Thus, changing the meridional mass transport implies a variation of the heat transport resulting in a warming/cooling of the northern hemisphere and a corresponding cooling/warming of the southern ocean, thereby causing the cross-equatorial SST dipole as found in climate model studies by DONG & SUTTON (2003), BENTSEN ET AL. (2004) and ZHANG & DELWORTH (2005).

A second mechanism possibly contributing to interannual and decadal current variability is associated with the variability of the STCs. Changes of the STCs are mainly related to wind changes causing transport variability of the surface and near-surface currents as well as upwelling variability at the equator. But there are also thermohaline variability components as indicated by ocean model sensitivity experiments by KRÖGER ET AL. (2005). They found a decadal signal, caused by heat flux anomalies only, in the equatorial SSTs which could be explained by corresponding southern hemispheric equatorward transport fluctuations. The amplitude of this signal represents about 1/5 of the whole STC variability signal but shows a coherent, equator-crossing structure which is indicative for a reaction of the MOC return flow. An interesting result together with this finding, but not discussed further in the work of KRÖGER ET AL. (2005)), is the occurrence of a northern STC as an anomaly structure during part of this decadal fluctuations, most clearly during the mid-eighties. Thus, the phases of weak MOC return flow might allow temporarily for a contribution of the northern STC to the variability of the equatorial currents.

Summarizing, the contributions to the equatorial upwelling variability cover a wide range of time scales and spatial patterns. Even if the wind fluctuations were found to dominate the current variability in this region there are several thermohaline forced mechanisms which have the potential to contribute to variations on longer timescales. Especially the interaction between the mainly wind-driven STC variability and the thermohaline driven MOC needs to be revisited. The questions addressed by this work will include first a description of the STC variability and patterns on interannual to decadal timescales and their underlying mechanisms. Second, the connection between the MOC and the dipole mode will be studied and last we focus on the interaction between the MOC and STC variability.

The results to be presented in this work build on the output of two different ocean models (the OPA-based ORCA-system and the FLAME-model) which differ in many of their technical details but show in general a good accordance about the mean circulation features. A high resolution FLAME 1/12°-case enables the investigation of the short spatial and temporal scales needed for the discussion of the pathways into the several zonal currents, while the eddy-resolving 1/3° FLAME-model as well as the ORCA-runs (1/2° at the equator) allow for sensitivity experiments to get insight into physical mechanisms triggering the (near-)surface variability of the tropical currents. Effects resulting from the coupled ocean-atmosphere system can

not be studied within this framework but will be discussed as far as they result from changes in the oceanic parameters.

This thesis is organized as follows: chapter 2 briefly introduces the ocean models and experiments used here and presents an overview of the Lagrangian technique used for the investigation of the pathways into the equatorial currents later. In chapter 3 the open questions concerning the mean circulation will be discussed. After a description of the mean circulation patterns, their annual cycle and possible influences of high-frequency variability, the sources and role of the eastward undercurrents will be investigated. A summary and discussion of the results is given before drawing the attention to the longer term variability processes in chapter 4. There, the variability of the STCs is the first focus and several sensitivity experiments will be used to clarify the underlying mechanisms. The effect of the MOC variability onto the upper-layer variations will be studied afterwards. A concluding summary and outlook will be given in the last chapter.

2 Models & diagnostics

The analyses in this work are based on the output of two different ocean models: the FLAME models, which form a hierarchy of Atlantic ocean models, and the OPA9 based ORCA-configurations which include the global ocean. Both models implement the primitive equations and were run for different longterm experiments. Because both models differ in many details they will be described separately. Then, the Lagrangian trajectory analysis, performed with the FLAME model, will be introduced.

2.1 FLAME

General features

The first set of experiments is based on the FLAME model hierarchy simulating the circulation of the Atlantic ocean. The z-coordinate models build on a highly modified version of the MOM2 code (PACANOWSKI (1995)) and implement the primitive equations on an Arakawa-B grid (ARAKAWA (1966)). The models of the FLAME hierarchy range from a non-eddy-resolving configuration of 4/3° to an eddy-permitting version with a resolution of 1/3° to an eddy-resolving model of 1/12° and have been extensively analyzed for several studies in the Tropical Atlantic (BÖNING & KRÖGER (2005), BRANDT & EDEN (2005)) and in the subpolar North Atlantic (EDEN & WILLEBRAND (2001), BÖNING ET AL. (2003)). The horizontal grid is characterized by an isotropic grid, which means that all grid boxes cover the same box volume, independent of latitude. All model cases described here use 45 levels in the vertical, with a 10m-resolution at the surface, smoothly increasing to a maximum of 250m below 2250m. In this work only experiments from the eddy-permitting (1/3°) and eddy-resolving (1/12°) model versions are discussed. While the 1/3°-model covers the whole Atlantic reaching from 70°N-70°S, 100°W to 30°E, the 1/12° configuration only covers the North Atlantic from 70°N-18°S, 100°W-16°E. The models topography was calculated from the ETOPO5 dataset.

Boundary conditions

Lateral boundaries

The northern and southern boundaries are handled differently, depending on the models' resolution. While the 1/3°-model has a closed northern boundary with restoring to hydrographic conditions (developed by DYNAMO GROUP (1997)), the 1/12° model uses adopted climatological inflow data from a low-resolution Arctic model (BRAUCH & GERDES (2005)) at the northern boundary. This has been a necessary change to maintain the water mass characteristic in the Labrador Sea and to correct the unrealistic high salinities in this area in the 1/3° version (CZESCHEL (2004)). It is worth to note, that this kind of northern boundary condition effectively inhibits interannual variability of the overflow water masses. That, it is possible to study the effects of subarctic variability in separation. The southern boundary of the 1/3° model is closed by streamfunction data along the inflow of the Antarctic Circumpolar Current. The 1/12° configurations southern boundary is given by streamfunction values calculated from the Sverdrup relation. The temperature and salinity fields at all boundaries are prescribed from a combined LEVITUS & BOYER (1994) and BOYER & LEVITUS (1997) dataset.

Surface forcing

For the surface boundary conditions monthly fields for wind stress and heat flux are used. They build on a climatological ECMWF mean (BARNIER ET AL. (1995)) and supplemented by interannual anomalies of the NCEP/NCAR reanalyses (KALNAY ET AL. (1996)) to conserve the models mean state after spinup. The formulation of the surface heat flux follows HANEY (1971) and some adaptions by BARNIER ET AL. (1995) and EDEN & WILLEBRAND (2001): the heat flux is determined by a prescribed value (Q_0, from climatology or time series) and a correction term including a relaxation of the models' sea surface temperature (SST) to a climatological mean value ($Q_2(SST_{model} - SST_{climatology})$). The strength of this relaxation is dependent on other meteorological parameters like wind speed and humidity, which are addressed by the value of Q_2. However, due to this condition, the longterm variability of the SST in the tropical Atlantic is strongly damped toward the climatology. The fluxes of fresh water into the ocean were determined by restoring to sea surface salinities (SSS) from the LEVITUS & BOYER (1994) dataset with a timescale of 15 days for the uppermost 10m.

Parameterizations

Small scale processes not resolved by the model play an important role in the surface and bottom layers as well as for mixing in the interior ocean. To include these effects, they have to be parameterized. The wind-induced mixing in the surface layers is calculated after KRAUS & TURNER (1967) and homogenizes tracers in the mixed layer. Lateral mixing acts along isopycnals (following REDI (1982)) and is parameterized by an harmonic operator. The 1/3° version also includes the parameterization of GENT & MCWILLIAMS (1990) tracer advection. The choice of isopycnal mixing leads to some deficits in the details of the equatorial circulation

(see KRÖGER (2001) and BÖNING & KRÖGER (2005)) but it is motivated by the need to capture aspects of the basin wide overturning and deep water formation at high latitudes. The values used for lateral mixing can be found in CZESCHEL (2004) in their table 2.2.

The vertical mixing is stability dependent (CUMMINS ET AL. (1990)) for tracers (κ_h=0.1-4.0 cm^2/s) and momentum (κ_m=2.0-10.0cm^2/s), with the higher mixing values if the water column is statically unstable. For details of implementation see BÖNING & KRÖGER (2005). Convection in the model is calculated using the scheme of RAHMSTORF (1993) which vertically homogenizes the water between the unstable model boxes. For a better representation of the overflows from the Nordic Seas the bottom boundary layer parameterization (BBL) of BECKMANN & DÖSCHER (1997) is used.

Experiments

Before performing different experiments both model versions were started from an initial state given by the combined LEVITUS & BOYER (1994)/BOYER & LEVITUS (1997) climatology. The 1/3° model was run for a 25-year spinup, the 1/12° version only for 10 years. During the spinup phase both models were forced with the climatological ECMWF surface fields.

Experiments at 1/3° resolution

After spinup 58 years of a climatological forced experiment were run (Exp. FLAME CLIM). For the period from 1958-2001 anomalies from the NCEP/NCAR climatology were added to this climatological forcing. Thus, all forcing components vary interannually and this experiment is used as the reference experiment at 1/3° resolution (Exp. FLAME REF).

To study the effects of thermohaline circulation changes in separation of the wind-driven changes two sensitivity runs were calculated. One of them is an experiment including interannually varying heat flux fields but climatological wind stress (Exp. FLAME HEAT) which is run over the whole period from 1958-2001. When comparing to the reference run, the effect of the interannual wind variability can be estimated. For the investigation of the influence of Labrador Sea Water formation on the meridional overturning circulation and the possible effects of MOC variability in the tropics, a climatological experiment was performed where deep convection was prohibited by capping surface temperatures below 5°C (Exp. FLAME NOLAB).

Experiments at 1/12° resolution

Due to the high computational costs of the 1/12° model only one experiment was performed after the spinup. It covers the years 1987-2004 and was calculated using interannual forcing for this period. We will refer this experiment as FLAME HIGH-RES. The last year of the 1/12° spinup is used for Lagrangian analysis and the discussion of the mean circulation.

For analysis monthly mean data of all FLAME experiments is used. For the last year of the 1/12°-spinup daily data can be obtained and for the period 1990-2004 3-daily average values from FLAME HIGH-RES are available.

2.2   OPA

General features

The second model analyzed in this work builds on the OPA system which covers
the global ocean. The experiments are based on the latest version of the ocean
model OPA9 (MADEC ET AL. (1998)) coupled to a dynamic-thermodynamic sea
ice model (LIM2, FICHEFET & MORALES-MARQUEDA (1997)). The model uses z-
coordinates as well, but it is implemented on a tri-polar grid (MADEC & IMBARD
(1996)) to avoid the singularity over the North Pole. The three poles are situated
over land, leading to a strong deformation, but no singularity, of the grid boxes in
the vicinity of the North Pole. On the other hand, this is a resolutional advantage
in the high latitude regions, as resolution turned out to be one of the main factors
for simulating realistic convection processes in the North Atlantic. For analysis
we use output of the model configuration ORCA05 (in the following named simply
ORCA) which has a resolution of $1/2°$ at the equator. Thus ORCA05 should be
comparable in the tropical Atlantic to the results of the FLAME $1/3°$ experiments.
The vertical discretization uses similar depth levels as the FLAME model (46 instead
of 45 z-levels with similar resolution in the upper 1000m) and the topography also
originates from the ETOPO5 dataset. However, the topography in the OPA model
can be represented better due to the use of the partial step algorithm by ADCROFT
ET AL. (1997) which can fill the models' bottom cells partially. Partial filling is
advantageous in regions with steep and narrow topography. In contrast to the
FLAME system, the model equations are solved on a Arakawa C-grid (ARAKAWA
(1966)), leading to an correct representation of oceanic boundary wave processes.

Surface boundary conditions

For the surface forcing the CORE-dataset, prepared by LARGE & YEAGER (2004),
is used. This dataset bases on the NCEP/NCAR analyses, too, but were corrected,
revised and globally balanced using the observational and satellite data by LARGE &
YEAGER (2004). The model calculates its own surface heat fluxes which is done by
the bulk formulae given by KARA & HURLBURT (2004). In contrast to the FLAME
model experiments, these bulk formulation includes a relaxation not to climatological
values but to interannual varying forcing fields at the surface. Thus, the SSTs can
not evolve freely. The fresh water forcing is given from the CORE dataset and is
restored with a weak timescale of 180 days towards the Levitus climatology. The
restoring is applied only at the surface but for the whole water column in the polar
oceans.

Parameterizations

As the ORCA configuration is not eddy-resolving, the eddy-parameterization fol-
lowing GENT & MCWILLIAMS (1990) is included. The mixing for tracers and
momentum is along isopycnals using a harmonic operator for tracers (a_{ht0}=1000
m^2/s) and a biharmonic one for momentum (a_{hm0}=-8.5*10^{11} m^4/s). The verti-
cal mixing, mainly at the surface, is determined by a TKE scheme and convection
is realized by enhanced vertical mixing. Tracer advection is determined by the

Experiment	Resolution	Years	Wind Forcing	Heat Forcing	Special
FLAME HIGH-RES	1/12°	1987-2004	interannual	interannual	
FLAME REF	1/3°	1958-2001	interannual	interannual	
FLAME HEAT	1/3°	1958-2001	climatological	interannual	
FLAME NOLAB	1/3°	0000-0020	climatological	climatological	capping of SST at 5°C, over Labr. Sea
ORCA CLIM	1/2°	0020-0066	climatological	climatological	
ORCA REF	1/2°	1958-2001	interannual	interannual	
ORCA HEAT	1/2°	1958-2001	climatological	interannual	
ORCA WIND	1/2°	1958-2001	interannual	climatological	
ORCA EQ	1/2°	1958-2001	climatological	climatological	interannual from 5°S-5°N
ORCA LS	1/2°	1958-2001	climatological	climatological	interannual from 45-68°N only in Atlantic

Table 2.1: Overview of model experiments

3-dimensional MUSCL scheme (monotonic upstream-centered scheme for conservational laws, HOURDIN & ARMENGAUD (1999)).

Experiments

Like for the FLAME model experiments, the ORCA configuration is started by temperature and salinity data from the Levitus climatology and spun up for 20 years. In the polar regions an additional dataset by STEELE ET AL. (2001) was used for a better representation of the polar oceans.

After that, similar experiments as for the FLAME models have been setup: there is a climatological run (ORCA CLIM), using only climatological forcing fields for the years 20-66, a reference run with full interannually varying forcing from 1958-2001 (ORCA REF), an experiment with only variability of the heat fluxes (ORCA HEAT), a corresponding experiment with only interannual wind-forcing (ORCA WIND). In addition to the runs comparable to FLAME, sensitivity experiments with interannual forcing in localized regions and climatological forcing elsewhere have been performed. In the context of this work a run with interannual variability only in the tropics (ORCA EQ) and an experiment including variability only in the region of the Labrador Sea (ORCA LS) will be discussed. The ORCA EQ-run is forced fully interannually in the band 5°N to 5°S with a linear decrease of the interannual forcing towards the climatological forcing at 15°N/S. This rather large transition zone is chosen to allow the whole tropical gyre to react to the interannual forcing, a smaller latitudinal range might lead to artifcial responses by forcing the poleward limbs of the gyre circulation to a climatological value. For the ORCA LS-experiment the interannual forcing is applied to a zonal band covering the North Atlantic at the latitudes of the Labrador Sea (50°N-65°N, with linear decrease until 45°N/68°N towards the climatological forced regions). Table 2.1 summarizes the models and experiments used in this work.

2.3   Lagrangian Analysis

For a part of this work the circulation is studied using trajectory analysis. This technique is used as a complementary view on the circulation. It admits a direct view of the circulation pathways instead of observing the velocity and tracer fields at fixed grid points as given by the model.

A trajectory of a particle is easy to calculate from a three-dimensional Eulerian velocity field by integration of the differential equation $\frac{d\vec{x}}{dt} = \vec{v}$, whereby $\vec{x}$ denotes the particles position and $\vec{v}$ the three-dimensional velocity field. This calculation can be done during the model run (online) or after it (offline) using the velocity output fields. The offline diagnostic has some advantages compared to online calculations: it is easy to perform different particle launches, to average or manipulate the velocity fields to exclude for example eddy motions and it is possible to integrate the trajectory backward and forward in time. The last point is advantageous for studying the source waters and the fate of a current.

The Lagrangian analysis is used mainly for FLAME HIGH-RES, due to its better resolution of the meridional small current bands near the equator. In some cases comparison to FLAME REF is made. For ORCA a similar analysis tool exists developed by BLANKE & RAYNAUD (1997) which has not been used here. Some ideas for interpreting the trajectory data proposed by these authors will be used in this work.

Launch strategy

To study the circulation by trajectories one can imagine the flow field to consist of finite particles, each associated with a certain amount of water. This value should be chosen in such a way, that the summed transport of all such particles through a section of the currents of interest is equal to the transport of these currents calculated from the models' velocity fields. Figure 2.1 illustrates this idea for a float launch in the Equatorial Undercurrent along the 23°W section. Each float is marked by a red cross. When calculating the trajectory of such a particle this gives the corresponding pathway of it through the ocean.

One task is to define, how "big" such a "water particle" should be to give a reasonable representation of the flow field. In other words, how many trajectories are needed to represent a current adequately? For their Lagrangian analysis in the tropical Pacific and Atlantic BLANKE & RAYNAUD (1997) and BLANKE ET AL. (1999) revealed a limit of 0.01 Sv per particle is needed to represent the Eulerian flow in an acceptable way in their coarse resolution model, i.e. an increase of the trajectories does not lead to a further change in the representation of the current pathways.

Their findings lead straightforward to a strategy about the distribution of the particles (in the following named "floats") along a desired section: in regions with high transports and correspondingly high velocities many floats are concentrated whereas in regions with weak flow only a smaller number is needed to represent the current (see Fig. 2.1). BLANKE ET AL. (1999) found this selective distribution strategy more adequate for covering currents than distributing the particles uniformly over the current section.
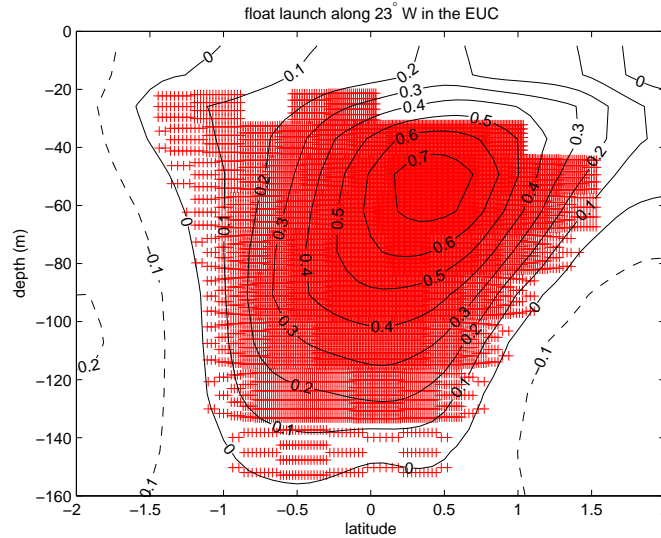
Figure 2.1: Example of a float launch along the EUC at 23°W. The contour lines indicate the zonal velocity in m/s and the red crosses show the launch positions of the floats. The 10861 floats represent the EUC transport of 9.15 Sv between the isopycnals σ_θ=24.5 and 26.8 kg/m^3. The launch strategy shows a concentration of floats in the EUC core and a smaller float density in areas of weak current velocities.

In the analysis in this work most experiments used more than 10.000 floats to make sure that even weak and meridional small currents bear a large number of floats in order to calculate reasonable statistics. The floats are distributed over the whole selected section weighted by the current transport, i.e. not all floats bear exactly the same transport value. In Fig. 2.1 10861 floats are distributed in the depicted manner, resembling a total transport of the EUC of 9.15 Sv between the isopycnals σ_θ=24.5 and 26.8 kg/m^3 and each particle is associated with a transport of approximately 0.0008 Sv. All Lagrangian float studies and their launches and transports can be found in table 2.2.

Trajectory calculation

The calculation of the trajectories within the given velocity fields in most cases leads to float positions which are not on the models' grid. For the calculation of the velocity field at the trajectory positions between grid points a linear interpolation between the next model grid points is used. Linear interpolations should be accurate enough due to the high horizontal resolution. The solution of the trajectory equation is done by a simple Euler scheme, which is sufficiently accurate if the integration time step is small enough (BÖNING & COX (1988)). The accuracy can be ensured by using an adaptive time-step scheme which couples a minimum number of calculation steps per float and model box to a function of the velocity at a point.

Model snapshots of the horizontal velocity were used as a basis for the trajectory integrations. The vertical component was calculated by the trajectory algorithm because reading the input velocity data is the most computationally expensive timestep

of the trajectory calculation. However, the dataset to hold in memory is still large (for example: 2 snapshots of FLAME HIGH-RES with 1.4 GB each, grid data and trajectory output). The integrations were performed on an ItaniumII-machine with 4GB memory. This amount of memory permits for calculations using the whole model domain.

For additional analysis of the float pathways it is possible to calculate salinity, temperature and density along the trajectory. These additional variables allow for direct insight into diapycnal processes and can be used as a measure for upwelling or to define mixed-layer depths. For the FLAME HIGH-RES integrations, daily and monthly output fields from the last year of the model spin-up were used. To point out the effect of the high horizontal resolution, these integrations are sometimes contrasted to trajectory runs with monthly and yearly means of FLAME REF.

Depiction of trajectories

One of the main advantages of the Lagrangian analysis is the direct illustration of water mass pathways. Because of the large number of calculated particle trajectories (in the following named "floats") it is neither possible to show nor to investigate every single trajectory. However, it is possible to study the trajectories passing a distinct section or depth and calculate transports through this section or over the layer boundaries. This possibility is shown in Fig. 2.2a. However, this method does not reveal what happens to the particles between the sections, and it is obvious that the mass balance between launched trajectories and transports reaching the boundary current and interior currents is not closed. Thus, recirculation waters or particles between the sections are not included in the transport calculation.

Another possibility is to sum up the transport of all trajectories passing through a 3d-box. Because every float is associated with a transport value (as described in the last section) this enables a transport calculation over the edges of each grid box. The transports are calculated for regular $1/10°$ boxes in the horizontal plane and vertical box size of 10m and referred as "transport function". Boxes passed by many trajectories thus will appear as maxima of the transport function. The transport function will be summed along the vertical to visualize horizontal maps of the floats or along longitudes to learn about the vertical flow structure.

The proposed transport function is not identical to streamfunction formulations of, for example, BLANKE ET AL. (1999) because we do not take into account the direction of the trajectory, i.e. if the float crosses a section north-, south-, east- or westward. The method used here has the advantage of detecting recirculation routes easily due to their high transport values which might exceed the initial transport of the float launch. For the streamfunction calculations of BLANKE ET AL. (1999) only trajectories that left the region of interest at the end of the calculation can be used. In that case, recirculation pathways in the studied region were explicitly excluded to calculate a streamfunction.

The vertical sum of the transport function from the floats in Fig. 2.2a can be found in Fig. 2.2b. The main pathway of the floats is visible in this depiction of the transport function as a region of maximum transport which can be associated with different current cores: in Fig. 2.2b the pathway from the NBC into the EUC appears as the main route for EUC waters. Directly visible is also a small recirculation
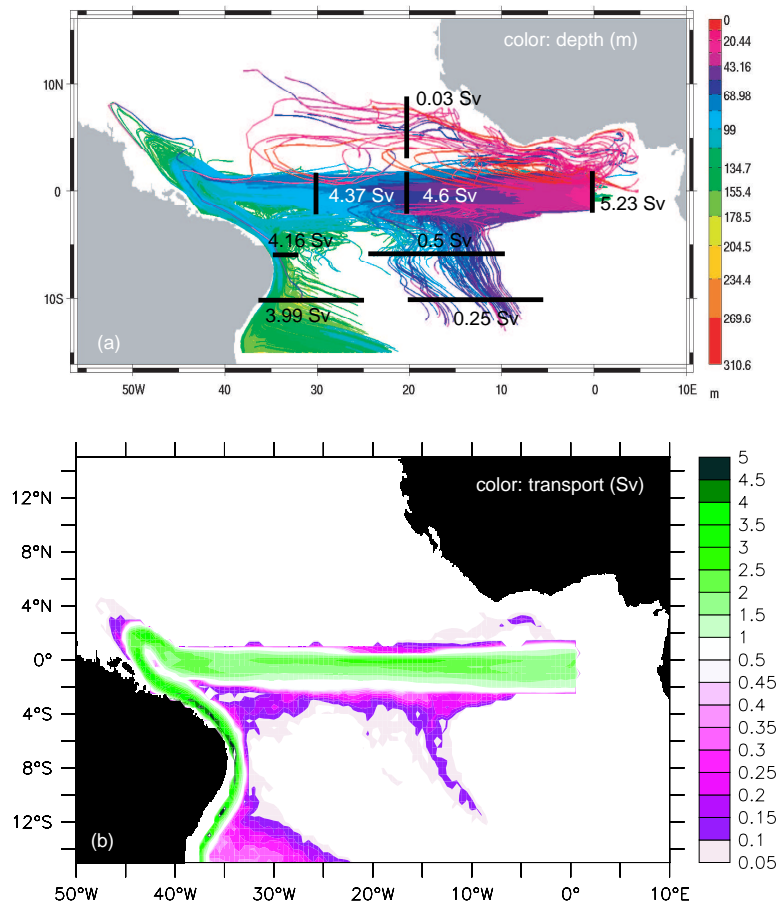
Figure 2.2: Two different ways of illustrating float trajectories: (a) the "traditional" possibility by showing the individual pathways of a float and examine transports along sections and (b) the vertically summed transport function. More details in the text.

cell between 25°W and the western boundary between 4°S and the equator. This recirculations cell is also the main pathway of interior flow from the south. The few trajectories originating from the northern hemisphere have too low transport to appear in Fig. 2.2b.

This kind of analysis helps to highlight the main pathways that have been generated by many following particles. In contrast, the individual trajectories along the main pathways are difficult to separate due the high float density per grid box (for example the trajectories in the EUC in Fig. 2.2a). Pathways joined only by few floats are easy to detect (for example the trajectories north of the EUC in Fig. 2.2a) by not necessarily significant. It should also be noted, that the figures depict the whole trajectory pathway after a certain integration time. Thus, float launches started in different seasons can reveal different distribution patterns after, say four years, due to their different spreading pathways in the first months of integration.

For the Lagrangian analysis presented in this work, all integrations are confined to one current core and a 4-year time-span because of limitations in calculation time

and because of the fast response timescales (see later chapters) within the tropical current system. Using the additional information of temperature and salinity along the float trajectory it is also possible to calculate the transport function as a function of density or temperature to get insight into diapycnal processes.

Table 2.2: Overview of Lagrangian experiments used in this work. Given are start sections, depth and density ranges, used velocity fields and associated transports.

launch date	latitude of launch	depth/isopycnal range in kg/m^3	total transp.	max. float transp.
NEUC 23°W using daily FLAME HIGH-RES velocity fields				
15 Feb	2.8°N-4.8°N	40-300m/σ_θ=24.5-26.8	2.34 Sv	0.5 mSv
15 May	3.2°N-5.0°N	40-300m/σ_θ=24.5-26.8	5.21 Sv	0.2 mSv
15 Aug	2.6°N-4.2°N	40-300m/σ_θ=24.5-26.8	1.57 Sv	0.15 mSv
15 Nov	2.6°N-3.8°N	40-300m/σ_θ=24.5-26.8	1.04 Sv	0.1 mSv
NEUC 23°W using monthly FLAME HIGH-RES velocity fields				
15 Feb	3.0°N-5.0°N	80-300m	2.04 Sv	0.5 mSv
15 May	3.5°N-5.5°N	80-300m	4.11 Sv	0.5 mSv
15 Aug	3.0°N-5.0°N	80-300m	1.72 Sv	0.5 mSv
15 Nov	3.0°N-4.0°N	80-300m	0.91 Sv	0.5 mSv
SEUC 10°W using daily FLAME HIGH-RES velocity fields				
15 Feb	4.5°S-2.5°S	50-300m/σ_θ=25.5-26.8	2.40 Sv	0.2 mSv
15 May	5.0°S-3.0°S	50-300m/σ_θ=25.5-26.8	1.57 Sv	0.15 mSv
15 Aug	4.5°S-2.5°S	50-300m/σ_θ=25.5-26.8	1.33 Sv	0.15 mSv
15 Nov	5.2°N-3.5°N	50-300m/σ_θ=25.5-26.8	2.30 Sv	0.2 mSv
SEUC 10°W using monthly FLAME HIGH-RES velocity fields				
15 Feb	3.5°S-5.0°S	60-300m	2.25 Sv	0.5 mSv
15 May	3.5°S-5.5°S	80-300m	1.37 Sv	0.5 mSv
15 Aug	3.5°S-5.5°S	80-300m	1.20 Sv	0.5 mSv
15 Nov	3.5°S-5.5°S	80-300m	2.39 Sv	0.5 mSv

EUC 0°W using daily FLAME HIGH-RES velocity fields

15 Feb	2.5°S-2.5°N	40-120m/σ_θ=24.5-26.8	5.8 Sv	0.5 mSv
15 Aug	1.5°S-1.5°N	40-120m/σ_θ=24.5-26.8	2.8 Sv	0.2 mSv
15 Oct	2.5°S-2.5°N	40-300m/σ_θ=24.5-26.8	7.05 Sv	1 mSv

EUC 0°W using 1/3°-model monthly velocity fields

| October | 1.5°S-1.5°N | 30-120m | 5.23 Sv | 5 mSv |

EUC 23°W using daily FLAME HIGH-RES velocity fields

| 15 Feb | 1.5°S-1.5°N | 20-160m/σ_θ=24.5-26.8 | 9.15 Sv | 1 mSv |
| 15 Aug | 1.5°S-1.5°N | 20-300m/σ_θ=24.5-26.8 | 18.54 Sv | 2 mSv |

Guinea Dome 23°W using daily FLAME HIGH-RES velocity fields

15 Feb	8°N-14°N	20-500m/σ_θ=24.5-26.8	3.96 Sv	0.4 mSv
15 May	8°N-13°N	20-500m/σ_θ=24.5-26.8	2.87 Sv	0.4 mSv
15 Aug	8°N-14°N	20-500m/σ_θ=24.5-26.8	5.33 Sv	0.4 mSv
15 Nov	8°N-14°N	20-500m/σ_θ=24.5-26.8	4.08 Sv	0.4 mSv

Runs with annual mean velocity fields

23°W	3.0°N-5.5°N	NEUC, 80-300m, 1/12°	2.31 Sv	0.1 mSv
10°W	2.5°S-5.5°S	SEUC, 40-300m, 1/12°	1.79 Sv	0.1 mSv
13°N	20°W-25°W	G. Dome 50-150m, 1/12°	0.41 Sv	5 mSv
13°N	20°W-25°W	G. Dome 50-150m, 1/3°	0.71 Sv	5 mSv

3   Aspects of the mean circulation

3.1   Introduction

The meridional upper-layer circulation in the tropical Atlantic can be understood as a superposition of the northward, interhemispheric flow associated with the deep meridional overturning circulation (MOC) and the shallow subtropical-tropical circulation cells (STCs). The STCs connect the subduction zones of the subtropical gyres with the equatorial regime of eastward currents and the equatorial upwelling. The MOC transfers about 15 Sv (Ganachaud & Wunsch (2001)) of warm water in the upper 1000m northward across the equator and the largest amounts of this transport are associated with the flow of the North Brazil Current (NBC) along the western boundary. Beside this large-scale transport patterns several small-scale zonal currents bands are found in the vicinity of the equator, both in thermocline and subthermocline layers. Their origins, sources and connections to the large-scale circulation features have been less investigated but are presently focused because their possible contributions to the coastal and off-equatorial upwelling. The aim of this chapter is to provide a description of the equatorial circulation which shows the interaction of the large-scale meridional circulation and the small-scale zonal current bands.

Meridional cells and large-scale transport pathways

The water masses forming the STCs are saline waters from the subtropics and introduced into the thermocline layers by winter-time homogenization. In spring a much shallower mixed layer establishes and uncouples the uniform watermass in the depth from the surface. This process is called subduction and occurs in the subtropics of both hemispheres.

 The theory of the "ventilated thermocline" by Luyten et al. (1982) describes the spreading of the subducted waters by geostrophic currents to the equator and feeding the Equatorial Undercurrent (EUC). Extensions of this theory were given by McCreary & Lu (1994) and Malanotte-Rizzoli et al. (2000). While McCreary & Lu (1994) combined the equatorward flow of subducted waters with upwelling along the equator and poleward flow in the Ekman layer to the idea of a closed cell (called the STC), Lu & McCreary (1995) and Malanotte-Rizzoli

ET AL. (2000) pointed out, that inside the STC different spreading pathways of the subducted waters exist. There have been found two pathways of watermass transfer between tropics and subtropics: one along with the western boundary current (the "western boundary exchange window") and another one directly through the interior ocean, associated with the SEC flow (the "interior exchange window"). Waters subducting to close to the western boundary recirculate in the subtropical gyre. In the eastern part of the basin there exist "shadow-zones", which are neither influenced by the subduction process nor by the surface poleward flow of the STC. These regions reveal a rather weak cyclonic circulation and an isopycnic doming, so they are referred as "domes". All this features are summarized schematicly in Fig. 3.1a for the southern hemisphere but also apply in general for the northern hemisphere.

However, the circulation of the tropical Atlantic is more complex and can not be explained fully by this simple STC concept. As mentioned above, the MOC return flow influences the upper-layer transports and a major consequence of this return flow is a marked asymmetry in the strengths of the Atlantic STCs (FRATANTONI ET AL. (2000), JOCHUM & MALANOTTE-RIZZOLI (2001)). Observational evidence based on hydrographic data clearly revealed that the major contribution to the EUC is of South Atlantic origin (METCALF & STALCUP (1967), TSUCHIYA (1986)), with the equatorward flow mainly is carried along the western boundary by the North Brazil Undercurrent (NBUC or NBC; SCHOTT ET AL. (2002)), with some additional contributions from interior pathways (LAZAR ET AL. (2002), ZHANG ET AL. (2003)). The equatorward flow of North Atlantic thermocline water is comparatively weak, carried mostly off the western boundary by the Guyana Undercurrent (WILSON ET AL. (1994), SCHOTT ET AL. (1998), BOURLES ET AL. (1999)). Possibly some additional interior pathway (ZHANG ET AL. (2003)) along the cyclonic geostrophic contours of the Guinea Dome area (STRAMMA ET AL. (2005a)) exists. The northern waters, however, do not appear to penetrate to the equator, but to join mainly the North Equatorial Countercurrent (NECC)/North Equatorial Undercurrent (NEUC)-system between 4°N and 8°N.

The understanding of the physical mechanisms governing the mean pathways and transports in the tropical Atlantic has been aided by several ocean modeling studies. The salient features of the observational picture, particularly the predominantly southern origin of the EUC, and the dominance of the western boundary pathway for the equatorward flow of the South Atlantic water, are generally well reproduced in high-resolution models of the wind-driven and thermohaline circulation, such as the 1/4°-OCCAM solution analyzed by HAZELEGER ET AL. (2003), or the 1/3°- and 1/12°-FLAME cases described by BÖNING & KRÖGER (2005) and STRAMMA ET AL. (2005b).

A main area for quantitative differences between recent simulations has been the contribution of the northern STC, suggestive of the sensitivity of this feature to the strength of the MOC. The investigation of the large-scale circulation patterns in the two ocean models thus has to address the questions how the STCs are simulated in the models, how the different equatorward STC pathways are represented, how they compare to observations and how strong they depend on the models' resolution and other model parameters.
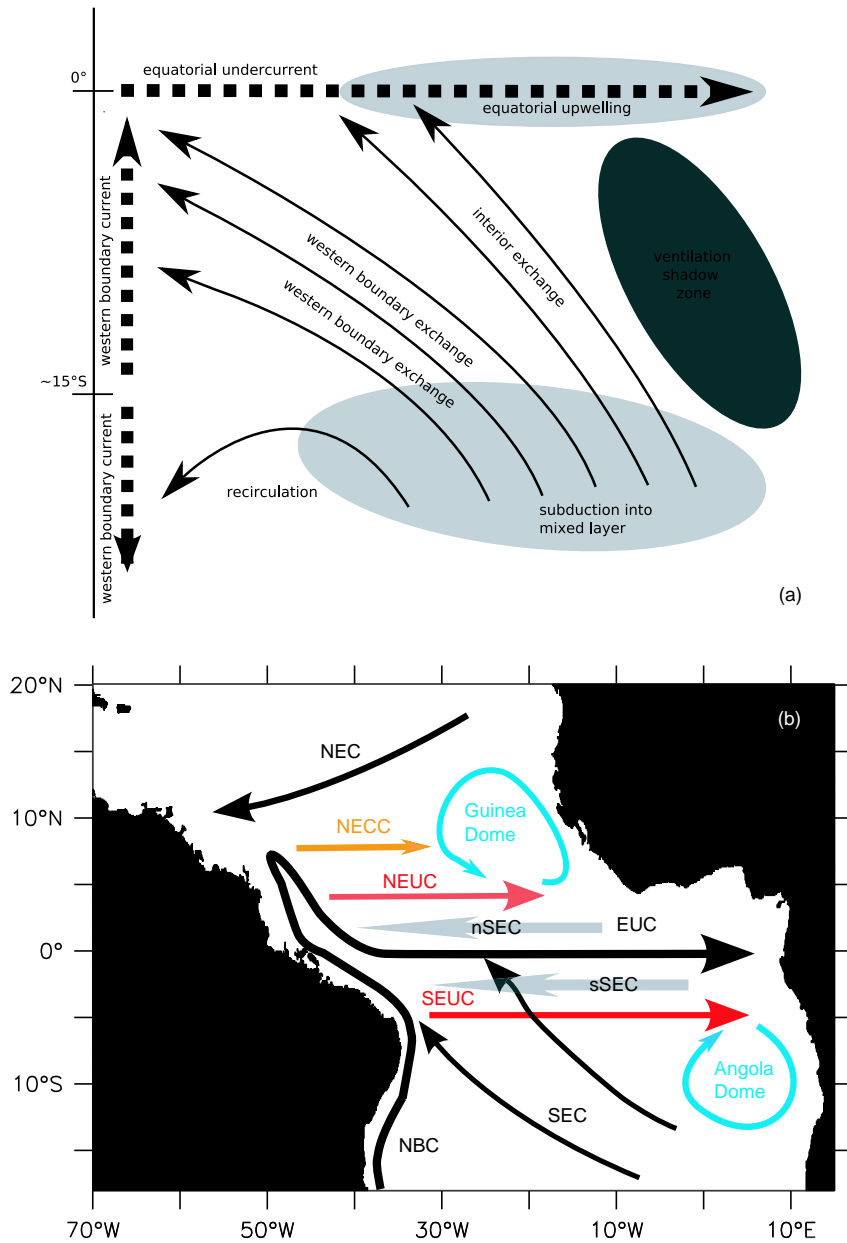
Figure 3.1: Schematics of the a) STC ventilation windows and b) the subsurface equatorial current system including the doming circulations. The westward flowing SEC bands between the EUC and NEUC/SEUC are shaded in light gray.
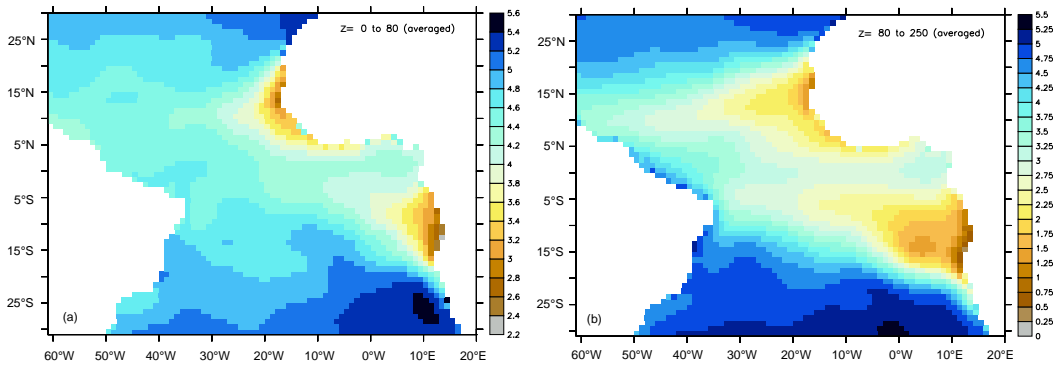
Figure 3.2: Oxygen content in ml/l from LEVITUS & BOYER (1994). Left: mean oxygen in the surface layer 0-80m, right: mean content in the eastward undercurrent layer between 80 and 300m. Clearly visible are the oxygen minimum zones of the Guinea and Angola Dome, the higher oxygen tongue of the EUC and the oxygen maximum regions in the subtropical subduction areas. Note the different scales of both sub-figures.

Circulation in the shadow zones

In contrast to the recently ventilated waters in the equatorward STC branch, the STCs also form regions of unventilated, oxygen-minimum watermasses in the shadow zones. In these zones a weak cyclonic flow pattern around the doming isopycnals has been observed (VOITURIEZ (1981)). In the tropical Atlantic shadow zones exist on both sides of the equator (see sketch in Fig. 3.1b): south of the Cape Verde frontal zone the Guinea Dome is formed between 28-16°W, 8-14°N (MAZEIKA (1967), SIEDLER ET AL. (1992), STRAMMA ET AL. (2005a)). Its southern hemispheric counterpart, the Angola Dome, between 5-10°E, 8-12°S (MAZEIKA (1967)) is bounded to the south by the Agulhas-Benguelas frontal zone.

 It is interesting to note that along the domes, visible as oxygen minimum zones below the surface in Fig. 3.2b, there is some upwelling (see low oxygen contents compared to the subtropics at the surface (Fig. 3.2a)). SCHOTT ET AL. (2004) calculated from Ekman divergences an upwelling of 4.4 Sv for the Guinea Dome area and 5.5 Sv for the region of the Angola dome. Both values include also the coastal upwelling in these regions and it remains unclear what the relative contribution of the upwelling along the domes and the coastal upwelling is. However, the upwelling along the domes has to be supplied by near-equatorial currents and the open question concerns the sources of this off-equatorial upwelling water.

The eastward zonal currents

In the early eighties the work by VOITURIEZ (1981) indicated a connection between the off-equatorial undercurrents occurring near 4°N/S in the subsurface layers between 50 and 300m and the upwelling in the domes, similar to the findings of TSUCHIYA (1975) in the eastern Pacific. The currents are called the North/South Equatorial Undercurrent (NEUC/SEUC) in the Atlantic while their Pacific counterparts are often referred as "Tsuchyia jets" or "subsurface countercurrents". Al-

though there exist other works investigating the Dome circulations (for example: HAGEN & SCHEMEINDA (1984), SIEDLER ET AL. (1992), YAMAGATA & IIZUKA (1995), STRAMMA ET AL. (2005a), DOI ET AL. (2006)) no new theories about the origin of the Dome waters have been proposed. In addition, the connection of the NEUC/SEUC and the Domes as suggested by VOITURIEZ (1981) have not been investigated further, partly because of sparse measurements in the eastern equatorial region, partly due to the fact that ocean models did not provide good simulations of the domes.

Also the dynamics of the off-equatorial undercurrents are still under discussion. There are different proposed theories on their formation but a theory explaining all observed features of the undercurrents is still missing. The first attempts to explain the currents were linear theories by MCPHADEN (1984) and MCCREARY (1981) assuming these currents as meridional lobes of the equatorial undercurrent, sustained by a balance between vertical diffusion of relative vorticity and advection of planetary vorticity. In contradiction to these theories observational studies in the Pacific (JOHNSON & MCPHADEN (1999), ROWE ET AL. (2000)) revealed the off-equatorial undercurrents forming separate current cores when flowing eastward and found the currents to diverge poleward on their way to the east.

The divergence phenomenon was already described by JOHNSON & MOORE (1997) proposing the jets are formed by inertial instability. Because the equatorial thermocline is shoaling to the east and the eastward flow has to conserve potential vorticity the jets have to diverge poleward. However, this theory could not explain why the jets shoal to the east, involving diapycnal processes. In the tropical Atlantic a poleward divergence of the undercurrents has been observed by BOURLES ET AL. (2002).

Another approach to understand the dynamics of the off-equatorial undercurrents is given by MARIN ET AL. (2000), MARIN ET AL. (2003) and HUA ET AL. (2003). The authors point out the similarities between the equatorial oceanic zonal current system and the atmospheric Hadley cell: the strong horizontal density gradient at their poleward boundaries, a pool of nearly uniform temperatures between the equator and the poleward boundary and the existence of a jet-like current above the region of highest horizontal gradients (the jetstream for the atmosphere, the off-equatorial undercurrent in the ocean). The atmospheric Hadley cell can be explained by conservation of angular momentum and so they explain the ocean counterpart too. However, a driving mechanism for the oceanic counterpart of the Hadley-circulation is still missing: the atmospheric cell is driven by releasing latent heat during convection, a corresponding diapycnal process in the ocean was not proposed.

A possible mechanism for the diapycnal transfer is proposed by JOCHUM ET AL. (2004a). They investigated the role of high-frequency variability for the establishment of the off-equatorial undercurrents. By studying the energy balance of the tropical current system they revealed the undercurrents resulting from the conversion of eddy kinetic energy from tropical instability waves (TIWs) to the mean kinetic energy of the zonal current system. The meridional heat flux associated with the instability waves flattens or steepens the isopycnals thus generating a geostrophic balanced flow which is only limited by dissipation. These findings are supported by other model results (ISHIDA ET AL. (2005)).

Another possible mechanism forcing diapycnal processes is associated with up-welling. MCCREARY ET AL. (2002) and FURUE ET AL. (2006)) propose the off-equatorial currents could be drawn by the off-equatorial upwelling along the doming regions, i.e. the undercurrents are the source waters for this upwelling. Wind-driven upwelling variability thus should generate variability of the undercurrents too. How-ever, this direct connection between a fast wind-driven response of the off-equatorial undercurrents and upwelling is contrasted by the low oxygen contents (see Fig. 3.2) of the upwelled waters which indicate long isolation of the upwelled watermasses from the oceans surface.

The remaining questions concerning the off-equatorial undercurrents thus include not only their connection to the off-equatorial upwelling but also their sources need to be investigated. In addition, the dynamics of the currents have to be revisited and discussed in the context of the present theories.

3.2   Mean circulation

3.2.1   Mean flow depictions

It is useful to precede the discussion of any variability by an examination of the mean current patterns comprising the subtropical-tropical current regime. The findings from ocean model output will be discussed and related to results obtained from observations. Figure 3.3 shows the mean current system at 100m depth from FLAME HIGH-RES and the ORCA REF solution. Both models reveal a strong eastward equatorial undercurrent (EUC) which is almost totally fed by the western boundary current, the North Brazil (Under)current (NBC). The NBC inflow occurs mainly south of 5°S, a result in good accordance with observations of SCHOTT ET AL. (2005). The retroflection pattern of the waters crossing the equator are heavily obscured in the long-term mean field due to its strong seasonal and intraseasonal variability in this regime. A detailed analysis of this patterns for the FLAME model can be found in BÖNING & KRÖGER (2005) and STRAMMA ET AL. (2005b).

Away from the western boundary different zonal current bands are observable: flanking the EUC two westward currents on each side of the equator are visible, and more poleward eastward currents centered around 4° latitude occur. The models differ in the magnitude as well as in meridional and zonal extent of the currents: while the ORCA REF-run gives a strong EUC reaching until the easternmost part of the basin, this current is much weaker in the FLAME REF-run near the eastern boundary. This differences are linked to the different vertical mixing schemes in the models (a simple stability dependent scheme in the FLAME runs and a complex TKE algorithm in ORCA) which allows a much sharper thermocline and EUC in the ORCA experiments.

A strong difference between both models can also be found in the inflow region of the SEC into the western boundary current on the southern hemisphere. While ORCA REF shows strong inflow westward of about 20°W between 6°S and the equator, this region is confined to a small meridional band between 1°S and 3°S next to the boundary in FLAME HIGH-RES and the bulk of the SEC waters has entered the NBC south of 10°S.

Both models indicate a southern hemisphere eastward flow (the SEUC) starting in mid-basin. In FLAME HIGH-RES the SEUC occurs at about 25°W, ORCA REF shows it eastward of 10°W. On the northern hemisphere the differences look less significant but ORCA REF shows a broad eastward flow north of 4°S while the FLAME solution indicates this flow to occur in two separate currents. For resolutional purposes ORCA REF does not resolve the NEUC adequately but shows part of it as a deepened flow of the eastward North Equatorial Countercurrent (NECC) north of 4°N, while FLAME HIGH-RES shows two different current cores (in the vertical) off the western boundary.

Seasonally, a second NECC core develops around 8°N in FLAME HIGH-RES which is the northernmost current band in Fig. 3.3a (as a residual of the averaging procedure). In both pictures it is not obvious what feeds these off-equatorial undercurrents (if recognizable): the SEUC develops in the mid of the basin and the NEUCs connection to western boundary can not be clearly stated even from FLAME HIGH-RES. Another point difficult to see in this picture is where the flow ends up after reaching the eastern basin. Because of the small meridional components of the shown velocities most of this flow has to be up- or downwelled in the east or to be shifted otherwise from the current. To get insight into this processes it is useful to look on results of Lagrangian float integrations. A detailed discussion of that will be given in section 3.4.

VOITURIEZ (1981) related the off-equatorial undercurrents to the thermal domes in the eastern part of the basin. The dome regions associated with the STC shadow zones are shown in Fig. 3.4 for FLAME HIGH-RES. The depth of the isopycnal σ_θ=26.5 kg/m^3 reveals a doming of the isopycnal near 10°N-18°N, 30°W-20°W in the region of the observed Guinea Dome and a second doming area near the southern boundary at 0°E-10°E, 12°S-16°S, which shows a elongated tongue to 10°W, 5°S. While the northern dome represents the observations, the southern pendant is found to be too far south, an attribute likely to be caused by the southern model boundary at 18°S and the corresponding buffer zone.

3.2.2 Zonal and meridional sections

Relation to observations

An assessment of the simulated mean current patterns and transports for the FLAME model is provided for an EUC-section at 35°W and a NBC-section at 5°S (Fig. 3.5), in comparison to the observational results presented by SCHOTT ET AL. (2003) and SCHOTT ET AL. (2005). While the FLAME REF-experiment appears capable of representing the broader-scale aspects of the current system, the higher resolution is obviously needed for capturing the details of O(100 km) or less. ORCA REF shows similar current characteristics to the FLAME REF results and therefore is not discussed separately here.

The observed core speed of the EUC of more than 65 cm/s is well reproduced in FLAME HIGH-RES. The maximum velocities are smaller (55 cm/s) in FLAME REF, along with a somewhat more diffuse meridional extent, both probably attributable to the use of a harmonic (Laplacian) mixing scheme for momentum in the model version considered here. BÖNING & KRÖGER (2005) and KRÖGER (2001) showed that using a biharmonic mixing scheme or higher resolution helps to sharpen
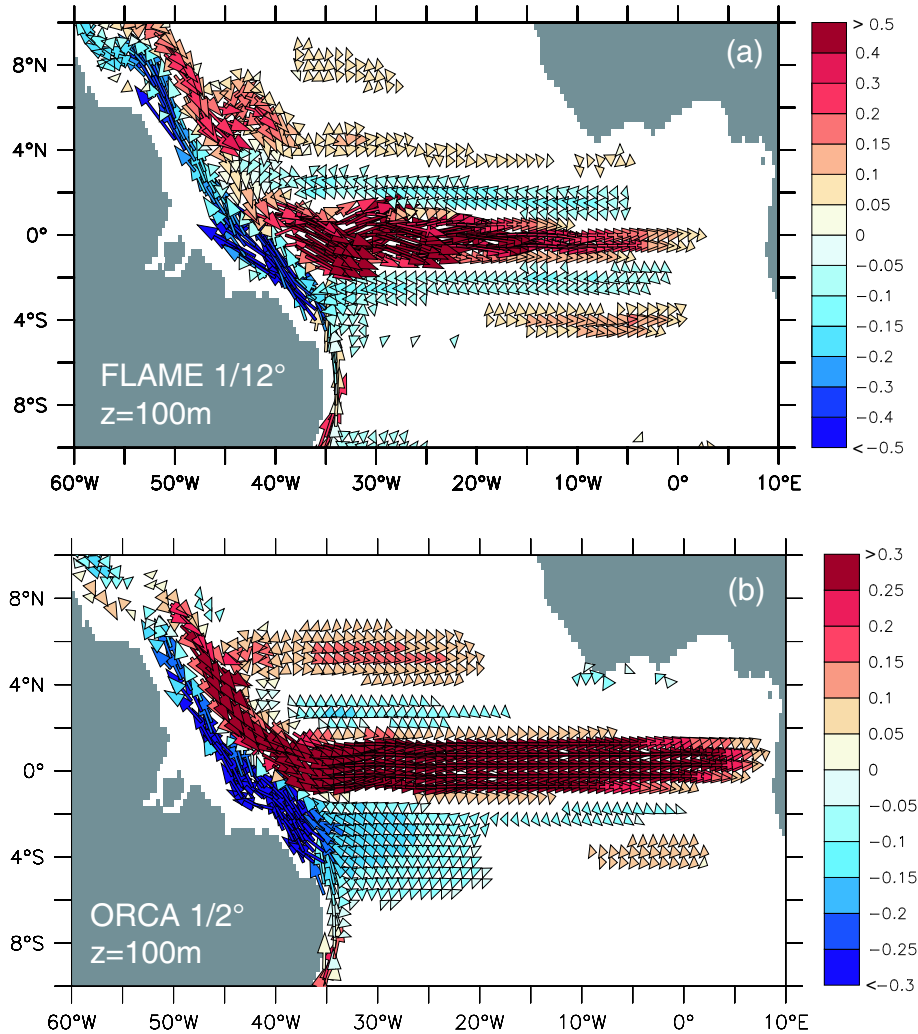
Figure 3.3: Annual mean circulation in 100m from a) FLAME HIGH-RES and b) ORCA REF. The vector color indicates the direction of the zonal current (red: eastward, blue: westward). FLAME HIGH-RES reveals the various small zonal current bands while the ORCA REF experiment gives a more general view of the circulation.

the eastward equatorial undercurrents and to maintain the equatorial thermocline structure to a more realistic representation. So one could expect a much better representation of the EUC and the vertical density structure in FLAME HIGH-RES.

In both models, the EUC core lies between 50m and 100m and between the isopycnals σ_θ=24.4-26.2 kg/m^3, at slightly lower densities than in the observations. The mean transports in this density range are 8.5 Sv for FLAME REF and 11.0 Sv for FLAME HIGH-RES (total eastward transports are 16.1 Sv and 22.2 Sv, respectively), in comparison to the observational estimates of 12.3 Sv (for the layer σ_θ=24.5 to 26.8 kg/m^3). The large differences between the two models results from the different vertical stratification (especially below σ_θ=26.2 kg/m^3) because FLAME REF is
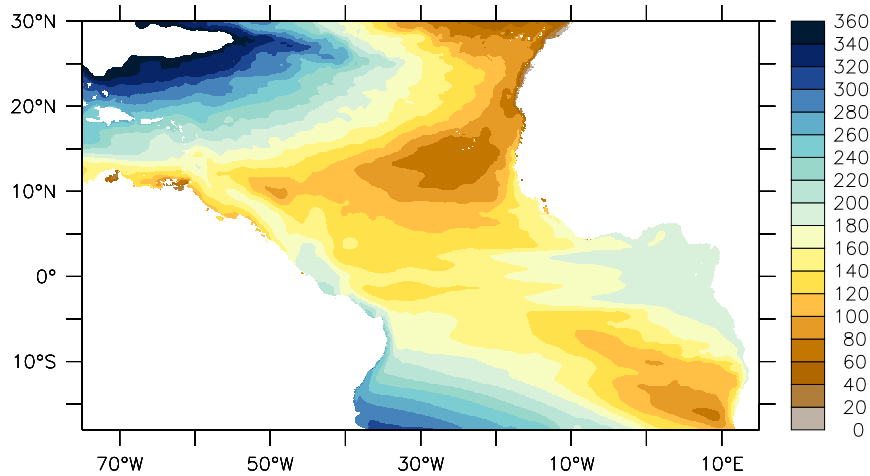
Figure 3.4: Depth of the $\sigma_\theta = 26.5$ kg/m^3 isopycnal. Clearly visible are the doming circulations near 15°N/S.

not able to maintain a very realistic thermocline structure for the reasons discussed above.

 The meridional velocity patterns at the western boundary (5°S) are all character-ized by a strong (90-100 cm/s) NBC, with a subsurface current core. Thermocline-transports associated with the NBC between σ_θ=24.5 to 26.8 kg/m^3 are 14.5 Sv for FLAME REF and 16 Sv for FLAME HIGH-RES, somewhat stronger than the observational value of 13.4 ± 2.7 Sv estimated by SCHOTT ET AL. (2002) from 6 repeated shipboard profiles. Moving to the density range given above, transports reduce to 9.3 Sv for FLAME REF and 8.7 Sv in FLAME HIGH-RES. The somewhat different locations of the core relative to the topography, and the deeper core-depth in the observational picture, might partly be attributable to sampling issues (no data from the shelf, and a possible seasonal bias due to the lack of winter data), and the varying degree of which topographic details are represented at the different model resolutions.

Resolutional effects

Discrepancies in the representation of the zonal current system turned out from Fig. 3.3 and 3.5 between both the ORCA and the FLAME experiments. Figure 3.6 illustrates this along zonal sections at 35°W, 23°W and 10°W. In all sections a deeper EUC core in ORCA REF is obvious which resembles much more the observed core depths. As discussed for example by OSCHLIES & GARCON (1999) this is related to the use of the TKE scheme for vertical mixing. However, the eastward transport in ORCA REF is much lower as in the FLAME-cases: 9 Sv at 35°W, 7 Sv at 23°W and 6 Sv at 10°W, an attribution to the weaker NBC in ORCA REF.

 Clearly visible in FLAME HIGH-RES is the NEUC at 35°W and 23°W between 80 and 300m as a deep extention of the near-surface NECC. The SEUC occurs as a separate current core (10cm/s) in FLAME HIGH-RES already at 23°W, while ORCA REF shows a small eastward core (5cm/s) at 10°W. While FLAME HIGH-
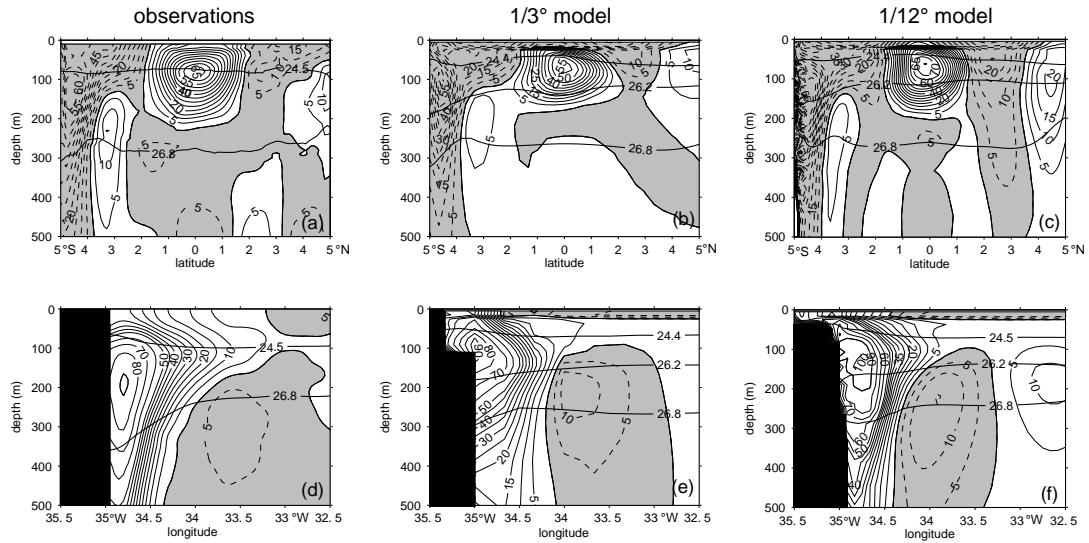
Figure 3.5: Current sections: a) EUC at 35°W from 13 observations by SCHOTT ET AL. (2003), b) mean EUC at 35°W in FLAME REF, c) mean EUC at 35°W in FLAME HIGH-RES, d) NBC at 5°S from ADCP- and current meter observations by SCHOTT ET AL. (2005), e) mean NBC at 5°S in FLAME REF, f) mean NBC at 5°S in FLAME HIGH-RES.

RES shows deep reaching westward currents between the SEUC/NEUC and the EUC, this flow is remarkably weaker and more surface confined in ORCA REF.

  For that, as an overall impression both models resolve the main currents forming the mean equatorial current system but ORCA REF has a too low horizontal resolution to resolve such narrow eastward jets as shown in FLAME HIGH-RES. In a regional model configuration of the 1/3°-FLAME model KRÖGER (2001) showed that it is possible to simulate the zonal current system in detail at this horizontal resolution when using biharmonic mixing and a stability dependent vertical mixing scheme. Thus, resolving the off-equatorial undercurrents depends not only on horizontal resolution but also on the choose of the mixing parameterizations. Due to the need to simulate a realistic behavior in the North Atlantic, the 1/3°-FLAME model was not tuned for equatorial processes and thus reveals not the best possible representation of the tropical current system at this resolution. In the following, the ORCA results and the FLAME 1/3° experiments (FLAME REF, FLAME HEAT, FLAME NOLAB) will be used mainly to describe the variability of the STC regime on longer timescales (see next chapter) while FLAME HIGH-RES will be used for analyzing the detailed structures and interactions within the zonal current system.

3.3   Mechanisms and patterns of the annual cycle

The basic physical mechanisms of the wind-driven annual cycle in the tropical Atlantic were first discussed by PHILANDER & PACANOWSKI (1986). They illustrated a direct link between thermocline depth, EUC transport and zonal wind stress but
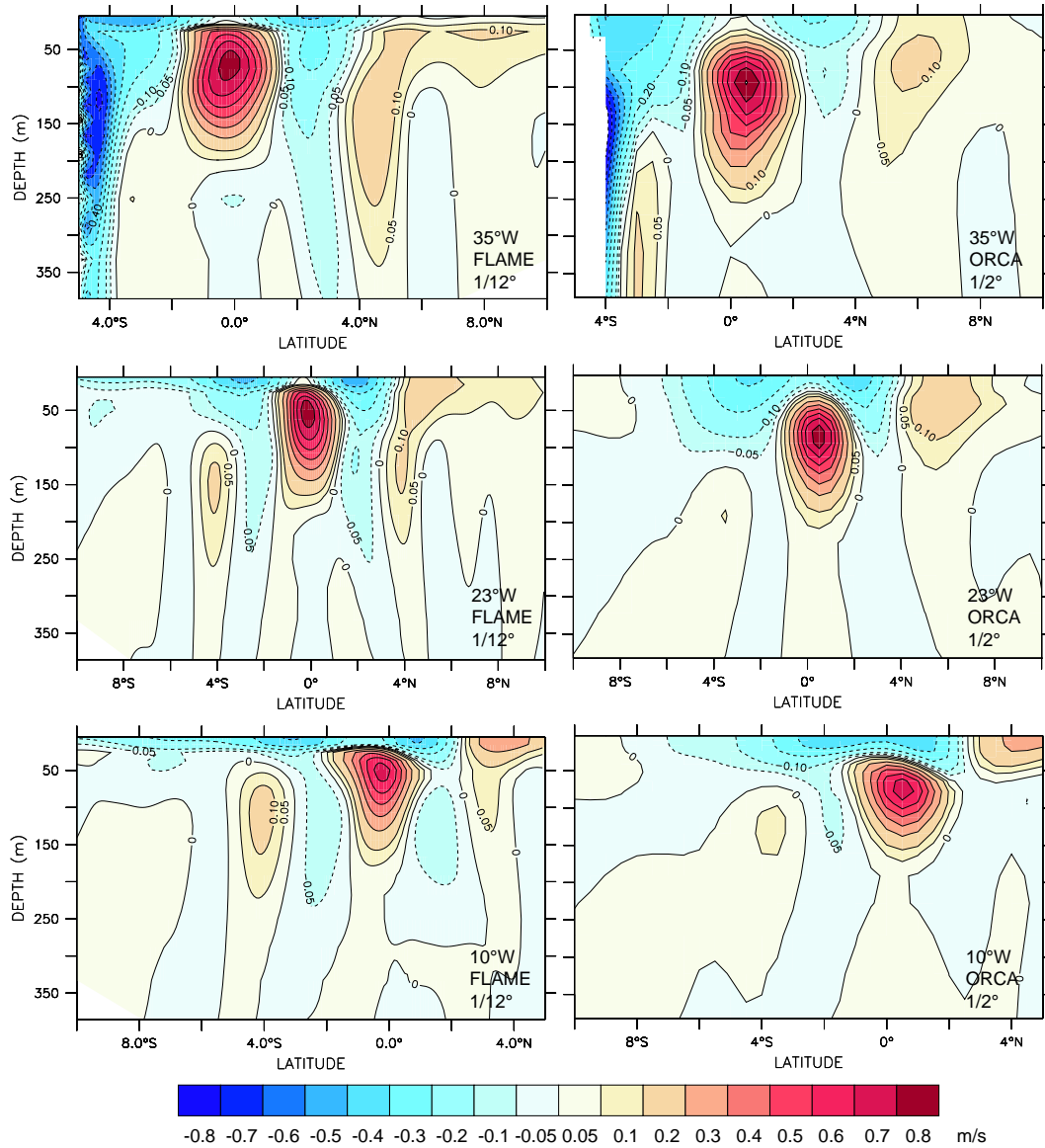
Figure 3.6: Zonal section from FLAME HIGH-RES (left panel) and ORCA REF (right panel). The main characteristics of the equatorial surface flow (EUC, NECC, SEC, NBC) are visible in both models. Differences occur in the representation of the off-equatorial undercurrents NEUC and SEUC as well as in the strength of the SEC westward flow between the eastward current cores.

also showed the importance of equatorial Rossby waves for the annual cycle. Various model studies have dealt with their generation and propagation characteristics (e.g. THIERRY ET AL. (2004)) and have examined their signatures in the deep (e.g. BÖNING & KRÖGER (2005)) and intermediate (BRANDT & EDEN (2005)) layers of the equatorial Atlantic.

An expression of the wave signal in the near-surface currents along the equator is given in Fig. 3.7, showing the anomalies of the zonal velocity component from the annual-mean, at 100m depth in FLAME REF. The wave signal extends nearly across the whole basin, characterized by an amplitude of O(10cm/s), intensified to O(15-20cm/s) between 20°W to 35°W, and decreasing to the western boundary. The phase propagation from 10°W to 35°W takes about 2 to 4 months. The horizontal structure (not shown) reveals a wave of the first meridional mode, with strongest amplitudes in the latitudinal range of about two degrees around the equator and reaching to about 6° latitude with decreasing amplitudes. Thus, all equatorial zonal currents are influenced more or less by the wave during their annual cycle. In FLAME HIGH-RES the wave behavior is less clear in the upper 500m because of a much stronger intraseasonal variability due to tropical instability waves (TIWs, WEISBERG & WEINGARTNER (1988)). The analysis of these waves and their role in the mean current structure will be discussed in a later in this chapter.
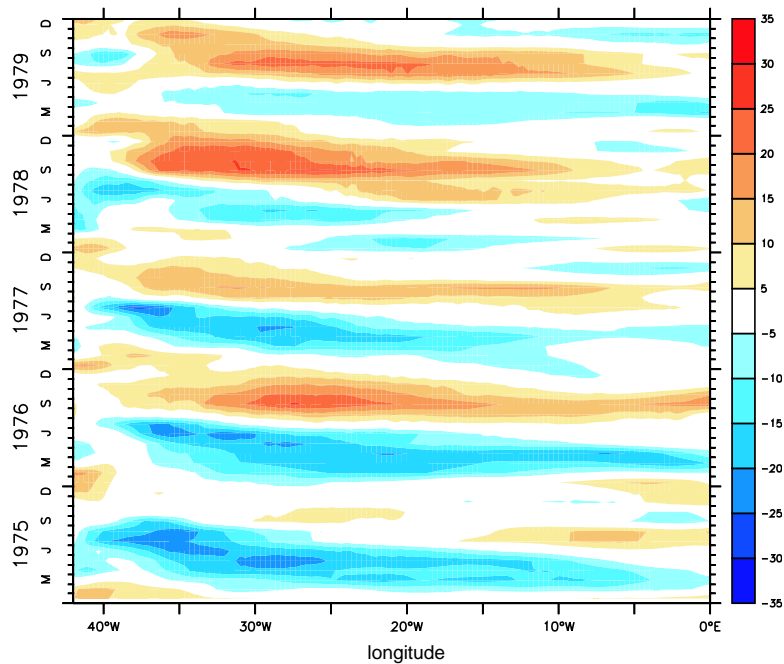

Figure 3.7: Hovmoeller diagram of zonal velocity anomaly at the equator in 100m depth from FLAME REF, indicating a Rossby-wave signal with interannual modulation.

A depiction of the annual cycle of the zonal current system in 100m depth is given in Fig. 3.8 from FLAME HIGH-RES. Strongest variability is visible in the westward flowing SEC band on both sides of the equator: enhanced westward transports
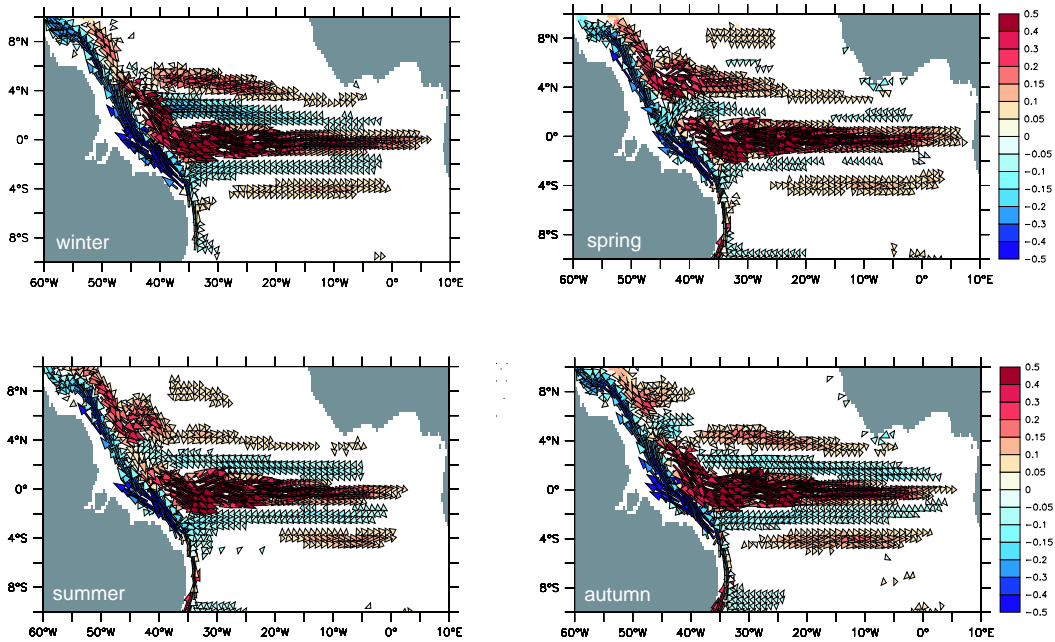
Figure 3.8: Annual cycle from FLAME HIGH-RES in 100m depth. The vector color indicates the direction of the zonal flow (red=eastward, blue=westward). The figure highlights the different zonal and meridional extents of the zonal currents.

in winter and a strong breakdown of the westward flow in mid-basin in spring. Interestingly, the minimum transport in May corresponds to with minimum eastward transport of the EUC in this season. Since this can not be related to the first meridional mode Rossby-wave signal (which has the same sign in the 3°N-3°S-strip and partly contributes to the spring minima in the eastward EUC transport), this indicates a connection of the EUC and the SEC flow, described by the concept of the tropical cell. This suggests a part of the EUC waters recirculates in the inner tropics.

Another interesting aspect of the westward flow is a split of the northern hemispheric NBC southward retroflection in spring and early summer. It seems that in spring there is additional northern inflow into the zonal currents north of 4°N because the southern waters do not reach further north than the EUC, thus are not connected to the NBC retroflection in spring. Nevertheless, it is difficult to estimate if a significant amount of northern hemispheric waters enters the tropical currents south of 4°N.

While the NEUC seems to be sometimes connected to the western boundary current and its retroflection, especially in spring and summer, the SEUC never shows such a linkage. However, the SEUC shows a east-west movement of its westernmost occurrence during the annual cycle. Its westernmost position the SEUC reaches in autumn (about 30°W) and its easternmost occurrence can be found in summer (about 20°W).

In all seasons none of the off-equatorial undercurrents is reaches the eastern boundary: the NEUC does not enter deep into the Gulf of Guinea and the SEUC can not be found east of 5°E. This implies a vertical or horizontal shift of the currents, i.e. up- or downwelling or horizontal recirculation. Like in the Pacific, some observations (Bourles et al. (2002), Mercier et al. (2003)) indicate a poleward shift of the off-equatorial undercurrents when flowing eastward, but this is not the case for the shown model currents. Instead of that, they seem to converge equatorward: the NEUC shows this behavior all the year, the northern part of the SEUC converges equatorward during spring and summer.

In spring and summer a deep reaching northern NECC branch develops north of 8°N near 35°W. This current has already been described by Richardson & Reverdin (1987) when analyzing float trajectories, surface drifters and buoy data in the NECC region and also was present in observations during fall 2002 discussed by Stramma et al. (2005a). Richardson & Reverdin (1987) also note the seasonal behavior of this northward branch: the two separate NECC cores between 33°W and 23°W exist from March to May and from July to September. Nevertheless, it is unclear what generates the deep northern NECC core: Urbano et al. (2006) propose a theory that both cores of the NECC result from the (seasonal) Sverdrup balance and are therefore generated by the particular structure of the wind field in the tropical Atlantic. However, Garzoli & Katz (1983) showed in an analysis of the vorticity balance in the tropical Atlantic that the Sverdrup balance does not hold for the western and eastern parts of the NECC, so the current can not be totally determined by Sverdrup balance. A study by Verdy & Jochum (2005) confirms this view by deducing from model results the balance does not hold for the NBC retroflection regime where the advection of relative vorticity is not negligible and therefore violates one of the assumptions for the use of Sverdrup theory.

Stramma et al. (2005a) discuss another possible connection between NECC and its deep northern part. They used model trajectories launched in the Guinea Dome and tracked them backward in time to investigate the watermasses reaching the Guinea Dome region. They found the westernmost watermasses in the Guinea Dome connected to the northern NECC core, which is formed from the NECC near the western boundary but partly shifted northward in the mid of the Atlantic basin. Monthly sensitivity runs revealed the northward shift to occur mainly in boreal summer and therefore tropical instability waves might be an important mechanism in transferring waters from the NECC or shallow parts of the NEUC to the northern NECC.

3.3.1   Annual variability of eastward currents

The different zonal currents have been observed and described for a long time one by one. Those forming the tropical and subtropical gyres and apparent near the surface have been extensively studied for their annual cycle and variability mechanisms. The zonal sections revealed also deeper undercurrents on both sides of the equator which only have recently found some attention because they might be the source of the upwelling waters along the African coast and in the doming areas.

The zonal sections, as shown in Fig. 3.6 show a heavily sheared current system, where the shear might creates instabilities and resulting from that, waves. As the

equator acts as a waveguide the currents in the vicinity of the equator show a fast response to changes, for instance in wind strength. But the equatorial waves show short meridional scales, thus the various zonal currents are influenced differently in time, space and amplitude by the same wave process. This might causes additional instabilities caused by waves itself leading to eddy-activity superimposed on the meandering currents. Such variability has the potential to mix waters from the different zonal currents, i.e. the expectation is a strong interaction between the various east- and westward flows.

However, it is difficult to study such processes by analyzing the Eulerian velocity fields which do not allow for a quantification if and how effective the interaction is. Hence, first the annual and seasonal variations of the eastward currents are discussed separately and for that part the possible exchanges between the currents is ignored. Using this approach, the variations can be related to observations and other model studies. The question about the degree of interaction between the currents will investigated afterwards by the help of Lagrangian analysis which will allow also for a determination of the sources and fates of the zonal currents.

North Equatorial Countercurrent

The annual cycle of the NECC is strongly related to the variations of the wind stress curl (GARZOLI & KATZ (1983)). The strength of the wind is directly related to the position of the ITCZ and the meridional NECC core position follows the ITCZ on interannual timescales (GARZOLI & RICHARDSON (1989), FONSECA ET AL. (2004)). Observations (GARZOLI & RICHARDSON (1989), RICHARDSON & REVERDIN (1987), FONSECA ET AL. (2004)) revealed a weak or even westward NECC west of 20°W in boreal spring and a rapid onset of the westward current during May and June. These findings are confirmed by all ocean models used here (see Fig. 3.9, left panel), although the NECC in the different models never reverses to westward flow in the westernmost part of the basin but is reduced remarkably.

RICHARDSON & REVERDIN (1987) pointed out, that it is difficult to see clearly an annual signal in observational data because it is overlaid by strong oscillations with a period of about one month (i.e. instability waves), lower frequency meandering and eddies originating from the NBC retroflection and from NBC rings. STRAMMA ET AL. (2005a) came to similar results using SSH analysis from altimeter data and output from the FLAME HIGH-RES. They find the tropical gyre, formed by the NEC in the north and the NECC in the south, to be dominated by short term variability and meanders. Additionally, due to the interannual variations of the ITCZ the latitude of the NECC fluctuates as well as its meridional width (GARZOLI & RICHARDSON (1989), HENIN & HISARD (1987)). Thus, the NECC and its variability is difficult to obtain completely and the question if the NECC reverses in boreal spring near the western boundary has to remain unclear.

The phases of the annual cycle compare quite well near the western boundary (35°W), only the amplitudes differ from model to model: FLAME REF gives 10 Sv, FLAME HIGH-RES and ORCA REF 8 Sv. However, observations in the western tropical Atlantic indicate a transport maximum of the NECC to occur two times a year: during the strengthening phase of the NECC from June to August and during October to November (FONSECA ET AL. (2004)). The models at 35°W show only
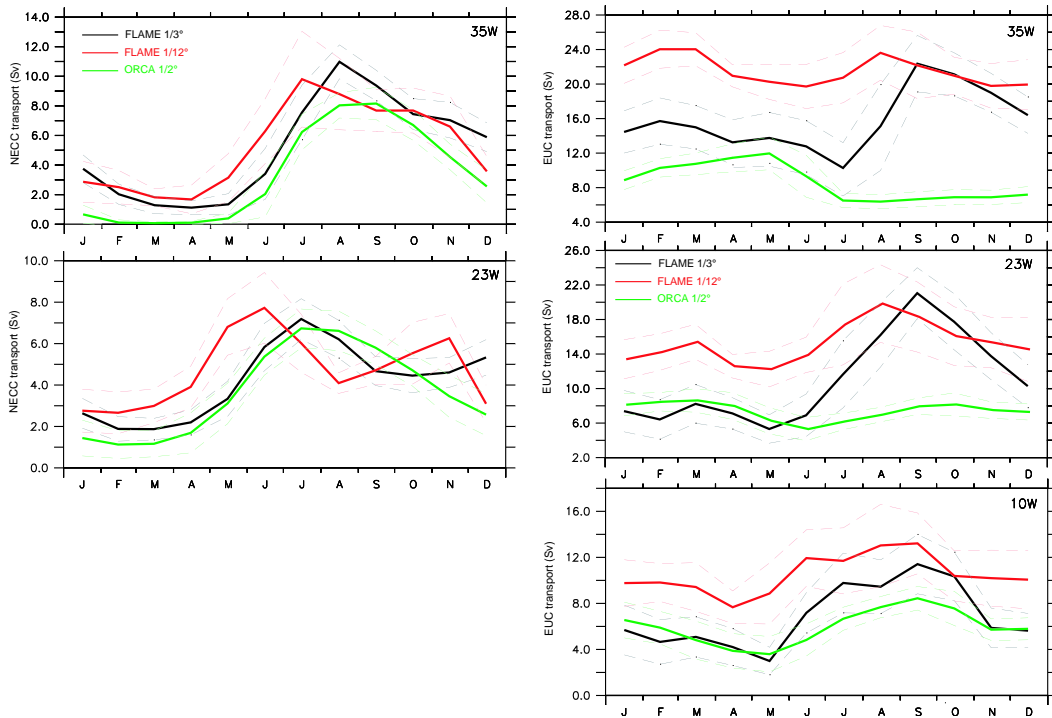
Figure 3.9: Annual cycle of the NECC (left panel) and EUC (right panel) at different longitudes in the different analyzed models. While the wind-driven variability of the NECC shows good correspondence between all models and findings from observational data, the EUC variability significantly differs between any of them. The dashed lines mark the RMS of the interannual variability.

one maximum which occurs quite earlier, in July (FLAME HIGH-RES), August (FLAME REF) and September (ORCA REF). In the mid of the basin (23°W) FLAME HIGH-RES reveals a more semi-annual cycle with an additional minimum in NECC transport in August and two maxima occurring in June and November, which resemble very much the observed transport variability. The August minimum in FLAME HIGH-RES is related to the strong intensity of the instability waves in this model due to sharper zonal jets and accordingly stronger horizontal shear.

Equatorial Undercurrent

Larger differences between the models can be found for the annual cycles of the equatorial undercurrent. The EUC (Fig. 3.9, right panel) indicates a latitudinal dependence of the differences in annual cycle: while near the western boundary (35°W) all used configurations give a different behavior, in the eastern part of the basin (10°W) at least the phases of the annual cycle are in agreement. Apparently, the annual cycle of the EUC is not coherent throughout the basin. This could be an effect of the upward motion of the EUC and the equatorial thermocline towards the east: in the east the EUC is more strongly related to the wind-induced upwelling variability, while near the western boundary it is much more dependent on the

annual cycle of the inflow from the NBC and its retroflection. Thus, it might gets complicated to determine which effects play a role for upwelling and EUC variability in the eastern tropical Atlantic.

The strong differences in the annual cycle of the EUC transport between ORCA REF and FLAME REF near the western boundary are also contrasted by results from (HAZELEGER ET AL. (2003) at 35°W and 23°W) and observations (SCHOTT ET AL. (2003) at 35°W). While HAZELEGER ET AL. (2003) find an annual cycle similar to FLAME HIGH-RES, the scatter in the measured values by SCHOTT ET AL. (2003) does not help to reveal a clear observed annual signal. For example, the three measurements from SCHOTT ET AL. (2003) in March at 35°W differ between 12 Sv and 15 Sv of eastward transport in the layer 50-300m. Thus, there seems to be strong short-term variability dominating the annual signal in some seasons. So, the ability of a model to represent intraseasonal fluctuations is maybe crucial to the representation of the annual cycle.

North and South Equatorial Undercurrent

Both, the NEUC and SEUC were found to be not resolved in detail in FLAME REF and in ORCA REF. Figure 3.10 shows the eastward transports below 80m and between 3°N/S and 5.5°N/S. Interestingly, some eastward flow also exists in the lower resolution experiments, revealing a similar but heavily damped annual cycle too. This eastward flow is related to the annual Rossby wave at these latitudes: while the EUC transports in May to July are reduced, the transports between 3°N/S and 5°N/S are strengthened. This view is also supported by the propagation of the annual cycle westward: the extrema of the transport time series first emerges in the eastern sections (23°W for the NEUC, 10°W for SEUC) and is found with a lag of one or two months at the western section (35°W for the NEUC, 23°W for the SEUC).

Surprisingly, the annual cycle of both off-equatorial undercurrents from FLAME HIGH-RES show similar amplitudes. But a more precisely investigation reveals the large interannual variability of this mean annual cycles. For the NEUC the standard deviation of the annual cycle shows values of comparable amplitude to the annual signal itself during May to June and November to March (23°W) and June to August and October to December (35°W), respectively. For the SEUC the interannual variability of the annual mean is year-round on the order of the amplitude of the annual cycle.

In the mean pictures, it is difficult to separate the NEUC from the NECC, but the annual cycle of the NEUC is quite different to that of the NECC: the transport maximum occurs 1 to 2 months earlier for the NEUC (another hint on the role of Rossby waves for the annual cycle of the NEUC, because the equatorial Rossby waves not only propagate westward but from bottom to top, see also BRANDT & EDEN (2005)) and the current is weak in winter, where the wind-driven NECC shows maximum amplitude.

The strong variance of the annual cycle is examined further by investigation of the time series of the off-equatorial undercurrents in Fig. 3.11. The NEUC (left panel) reveals interannual variability which is a modulation of the annual cycle, although with amplitudes up to twice as large as the annual signal. This variability is clearly
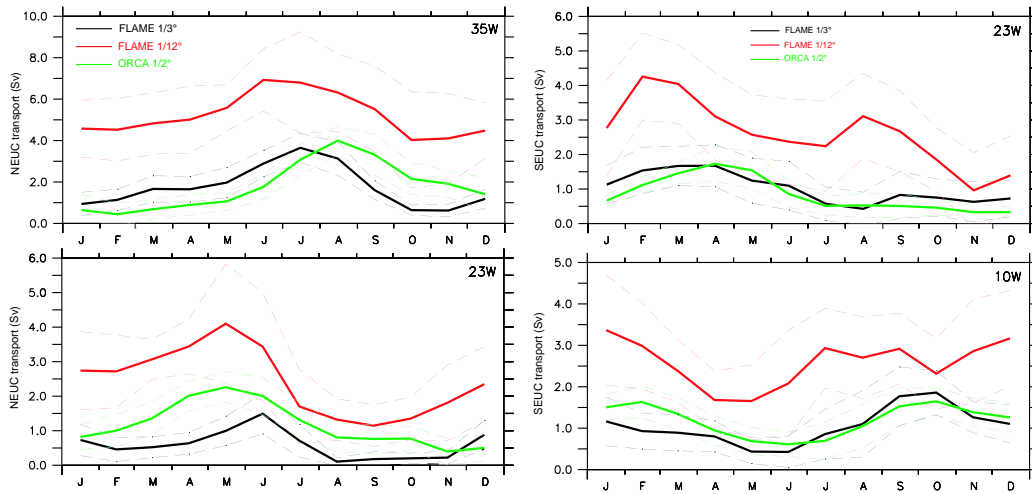
Figure 3.10: Annual cycle of the off-equatorial undercurrents. Left panel: NEUC,
right panel: SEUC. The lower resolution models which do not resolve the undercur-
rents in detail show similar results for both currents and therefore might be a result
of the wind-driven annual cycle. FLAME HIGH-RES shows a more complicated
annual cycle and significantly higher eastward transports throughout the year. The
dashed lines mark the RMS of the interannual variability.

related to the high frequency fluctuations as visible by a comparison between the
monthly mean values and the overlaid 3-daily time series for the years 1997-1999
(compare Fig. 3.11). However, these interannual changes do not occur in accordance
between the western (35°W) and the central (23°W) part of the current, i.e. their
zonal coherence is rather limited.
  The southern undercurrent (right panel) highlights the nearly independent vari-
ability behavior of the SEUC at 23°W and 10°W. As for the NEUC, the short-term
variability determines the interannual fluctuations but these are not simply an in-
tensification or reduction of a mean annual cycle and occur year round. Thus, is
is difficult to determine if the mean annual cycle calculated from this 15-year time
series is a meaningful quantity for the SEUC. From Fig. 3.11 the SEUC can be
regarded as a weak mean current that is dominated by different wave processes
which more or less influence the whole variability of the flow. So, it is difficult to
compare the mean models value and the observational means given by BOURLES
ET AL. (2002) or by BRANDT ET AL. (2006), as these values can differ significantly
depending on the length and the members of the average record.

3.3.2   Tropical Instability Waves

Timescales and variability patterns

As indicated by all time series analyzed yet, there is strong intraseasonal variability
along the near equatorial currents. Using Fourier-analysis of daily velocity fields
for the NEUC and SEUC (not shown) in FLAME HIGH-RES, enhanced energy in
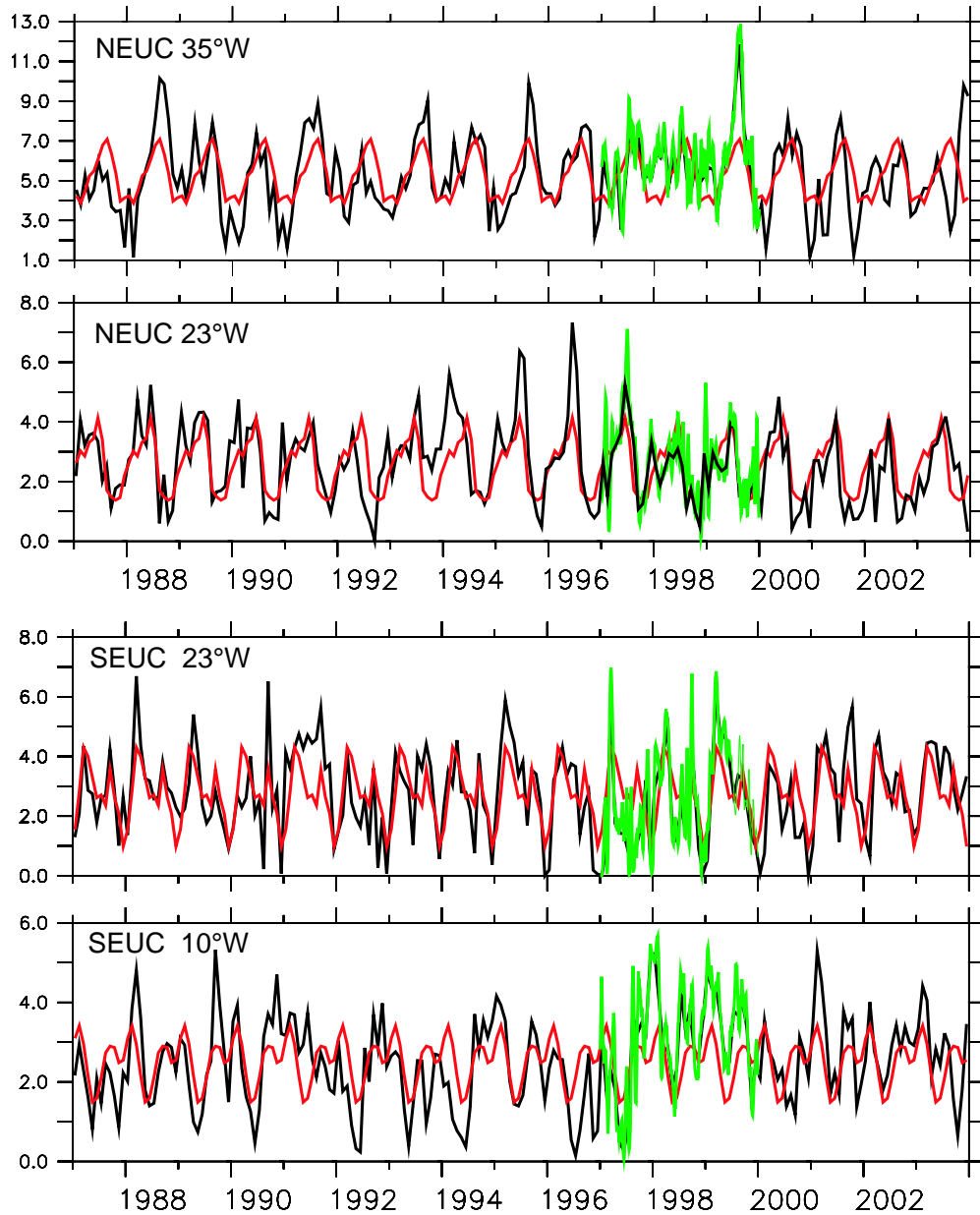the 30-40 day band and between 50 to 60 days is found. These timescales are in

Figure 3.11: Time series (black) and annual cycle (red) of the off-equatorial undercurrents from FLAME HIGH-RES. Upper panel: NEUC, lower panel: SEUC. Overlaid in green are the transports from 3-daily output for the years 1997-1999. It is obvious that the interannual variability of both currents is strongly influenced by the seasonal variability and almost as large (NEUC) or larger (SEUC) than the mean annual cycle. Especially for the SEUC in the eastern basin is difficult to determine if the mean annual cycle is a meaningful quantity.
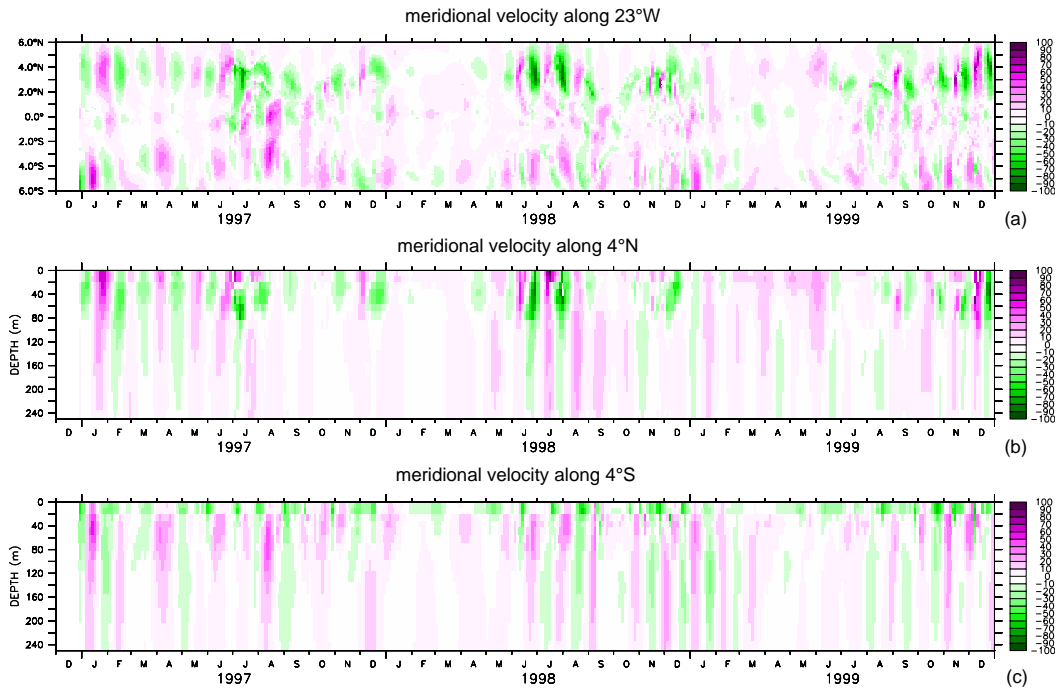
Figure 3.12: TIW structure from meridional velocity anomalies in FLAME HIGH-RES: a) horizontal structure and b, c) vertical structure along 4°N/S

good accordance with results from all observational records of instability waves (for example: WEISBERG & WEINGARTNER (1988), GRODSKY ET AL. (2005), BRANDT ET AL. (2006)). Interestingly, both timescales are connected to the same wave phenomenon created by shear instability: the 50-60 day undulations belong to westward propagating eddies slightly north (1° as indicated by WEIDMAN ET AL. (1999)) of the original instability and is related to the meridional shear between the NECC and the SEC (PHILANDER & PACANOWSKI (1986)). Some authors refer them as "tropical instability vortices" (FOLTZ & CARTON (2004)) or "Legeckis eddies" (WEIDMAN ET AL. (1999)). The 30-40 day variability is linked directly to the shear instability of the SEC-EUC system (see for instance QIAO & WEISBERG (1998)).

  Using longer interannual time series for the years 1987-2003, a 90-day band is obvious and the semiannual and annual components occur as the strongest signals. As suspected from Fig. 3.11 no preferred longer term variability timescale can be found. The Fourier decomposition also supports the result that the annual cycle is the dominating signal for the NEUC, while the semi-annual component is the strongest signal for the SEUC. Both of these spectral maxima are stronger than the spectral peaks associated with the different kinds of intraseasonal wave signals, i.e. the annual/semi-annual cycle of the off-equatorial currents is not totally defined by these waves. This indicates, that a mean annual cycle even for the irregular varying SEUC is not an artificial quantity as suspected from the time series in Figs. 3.10 and 3.11.

  The zonal currents in the mean reveal only small meridional velocities. Thus, strong meridional velocity components do not occur and if so, they are a good measure of
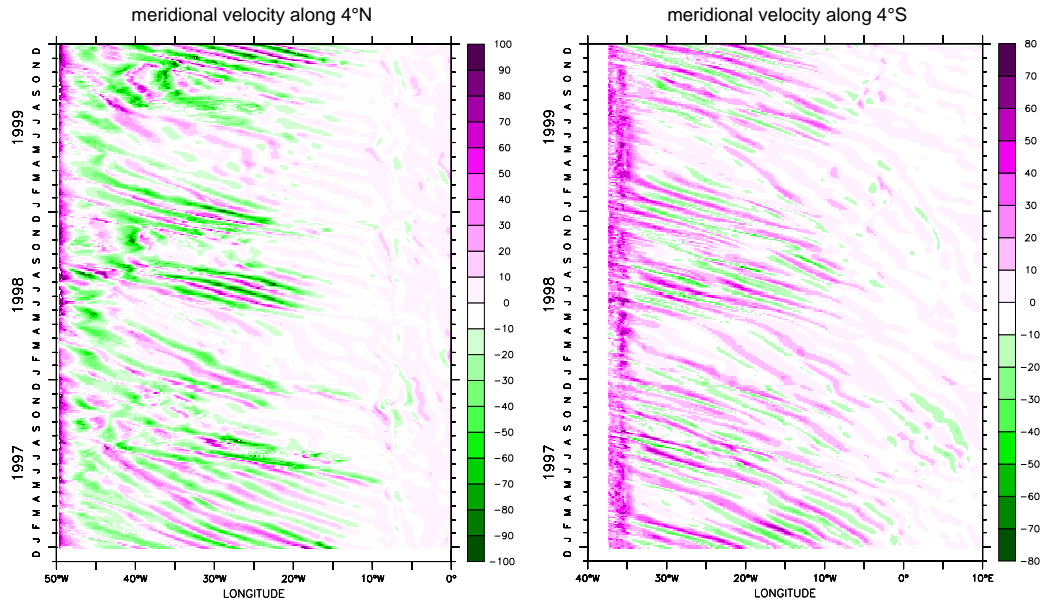
Figure 3.13: Hovmoeller diagrams of the meridional velocity anomaly along 4°N/S in 100m depth from FLAME HIGH-RES showing TIWs with eastward group and westward phase velocity.

any wave activity. Instability waves reveal a meridional anomaly signal clearly visible in Figs. 3.12 and 3.13. The meridional structure (Fig. 3.12a) of the waves at 23°W shows a nearly equator-symmetric wave pattern, although northern and southern hemispheric anomalies are slightly out of phase by about 15 days to one month and the northern hemispheric wave exhibits larger amplitudes. Strongest anomalies are found right on the equator and in the region between 4°N/S and 6°N/S. Interestingly, the wave signals do not occur in boreal summer only, but there is a second maximum of the waves in boreal winter from October to February. This semi-annual generation cycle was already observed by WEISBERG & WEINGARTNER (1988) and is evident in the data discussed by GRODSKY ET AL. (2005) and BRANDT ET AL. (2006). While the onset of the summer TIWs is nearly as observed, the winter waves in the model occur and vanish earlier by one or two months than the BRANDT ET AL. (2006) data analysis indicates.

The vertical structure of the anomalies (Fig. 3.12b) show the strongest anomalies are confined to the upper 250m, with largest amplitudes above 50m. The vertical and horizontal structures also give an explanation for 90-day timescale found in the Fourier-analysis as it is the preferred timescale for a packet of TIWs to cross a certain location. This most clearly visible for the waves in summer 1998 and the following winter.

The zonal propagation and wave lengths can be obtained from Hovmoeller diagrams along the signal maximum latitudes 4°N and 4°S (Fig. 3.13). At both latitudes several wave packets are visible. Also, the waves occur mainly in the central and western parts of the basin. At 4°N no waves occur further east than 10°W where

the equatorial Atlantic forms the Gulf of Guinea. At 4°S the waves reach until 0°W, at about the latitude where the SEUC vanishes in the mean.

According to linear theory (see GILL (1982)), tropical instability waves always show eastward energy propagation but phase propagation can be as well east- as westward. The waves in FLAME HIGH-RES clearly show westward phase velocities ranging between 30 to 40 cm/s and eastward energy propagation with group velocity between 15 to 20 cm/s (indicated by the black arrows in Fig. 3.14). The zonal wavelength ranges between 1000 and 1500 km. All these results are in the range of observations. The eastward energy propagation associated with the wave groups velocity indicates a wave generation near the western boundary.

Generation mechanism

The generation mechanism of the TIWs is the meridional shear between the near equatorial currents (PHILANDER (1976), WEISBERG & WEINGARTNER (1988), JOCHUM ET AL. (2004b)) which reverse meridionally in a few 100km from an strong eastward jet (EUC, NECC, NEUC or SEUC) to a strong westward flow (the nSEC, sSEC or NEC). The waves are thought to occur if the shear between the zonal currents reaches a critical value. This TIW generation is suggested to be mainly due to barotropic instability (PHILANDER & PACANOWSKI (1986)) and strong evidence for that was found by analyzing moored ADCP data from the tropical Pacific by QIAO & WEISBERG (1998)). Numerical studies by COX (1980) revealed also baroclinic instability as a energy source for the waves by providing available potential energy (APE, see also OORT ET AL. (1989) for an overview of energy conversion mechanisms). A more recent study by MASINA ET AL. (1999) confirms this result by finding the TIWs to grow both from barotropic and baroclinic energy sources.

JOHNSON & PROEHL (2004) reported for TIWs in the Pacific a correlation between seasonal and interannual variations of the strength of the zonal current system and revealed the waves reduce not only the shear of the currents but their thermal structure, too. A more recent study concerning the Atlantic TIWs by GRODSKY ET AL. (2005) supports this finding and emphasizes also salinity fluctuations associated with the waves to be important for the energy budget of the waves themselves.

Such a TIW mechanism is supported by the model, too: Fig. 3.14 shows the meridional shear (defined here as the maximum velocity difference between east and westward flow) of the zonal currents at 35°W between the nSEC and the NECC/NEUC and the EUC regime (Fig. 3.14a), between the sSEC and the EUC and SEUC (Fig. 3.14b) and the corresponding meridional velocity anomalies at 4°N (Hovmoeller diagram in Fig. 3.14c). Note, that only positive shear values, indicating stronger eastward than westward flow, are shown. The sign of shear reverses due to wave activity sometimes to negative values, which are omitted for reasons of clarity. It is obvious that the shear on the northern hemisphere is much stronger than the southern one. This is related to the occurrence of the NECC on the northern hemisphere that forces a sharper westward flow than on the southern hemisphere where the sSEC is weaker, broader and with stronger westward transports. This indicates a generation of the TIWs north of the equator like suggested by COX (1980) and JOCHUM ET AL. (2004b).
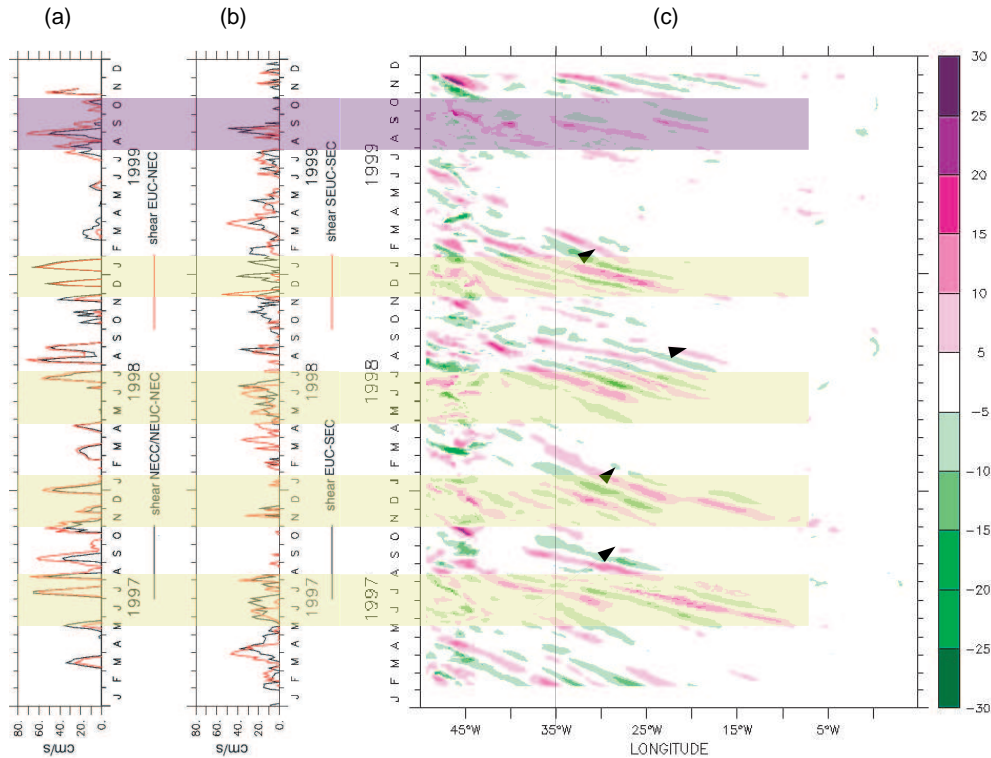
Figure 3.14: Shear between the zonal currents and their relation to instability waves from FLAME HIGH-RES. The shear between westward and eastward currents is calculated as a mean of the upper 50m at 35°W. Figure (a) shows the difference between the maxima of NECC/NEUC and the nSEC (black) and the EUC and the nSEC (red), (b) the difference between the maxima of the EUC and sSEC (black) and the SEUC and sSEC (red). Negative values occur due to the wave activity and are omitted for reasons of clarity. As a measure for the TIWs a high-pass (cut-off: 90d) filtered time series of the meridional velocity anomalies from the 3-daily dataset for the years 1997-1999 is shown in (c). The arrows indicate the direction of the wave energy. For more details see text.

A comparison between the shear and the corresponding wave patterns (Fig. 3.14) shows the occurrence of eastward propagating waves some days after a maximum in shear between the NECC/NEUC (May 1997, April 1998, November 1998, marked yellow in Fig. 3.14) and SEC and between EUC (November 1997, April 1998, November 1999, also marked yellow) and SEC respectively (maximum correlations are found for a lag of 6 days). However, the strength of the shear is not always reduced by waves: in July/August 1999 (marked in magenta) the shear is as strong as in the years before, but no waves are visible on the northern hemisphere (at 4°S there is a clear wave signal visible, see Fig. 3.13). Thus, the shear is related to the waves but it is not clear what sets the amplitudes of them. Hence, baroclinic processes have to play a role for the waves, at least for the growth/decay.

Interestingly from Fig. 3.14, the strength of the waves actually does not seem to be linked to the strength of the shear itself. A possible explanation is, as suggested by the work of Cox (1980) and Grodsky et al. (2005), that salinity and temperature anomalies going along with the instability waves might influence the density gradients between the alternating current bands and thus acting on the energy sources of the waves themselves. Another possible mechanism are different watermass properties in 1999 in the zonal currents north of the equator: the NECC shows weakened inflow from the NBC during early summer 1999 (June/July) and that, the meridional gradient between NECC and nSEC is weakened too, thus leading to a strongly decreased wave activity in this particular year. Thus, also baroclinic mechanisms contribute to the variability of the TIWs. The results obtained from FLAME HIGH-RES suggest mainly an influence on the amplitudes of the waves.

Effect of the TIWs on the circulation patterns

In the analysis of tropical instability waves by Foltz & Carton (2004) and Menkes et al. (2002) together with the waves themselves anticyclonic eddy circulations have been found. These vortices show spatial scales of about 400km, and propagate westward towards the western boundary and were found to occur with the summer maximum of the TIWs. As discussed earlier in this chapter, such eddies can be associated with a meridional mass transfer and a mixing between the several tropical zonal currents. Hence, it is useful to analyze the models waves in view of such instability vortices.

Figure 3.15 shows the absolute velocities in 100m depth during two summer and two winter months of the years 1998/99 during which two separated maxima of TIW activity were found to occur (see Fig. 3.13). Both timeseries (from top to bottom) reveal first a meandering of the circulation around 4°N/S which breaks up into anticyclonic eddies some days later. These eddies were found to propagate towards the western boundary where they end up in the North Brazil Current (NBC). The anticyclones are formed on both hemispheres and show also similar intensities north and south of the equator. The spatial structure of the eddies is about 5°longitude, i.e. shows good correspondence with the observed vortices of Menkes et al. (2002) and Foltz & Carton (2004). On the northern hemisphere the TIW induced eddies might interact with the North Brazil Rings near the western boundary and hence are possibly linked to the higher TIW fluctuations north of the equator.

The eddies occur in mid-basin, but at slightly different longitudes on both hemispheres. On the southern hemisphere the first eddy structures in summer are visible between 15°W and 20°W (Fig. 3.15a) which intensify during the westward propagation (20°W-25°W in Fig. 3.15b and 25°W-30°W in Fig. 3.15c) and reach the western boundary after 1.5 months (see Fig. 3.15d). The propagation speed thus is between 40-50 cm/s, which is in the upper range of the observed values from Foltz & Carton (2004). On the northern hemisphere the eddies form west of 20°W and show the same properties as their southern counterparts.

Like the TIWs itself, the eddies also occur in winter. As Fig. 3.15 e-h indicate, the formation region is shifted about 5° towards the west and the southern eddies occur shifted about 2° to the south. On the northern hemisphere Fig.s 3.15 f and h
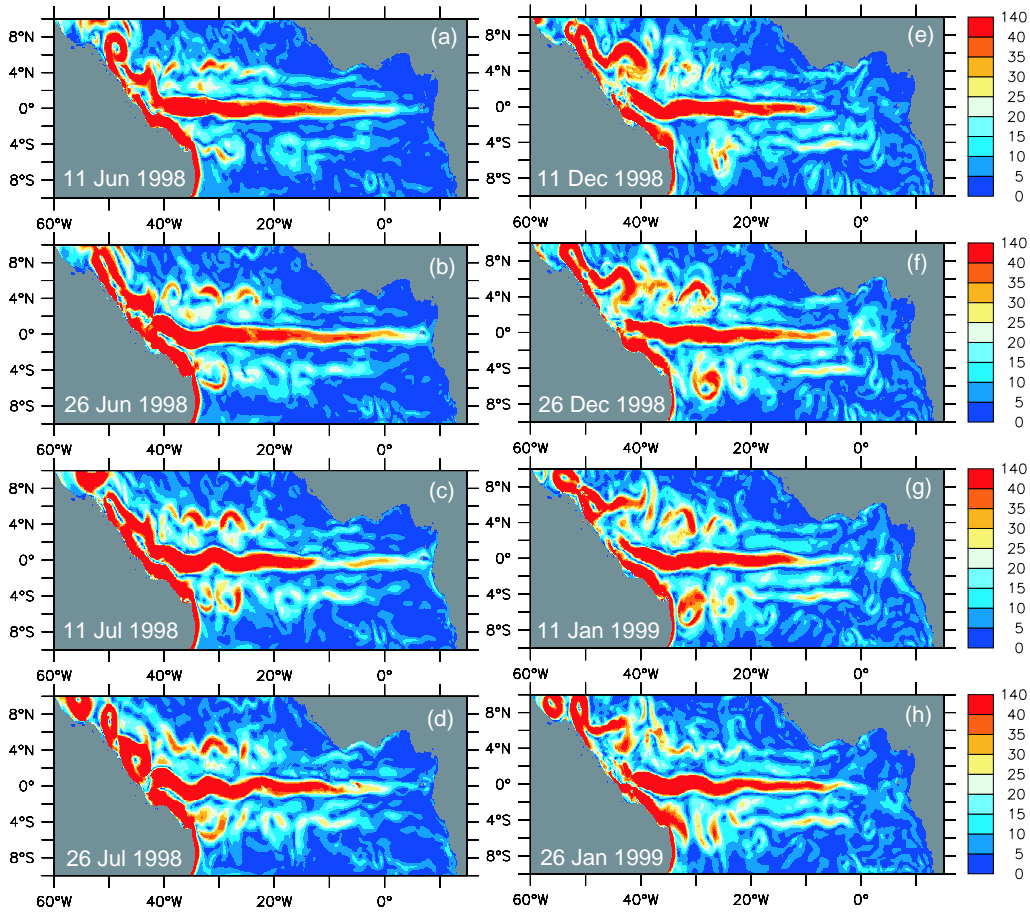
Figure 3.15: Absolute values (in cm/s) of horizontal velocity in 100m depth from FLAME HIGH-RES. The subfigures a-d represent the flow field during June-July 1998 and e-h the currents during December 1998 to January 1999. Strong subseasonal variability associated with the TIWs is visible. The TIWs cause a meandering of the currents which breaks up in mid-basin to eddies. These eddies propage towards the western boundary and on their way mix properties across the currents.

indicate interaction of the northern instability vortices with the NBC rings, leading also to variability north of the the eddy pathways.

Thus, the eddies triggered by the TIWs are present in the results of FLAME HIGH-RES and exist both during winter and summer. Their amplitudes exceed the mean current velocities and the strengthening on their way towards the western boundary indicates a strong transfer of available potential energy to eddy kinetic energy by eroding the density stratification via mixing of the different watermasses in the zonal currents. Hence, the eddies represent the baroclinic part of the TIW variability which has been discussed for setting the wave amplitudes.

3.4   Sources and fate of the zonal current system

3.4.1   Equatorial Undercurrent

The equatorial undercurrent is the strongest of the eastward (near-)equatorial currents. Early it has been recognized as a source of the cold waters in the eastern tropical Atlantic. Thus, the undercurrent and its possible sources have been extensively studied. Hydrographic measurements by METCALF & STALCUP (1967) showed that the current is mainly formed by southern hemispheric subtropical thermocline waters. With the help of the ventilated thermocline theory (LUYTEN ET AL. (1982)I and its extensions (MCCREARY & LU (1994) and LU & MCCREARY (1995)) the subtropical origin of the EUC waters was clarified and studies concerning the MOC in the Atlantic revealed a missing northern STC cell due to the northward transport in the upper 1000m of the tropical Atlantic.

What remains unclear is the distribution of the EUC waters along the different equatorward pathways discussed in Fig. 3.1a. A sensitivity study by INUI ET AL. (2002) revealed the importance of wind-stress patterns for the strength of the interior vs. the western boundary pathway. Thus, it might be possible that the strength of the interior pathway varies interannually. This aspect will be discussed not in context of the mean EUC sources and sinks, but in a later section.

Sources of the EUC

The sources of the EUC are delineated most clearly by a back-tracing of water parcels. For that, different backward integrations of the EUC water masses at 0°W were performed using output from the FLAME models. The integration was done using the mean annual cycle of the FLAME REF and FLAME HIGH-RES-experiment, i.e. 12 monthly means that are repeated after one year integration. The calculations start at different seasons of the year and are integrated backward in time for 4 years in each experiment. Using companion experiments of the 1/3° and 1/12° model allows for an estimate of the effects of higher resolution, i.e. better resolved off-equatorial currents. For an overview of experiments see Table 2.2.

The different realizations of FLAME REF, started in different seasons, appear fairly robust in the main features: the bulk of the EUC is supplied by the NBC and some weak interior flow, whereas there is no clear connection to the northern hemisphere subduction region. However, the southern interior transport shows some seasonality with strongest supply from the interior pathway when floats at 0°W are inserted in February. Figure 3.16a examines the pathways of the various contributions to the EUC from the October run in FLAME REF, where there is nearly maximum EUC transport at 0°W. The transport across this section, 5.23 Sv in the density range σ_θ=24.4-26.2 kg/m^3 is fed almost exclusively by southern hemispheric thermocline waters: while the main path along the western boundary is clearly dominating, a small (5-10%) fraction is due to an interior window between 10°W and 20°W. This pathway is rather difficult to see in a Eulerian picture of the velocity field because velocities are very low (less than 1 cm/s) in this area. This interior window is not confined to a certain density or depth range and covers the whole thermocline. The transport values in Fig. 3.16 resemble the transport through this section at the end
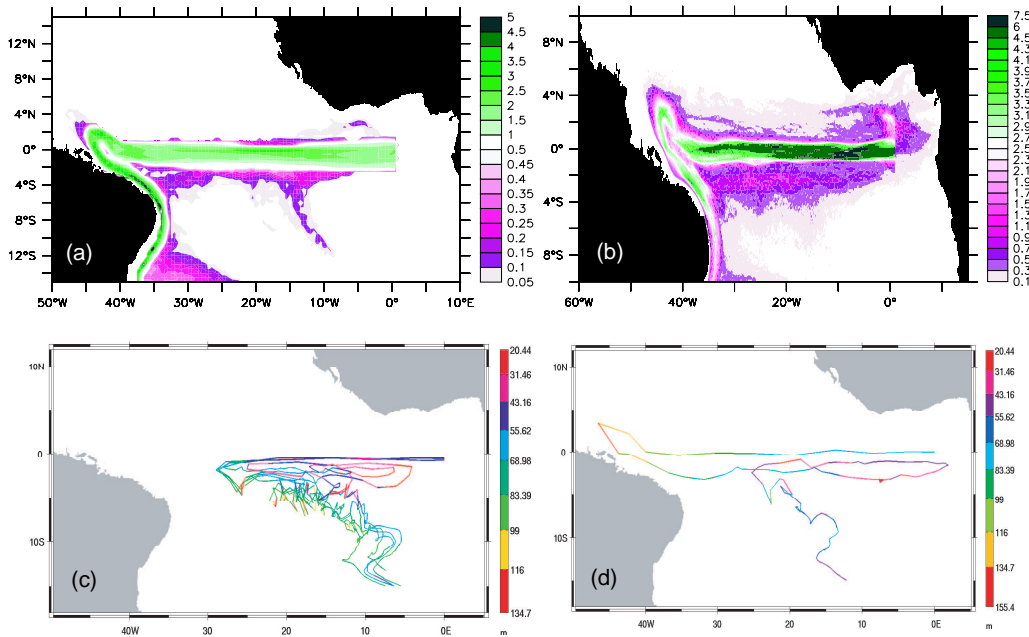
Figure 3.16: Sources of the equatorial undercurrent: a) transport function (in Sv) obtained from a 1/3° (FLAME REF) backward integration started in October, b) transport function (in Sv) from FLAME HIGH-RES also started in October, c) several trajectories from FLAME HIGH-RES illustrating an interior pathway from the subtropics to the tropics in FLAME HIGH-RES, d) trajectory ending up in the EUC showing a typical zig-zag-pathway through the zonal current system. The colorbars in a), c) and d) give the depth of the trajectory.

of the integration (i.e. after 4 model years), giving an indication for the importance of the various EUC sources.

The findings of FLAME REF are also valid for FLAME HIGH-RES (see Fig. 3.16b) with some refinements, especially in regard to the interior pathway. First, the interior supply is weaker (O(0.3Sv) at 5°S) and more shifted to the east than in FLAME REF and second, the trajectories have to join zig-zag-pathways through the SEUC and SEC to get into the EUC (see Fig.3.16c, d): along their equatorward way the trajectories show different meridional excursions and recirculation ellipses along the SEC, then entering the SEUC, getting upward towards the east and between 10°W and 0°W entering the SEC, flowing westward and entering the EUC near 30°W or after a detour along the NBC retroflection. Additionally there is a recirculation cell between 4°S and the equator, mostly west of 10°W (the TC) where about 1 Sv of the water found in the EUC originates from. Thus, the fully resolved SEUC seems to block the direct interior southern pathway found for FLAME REF, but does not prevent it by causing the waters to make a westward detour through the SEC before entering the EUC more westward than indicated by Fig. 3.16a. Additionally, the recirculation between the EUC and SEUC seems to play a role for the EUC.

The Lagrangian analysis clearly emphasizes the negligible contribution of northern hemispheric source waters to the EUC, indicating an even more pronounced hemi-

spheric asymmetry than previous model studies: while JOCHUM & MALANOTTE-
RIZZOLI (2001) and KRÖGER (2001) reveal some float trajectories following zigzag-
pathways from the NEC, via the NECC and nSEC to the equator, the blocking of
such communication by the potential vorticity ridge associated with the northward
shift of the ITCZ in the equatorial Atlantic (MALANOTTE-RIZZOLI et al. (2000))
appears very effective in the present model. The analysis of HAZELEGER et al.
(2003) also indicated subducted waters from the north enter the EUC. In their work
about 1/10 of the EUC transport is made up of northern hemisphere subduction wa-
ters, probably due to differences in the deep MOC and a different vertical structure
of the equatorial undercurrent.

  Thus, in accordance with observational data and other ocean models, the main
source pathway of the Atlantic EUC in FLAME HIGH-RES is along the western
boundary within the NBC, with a vanishing small part of northern and interior
watermasses (only in FLAME HIGH-RES). The differences in the interior pathways
of 1/3°and 1/12°FLAME indicate the interaction between the east- and westward
current bands and their influence on the watermass properties of the EUC.

Fate of the EUC

According to STC theory, the waters transported eastward by the EUC upwell in
the east and are transported back to the subtropics by the surface Ekman flow. One
concern about that is, not all EUC waters upwell in the eastern basin and take part in
the STC. The subsurface waters recirculate and possibly remain in the zonal current
system for several years before entering the EUC again, or reaching the surface and
the subtropics. BLANKE ET AL. (1999) (their Fig.s 5 and 7) show from Lagrangian
analyses of the ORCA2 model a strong zonally elongated recirculation gyre along
the southern flank of the EUC, consisting mainly of upwelled thermocline water.
They find the EUC and SEUC in the eastern basin to be the main recirculation
pathways in the tropics, in accordance with the indications from FLAME HIGH-
RES discussed for the EUC sources in Fig. 3.16b. This result is found to be in
accordance with findings obtained for the tropical Pacific, too.

  Slightly different results were obtained by the analysis of HAZELEGER & DE VRIES
(2004). They traced the EUC watermasses forming the EUC at 20°W in the 1/4°
OCCAM model and found only 1/3 of the particles (in contrast to more than 50%
found by BLANKE ET AL. (1999)) recirculating in the STC and about 2/3 of the
trajectories taking part in the MOC and leave the subtropics to the south after
on average 370 years. They find the shallow recirculation waters confined to the
southern hemisphere, too and the recirculation time scale within the STC to be
less than 10 years without a pronounced peak for any year. As a typical pathway
of recirculating EUC waters they investigated the particles making several zonal
excursions in the near-equatorial region. On average the particles up- and downwell
five times in the tropics and finally get back to the subtropics by surface Ekman
flow. After that the trajectories join the NBC to flow back equatorward.

  The fate and upwelling rates of the EUC waters in FLAME HIGH-RES are illus-
trated in Fig.s 3.17, 3.18 and 3.19. In the figures, the launches from February and
August are chosen because the May/Nov and February/August runs show similar
float distribution patterns. Note, that the figures illustrate the summed transport

of the trajectories during the four years of integration and the distribution patterns
between the seasons differ because of the seasonal varying pathways in the first
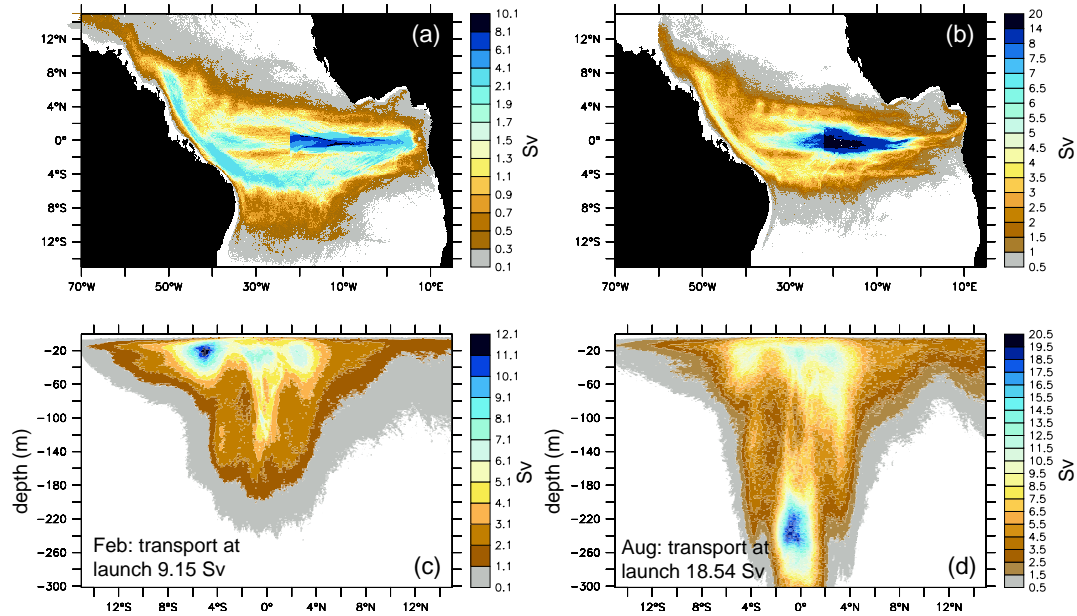months of integration.

Figure 3.17: Distribution of EUC waters at 23°W traced forward in time for 4 years.
The upper figures show the vertical sum of the transport function, the lower figures
illustrate the longitudinally summed floats. Obviously there are strong differences
of the transport distribution on seasonal timescales. For details see text.

Fate of the EUC at 23°W   At 23°W the EUC is a well-defined and strong east-
ward current between 1.5°S and 1.5°N (see Fig. 3.6), transporting 9.15 Sv eastward
in February and about 18.54 Sv in August. Indeed, the transport pathways of the
EUC waters differ significantly. The February launch reveals eastward flow until
about 5°E and a recirculation mainly to the southern hemispheric SEC and a re-
entering of the water into the EUC. This pathway nearly vanished in the August
launch and is replaced by an meridional transfer of waters to both sides of the equa-
tor. A strong EUC in August is visible until about 0°E, where a small part of the
EUC continues northward to the African coast but most of the transport is split-
ted in comparable fractions to north and south of the equator. In accordance with
the findings of Hazeleger & de Vries (2004) and Blanke et al. (1999) the
recirculation mainly occurs near the surface and is much stronger on the southern
hemisphere (see Fig. 3.17c). The retroflection to the northern SEC occurs mainly
between 10°W and 20°W, while the upwelled EUC waters in the east retroflect to
the south.

  The August launch also reveals a strong recirculation of the EUC waters in depths
below 150m: the launched transport below 150m is 6.1 Sv, but the summed trans-
ports in Fig. 3.17d reveal a strong transport of about 18 Sv in this region, indicating
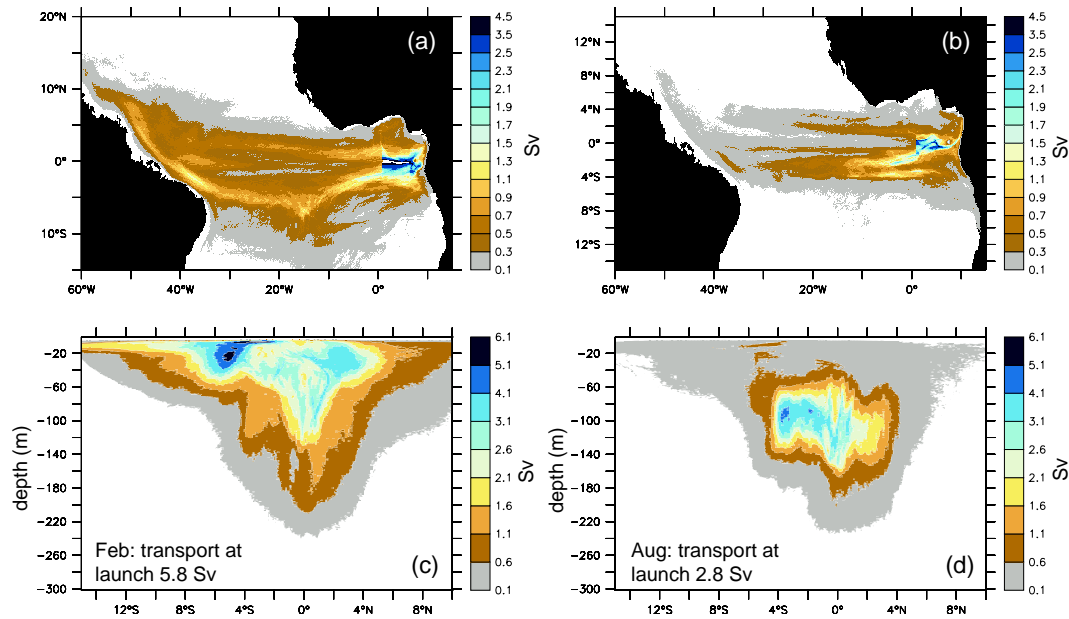
Figure 3.18: Like Fig. 3.17 but for the EUC waters at 0°W.

on average 3 recirculations around 23°W during the 4 years of integration. Additionally, this recirculation is shifted to the southern hemisphere too and seems to be confined to the region between 2°S and 1°N. These waters might correspond to the 2/3 of EUC transport of HAZELEGER & DE VRIES (2004) which take part in the MOC and never upwell in the vicinity of the equator. It might be, that the recirculation is bounded by the off-equatorial undercurrents (NEUC and SEUC) which seem to be fed partly by the EUC too, as the slight maxima of transport along 4°S and 3°N between 100m and 200m in Fig. 3.17d indicate.

In contrast, the February transport shows the strongest recirculation near the surface along 4°S to 6°S and a weaker one between the equator and 2°N to 3°N. Compared to the August run there is also a poleward Ekman transport reaching to about 10°S observable, which feeds partly into the NBC. Also, a larger fraction of recirculated EUC trajectories enter the NBC near the equator and flow northward, reaching the Gulf Stream and leave the subtropics to the north. Some of these trajectories also enter the NECC and the Guinea Dome region.

Also, there is seasonality concerning the EUC upwelling. While about 2/3 of the EUC launch from February takes part in the upwelling, only half of the August trajectories get to the surface layers. As Fig. 3.19 reveals, most of the upward motion occurs in the first year and mainly on the southern hemisphere. Also, the upwelling occurs along the whole EUC at the equator and is not confined to a region eastward of a certain latitude. The February launch shows not only upwelling along the EUC but also a strong upwelling along the westward flowing SEC, i.e. the retroflection to the west occurs below the mixed layer and upwelling occurs on the way westward. The August launch shows some connection of the EUC to the upwelling along Africa: as indicated by the horizontal structure (see Fig. 3.17b) there is a connection to the coastal current regime and part of the EUC upwells in the Gulf of Guinea during
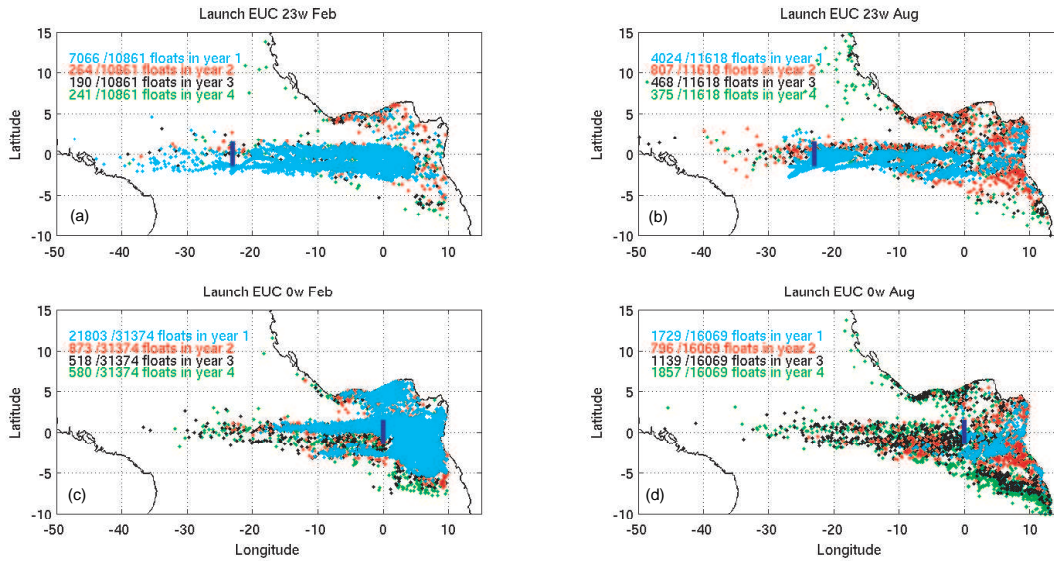
Figure 3.19: Upwelling sites of the EUC launches. The points indicate year and position when the trajectory enters the mixed-layer (0-30m). The EUC mainly upwells on the southern hemisphere and shows a strong seasonally dependent coastal upwelling part.

the 1st and 2nd year of integration. Also, a stronger connection to the southern hemisphere is visible.

Fate of the EUC at 0°W   At 0°W the EUC has already lost much of its eastward transport, partly due to upwelling, partly due to recirculation. The current core has moved to shallower layers and is found above 50m, while the current has almost vanished in depths below 150m. The eastward transport in February is 5.8 Sv, in August only 2.8 Sv are found at this longitude. Compared to the corresponding transports at 23°W, the EUC in August has to recirculate or upwell mostly west of 0°W, while in February a strong recirculation near the surface occurs between 5°E and 10°W, i.e. the fates of the EUC in both February launches should be comparable, while the August ones might differ significantly.

 This is the case indeed, when analyzing Fig. 3.18. The February launch at 0°E reveals nearly the same pathways than the 23°W launch although with diminished amplitudes: near 5°E the EUC recirculates largely to the southern hemisphere and a weak recirculation to the northern hemisphere is visible too. The trajectories entering the southern SEC flow westward to join the NBC and re-enter the EUC or flow northward along the NBC. The vertical structure of the February launch points out similar transport maxima in the upper 100m. In contrast to the 23°W launch, most of the trajectories of the EUC at 0°W upwell in the whole eastern basin, not only along the equator (see 3.19). The upwelling reaches as far north and south as 5°N/S during the first year of integration. The August launch shows interesting behavior: while some transports enters the coastal current system along Africa, the

bulk of trajectories retroflects southward, joins the westward SEC and enters the
upper branch of the SEUC between 30°W and 10°W.

This transport occurs in layers between 60m and 180m depth. In contrast to
the February launch, where 4/5 of the EUC upwell, the August launch shows an
upwelling of only 1/3 of the original launch. Interestingly, the upwelling does not
occur along the eastward path of the EUC, but mainly along the SEC, north of
the Angola Dome and along the African coastline (see Fig. 3.19c,d). The upwelling
east of 0°W is reduced significantly due to the southward excursions of the EUC
in August and the trajectories do not reach the surface layers as indicated by the
vertical structure of the August launch (Fig. 3.18d). The upwelling maximum of this
launch occurs after 4 years. Thus, at least seasonally, the EUC is connected to other
zonal currents and thus might influences the watermasses within these currents.
This aspect will be investigated in more detail when analyzing next the sources and
fates of the northern and southern off-equatorial undercurrent, i.e. the NEUC and
SEUC.

3.4.2   North and South Equatorial Undercurrent

Source Waters from annual means

NEUC   From an Eulerian view like Fig. 3.3 it is difficult to see, what watermasses
enter the NEUC and which pathways they take. This will be discussed further in this
section. For Lagrangian analysis of the NEUC sources and sinks the launch of the
floats is done at 23°W, where the NEUC is clearly separated from the western bound-
ary regime and not too far in the east where part of the NEUC enters seasonally
dependent the Gulf of Guinea (ELMOUSSAOUI ET AL. (2005)). Several experiments
were performed to rule out the effects of seasonality and tropical instability waves
on the pathways.

The sources of the annual mean NEUC are shown in Fig. 3.20. Here, the trajectory
integration was done using a repeated annual mean. Thus, all seasonal effects like
waves should be averaged out. However, this does not seem to be the case when
looking in more detail on the figure. The pathway of most of the trajectories is
influenced by eddy-or wave-activity connecting the NEUC directly to the western
boundary current, to the northern edge of the EUC and to the NBC retroflection
between 4°N and 14°N, where some trajectories belong to a NBC ring. Thus, the
eddy or wave activity in the Tropical Atlantic seems to be still a dominant signal
when excluding the annual cycle, i.e. the eddy activity has some influence on the
interannual variability especially in regions where the mean flow is weak.

Figure 3.20 shows two main pathways of the NEUC waters: one which is fed by
the NBC (≈1.5 of 2.3 Sv, value obtained at 5°S in the NBC) and another pathway
(≈ 0.8 of 2.3 Sv, values obtained at 35°W in the EUC) transferring waters from the
(deep) northern edge of the EUC westward through the nSEC and then discharging
into the NEUC. At least, most of the water originating from the EUC comes from
the NBC (see discussion of EUC-sources). So, a northern hemispheric source for
the NEUC is missing and the eastward current is made up of NBC water or even
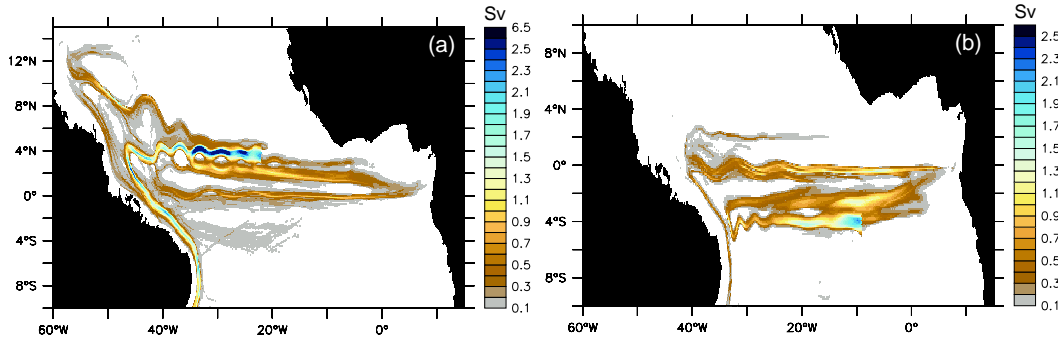recirculated NBC water.

Figure 3.20: Transport pathways into the NEUC at 23°W (a) and SEUC at 10 °W (b) obtained from Lagrangian analysis using the annual mean of the velocity field. Clearly visible are complicated interactions between the different east-west currents and the strong influence of wave processes, which were a the dominating signal in some regions and aliased in this figure by using the annual mean. The mean transport values for the NEUC at 23°W and the SEUC at 10°W are: 2.3 Sv (NEUC) and 1.7 Sv (SEUC).

SEUC As indicated by observations (SCHOTT ET AL. (1998), BOURLES ET AL. (2002)) and by Fig.s 3.3 and 3.8 the SEUC is found to occur as a jet-like current in mid-basin around 25°W most of the year. There are some observations of the SEUC at 35°W, too, but the weakly developed eastward current found near 3°S might be related to the southward retroflection of the NBC. However, the current strengthens remarkably some degrees off the western boundary. This already indicates a significant inflow of SEC waters into the SEUC.

From the model figures, there is no direct and obvious pathway of the watermasses entering into this undercurrent. A first Lagrangian analysis with annual mean velocity data is given in Fig. 3.20. It shows the SEUC at 10°W is consisting mainly of EUC and sSEC water, with almost no direct inflow from the western boundary current. West of about 25°W the SEUC shows strong overlaid wave activity, i.e. if there is direct inflow from the NBC this is connected to waves transferring the trajectories eastward by influencing the density stratification in this region.

The trajectories coming from the EUC show two ways to enter the SEUC at 10°W: initially, all pathways reaching to the SEUC originate from the EUC west of 5°E, then retroflect into the westward flowing sSEC and get introduced into the SEUC directly by a meridional shift between 15°W and 0°W (about 0.9 of 1.7 Sv, value obtained at 10°W in the sSEC) or by flowing westward within the sSEC and entering the SEUC near the western boundary (0.6 of 1.7 Sv, value obtained at 35°W in the sSEC). Some trajectories indicate also a connection of the SEUC watermasses to the waters of the nSEC which was shown to be connected to the NEUC, i.e. there is interaction between all equatorial zonal current bands.

Anyway, a mechanism transferring the waters from one band to another one is needed to fully understand these interactions. The equatorial waves discussed in the last section might be the key mechanism in supporting the meridional transfer between the currents. For gaining insight into that and to overcome the obvious

wave aliasing effects visible in the regions where mean flow is weak, from now on daily velocity fields (one repeating year) and monthly averaged fields, to average out the main TIW signal, are used for the calculation of the trajectories.

Role of the Annual Cycle

To study the influence of the annual cycle of the off-equatorial undercurrents float launches in different seasons were realized. This is done by starting the trajectory calculation at 15th of February, 15th of May, 15th of August and 15th of November. Sensitivity calculations with initializations at the first and last day of these months do not show strong differences between launches at the beginning or end of a month with exception of August, where the TIWs cause strong seasonal variability on the currents. The effect of the waves will be discussed in a separately chapter. However, these experiments help to gain insight into how the inflow conditions into the off-equatorial undercurrents might change within one annual cycle.

NEUC   The results of the different trajectory calculations for the NEUC water masses at 23°W are given in Fig. 3.21. Strong seasonal differences are visible: while the November-NEUC is mainly made of recirculating SEC water, in spring the NEUC waters consist partly (2.25 of 5.21 Sv at 2°S) of directly introduced NBC waters. In February and August this direct connection is missing as in November and the NEUC is made up of NBC water getting introduced in the deep northern EUC, flow eastward until reaching 10°W- 0°W, after that penetrating westward again and enter the NEUC between near the NBC retroflection at about 35°W (August) or in a broader longitudinal range between 35°W and 20°W (February).

  The way along the northern flank of the EUC and the nSEC is followed by about 1/3 of the floats launched in February, about half of the launch from May and November and by about 2/3 of the August NEUC launch (exact numbers at 35°W see table 3.1). It is also interesting to note that all launches show a recirculation of floats (recognizable by the transports exceeding the launch transport) not further than 20° longitude westward of the launch position. This indicates that these trajectories are affected by waves in the region westward of 23°W and thus perform cyclic or elliptical orbits around their initial position. In most cases the waves lead to the spin-off of eddies along its westward path. These propage westward with a differing meridional components. This eddy transport is found to be responsible for the wave-induced transfer between the several zonal currents as visible in Fig. 3.15 and discussed in section 3.3.2.

  Thus, the direct inflow from the western boundary is not needed to maintain the NEUC, but clearly contributes to the higher transports of the NEUC during the first half of the year. Additionally, a large part of the NEUC waters recirculates between the different zonal current bands during the 4 years of the integration. The fraction of NBC water (south of 5°S) younger than 4 years entering the NEUC is also seasonal dependent and ranges from about one third (Aug, Nov) to one fourth (Feb, May) of the total NEUC transport.

SEUC   The pathways of watermasses into the SEUC have been found to be a complicated zig-zag through the zonal current system in the analysis of the annual
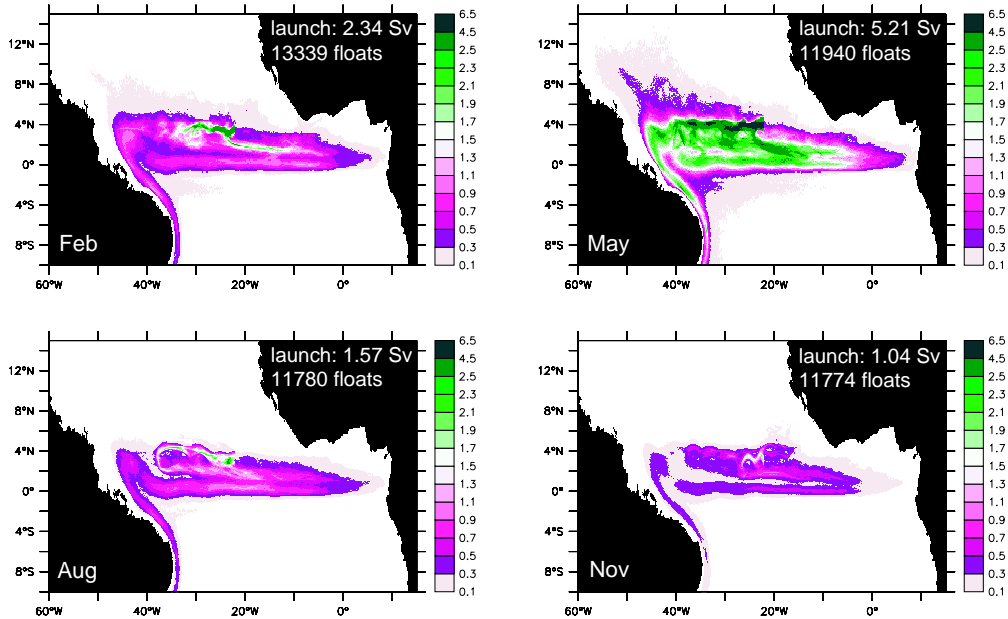
Figure 3.21: Source waters of the NEUC at 23°W obtained from 4-year backward integration. The figures show the vertically summed transport function at every grid point for launches in different seasons. The strong seasonality and a decoupling of the NEUC during the second half of the year is obvious.

mean. This view can be confirmed for seasonal timescales too. Fig. 3.22 reveals the complicated path of the SEUC waters through EUC and sSEC to be present all in months.

A direct connection and inflow from the western boundary is not recognizable. Instead, a strong part of the SEUC in all seasons is recirculating between 20°W and 10°W, indicating similar to the NEUC that wave or eddy activity is the only major flow component in this area. Between 60 and 75 % of the SEUC launch can be traced back to the EUC at 10°W, while the strongest fraction is shifted southward from the EUC in August (for exact values see Tab. 3.2). Only about one third (Feb) to one fourth (May-Nov) of the SEUC is formed by NBC water which is younger than 4 years. This water almost exclusively has made its way through the southern flank of the EUC, got shifted to the sSEC between 10°W and 0°W and after that got shifted a second time to the SEUC in the vicinity of 30°W to 25°W. The more westward inflow can be found during Nov-Feb, a more eastern inflow in the months May and August. This corresponds quite well with the findings from the Eulerian analysis from Fig. 3.8. Thus, the SEUC is found to be formed in the interior of the basin and is strongly related to the interaction between the different zonal current bands. The eastward transport of the SEUC should be sensitive to changes in the intensity or frequency of the wave processes in this region, too.

launched	EUC 35°W	NBC 0°S	NBC 5°S	total
Feb	0.82	1.02	0.66	2.34
May	2.48	2.21	1.49	5.21
Aug	0.95	0.62	0.5	1.57
Nov	0.5	0.46	0.32	1.04
without TIWs				
Feb	0.45	1.04	0.92	2.04
May	1.85	2.26	1.79	4.11
Aug	0.25	2.03	1.42	1.72
Nov	0.4	0.43	0.43	0.91

Table 3.1: Contribution to the NEUC obtained by 4-year backward integrations of particles launched in four different months at 23°W. The transport values were obtained by the vertically summed transport function values at the 35°W, 0°N and 5°S sections.

launched	EUC 35°W	EUC 10°W	NBC 5°S	total
Feb	0.97	1.37	0.77	2.4
May	0.85	1.11	0.47	1.57
Aug	0.75	0.98	0.43	1.34
Nov	1.02	1.39	0.61	2.31
without TIWs				
Feb	0.47	0.7	0.39	2.25
May	0.52	0.8	0.37	1.37
Aug	0.69	1.25	0.38	1.2
Nov	0.77	1.39	0.47	2.39

Table 3.2: Contribution to the SEUC obtained by 4-year backward integrations of particles launched in four different months at 10°W. The transport values were obtained by the vertically summed transport function values at the 35°W, 10°W and 5°S sections.
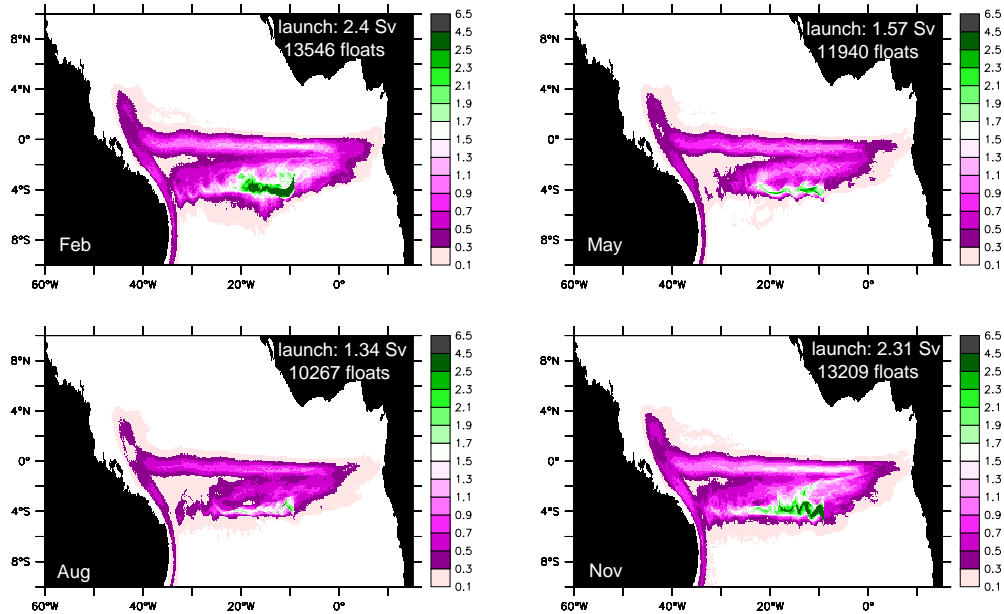
Figure 3.22: Source waters of the SEUC at 10°W obtained from 4-year backward integration. The figures show the vertically summed transport function at every grid point for launches in different seasons. All four pictures reveal a missing direct connection between the SEUC and the western boundary current and the major pathway of watermasses through meridional shift from one zonal current to the next (from EUC to sSEC to SEUC).

Role of the TIWs

The analysis of the seasonally launched floats revealed a strong influence of the tropical instability waves on the mean pathways of the SEUC and NEUC source water masses. To investigate the effect of the TIWs more precisely, experiments with monthly mean velocity fields were performed in which the waves should be nearly averaged out. The results are shown in Fig. 3.23 and 3.24 and the transport values can be found in Tab. 3.1 and 3.2. The effect of the waves is slightly different for the northern and the southern undercurrent and thus will be discussed separately.

NEUC Due to the strongest occurrence of the TIWs in boreal summer the biggest effect of them should be visible in the August launch. This is indeed the case when comparing the daily and monthly forced experiments. The (nearly complete) elimination of the instability waves favors the inflow of NBC waters into the NEUC and almost excludes the pathway from the northern EUC flank into the undercurrent. As a consequence, a higher percentage of the southern hemisphere waters from the boundary current can be found in the NEUC (for Aug 1.42 of 1.72 Sv, i.e. 83% of the trajectories) and the waters transported eastward should be less mixed.

  However, this possible change in watermass properties can not be verified from the Lagrangian analysis because salinity and temperature data are prescribed by the

model output. In the other seasons the NEUC from the monthly mean run contains also a fraction of EUC waters which are transported there likely by the aliased wave processes or simply the meridional migration and reversal of the zonal currents in the monthly mean runs. But all months show an increased transport of NBC waters when comparing to the experiments resolving the instability waves. Thus, the conclusion can be drawn that tropical instability waves decouple the NEUC seasonally from a direct western boundary current inflow and shift a large fraction of the waters between the various zonal current bands. This causes the zig-zag pathways through EUC and nSEC visible independently in nearly all backward integration NEUC launches.
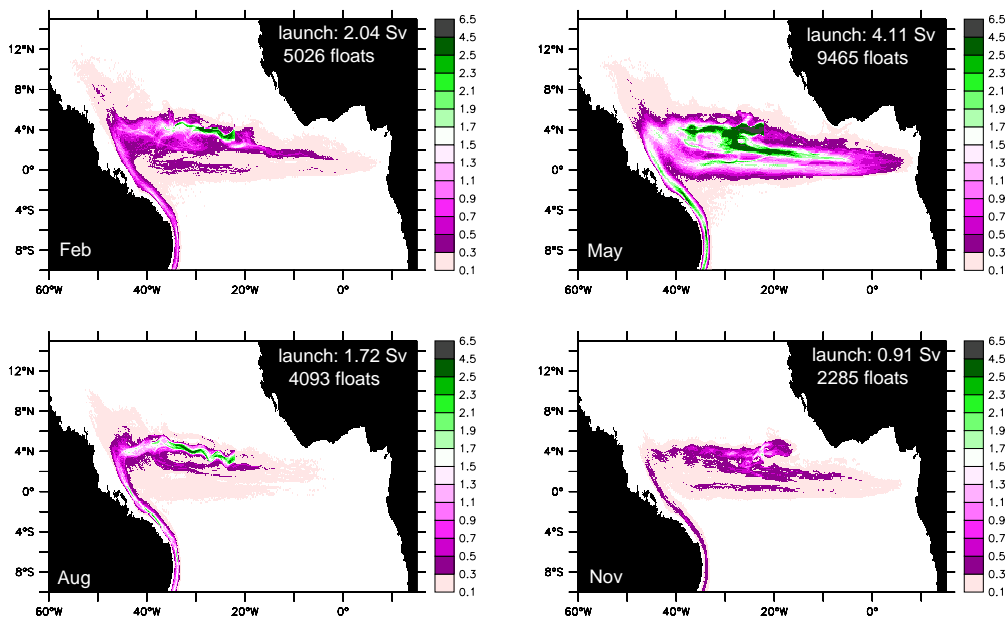

Figure 3.23: Like Fig. 3.21 but using monthly averaged velocity fields to integrate the trajectories. This almost totally excludes the instability wave processes. Without the waves the NEUC at 23°W is maintained by direct inflow from the western boundary all year. The zig-zag pathway through the zonal current system, clearly visible in Fig. 3.21 is heavily reduced.

SEUC   The missing meridional transfer associated with the wave processes should have strong impact on the sources of the SEUC. As the southern undercurrent never showed a link to the western boundary this has to lead to a breakdown of the sources of the SEUC and in consequence to a breakdown of the SEUC (which can not occur in the current model simulations because the velocities were prescribed). Figure 3.24 confirms this hypothesis by showing only weak connections to the deep southern EUC and even smaller transports originating from the NBC. Strongest differences can be found in February (i.e. the southern hemispheric summer, when a second TIW phase happens which is weaker than in boreal summer). But all

seasons show a reduced inflow from the EUC and much more recirculation near the launch positions than the corresponding runs with explicitly resolved waves. Also the connection pathways are strongly blurred. So the conclusion here is that the sources of the SEUC depend strongly on strength of interaction between the current bands due to the missing linkage to the direct western boundary inflow.
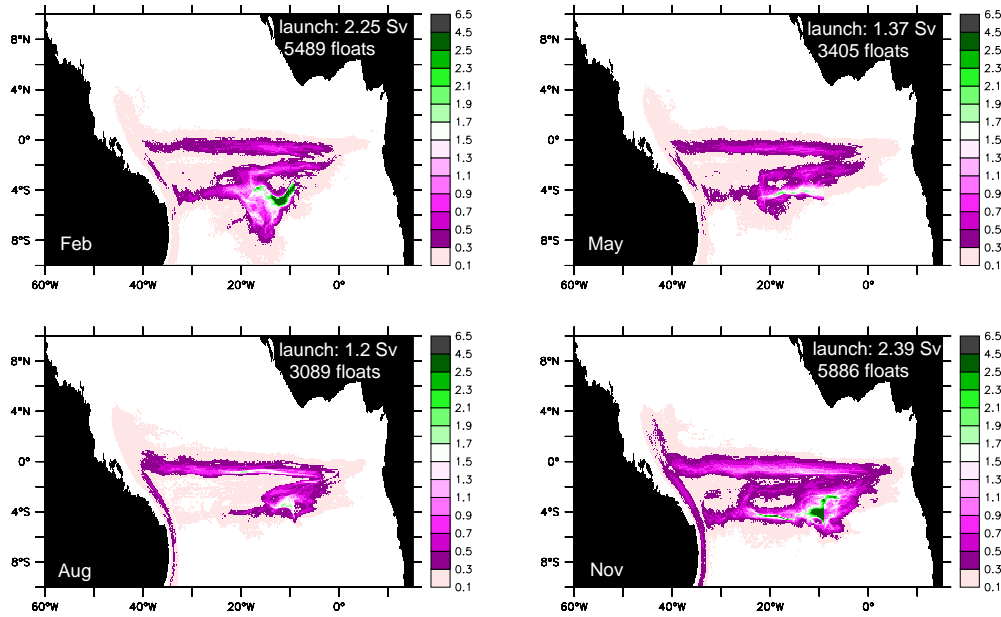

Figure 3.24: Like Fig. 3.22 but using monthly averaged velocity fields to integrate the trajectories. This almost totally excludes the instability wave processes. Without the waves the SEUC pathways are blurred very much and show a weakened connection to the EUC which is the source for the SEUC at 10°W.

Fate and connections to upwelling regions

In the last sections the source waters and pathways that maintain the system of eastward undercurrents in the Tropical Atlantic were described. But it is also interesting to see what the "fate" of these undercurrents is, particularly in the context of how they are connected to the upwelling regions near the eastern boundary and to the doming circulations. Such a direct connection has been stated mainly for the northern hemispheric dome (the Guinea Dome, VOITURIEZ (1981), SIEDLER ET AL. (1992), YAMAGATA & IIZUKA (1995)) and much less investigations were carried out for the southern hemisphere in the Angola Dome region (MERCIER ET AL. (2003), YAMAGATA & IIZUKA (1995), DOI ET AL. (2006)). But, observational data in the equatorial eastern basins are sparse, so most analysis concerning the source waters for the eastern circulations base on model results.

NEUC   Figure 3.25 gives results from the forward-in-time integrations of the NEUC 23°W launch. It is obvious that there are strong differences in the dispersion of the

trajectories after 4 years. While the launch in May shows a widespread pattern of
the trajectories, the November floats are confined to a well-defined region between
8°N and the equator. A particular pathway of the floats is visible just as little as a
strong connection to the Guinea Dome upwelling. The distinction of the "trajectory
patches" in the different months is related to wave induced eddy activity and in
particular the westward recirculation into the nSEC and the EUC vanishes when
the TIWs are averaged out from the velocity fields.

Thus, most of the floats drift to the north-east and reach the coastal upwelling
north of 5°N. From the May launch some floats enter the Gulf of Guinea and upwell
there. However, most trajectories (about 3/4 of the launched floats) recirculate more
than 4 years between the equator and 10°N and never end up in the upwelling. The
consequence of this behavior in the real-world ocean are the low oxygen contents of
the watermasses in the off-equatorial undercurrents which were visible in Fig. 3.2b.
It also fits to the even lower oxygen values in the doming regions. That implies if the
trajectories would not be subject to the meridional transport due to the subseasonal
variability, the watermasses in the undercurrents and the coastal upwelling regions
would be more oxygenated.

The part of NEUC water feeding the coastal and equatorial upwelling is shown in
Fig. 3.26. It reveals the seasonal dependence of the upwelling into the mixed layer
(0-30m) as well as the locations and timescale to be introduced into this layer. The
launches from February to August show the strongest connections to the equatorial
upwelling regions and enter the surface layers during the first year. In November
nearly no interactions between the zonal current bands exist and therefore a vanish-
ing fraction of the inserted floats reaches the equatorial upwelling. After the second
year the floats have reached the eastern boundary and partly upwell in this time
span. The bulk of upwelling north of 5°N occurs during year 3 and 4 of the integra-
tion. Especially, only some of the trajectories off the coast reach the Guinea Dome
region during year 4. The strong annual cycle of this upwelling is obvious: from
the February launch about 40% get upwelled during the four years, while from the
November run less than 10% were introduced into the mixed layer (exact values see
Tab. 3.3). In time-mean about 25% of the launch is transferred into the upper 30m.
It is interesting to note, that the mid- to eastern basin NEUC does only show a weak
connection to the Guinea Dome region. As indicated by the analysis of STRAMMA
ET AL. (2005a) the Dome is connected to the western part (mainly west of 20°W)
of the NEUC. This point will be discussed in more detail in the description of the
sources of the Guinea Dome in the next section.

Although, a large part of the NEUC water does not take part in upwelling. Also it
is obvious from Fig. 3.8 that the NEUC vanishes near 10°W. So, the waters trans-
ported eastward by the current have to move vertically or to recirculate meridionally.
The recirculation pathways were already discussed for Fig. 3.25 but this view does
not allow for evidence for any vertical or diapycnal motion. Thus, this picture is
supplemented by Fig. 3.27.

The figure shows the density distribution of the floats at launch and after 4 years
forward integration, i.e. diapycnal processes associated with upwelling or down-
welling are easy to detect. The main transports of the NEUC is in the density range
σ_θ=26.2-26.8 kg/m^3 for all launches, higher or lower density classes show a much
lower transport.

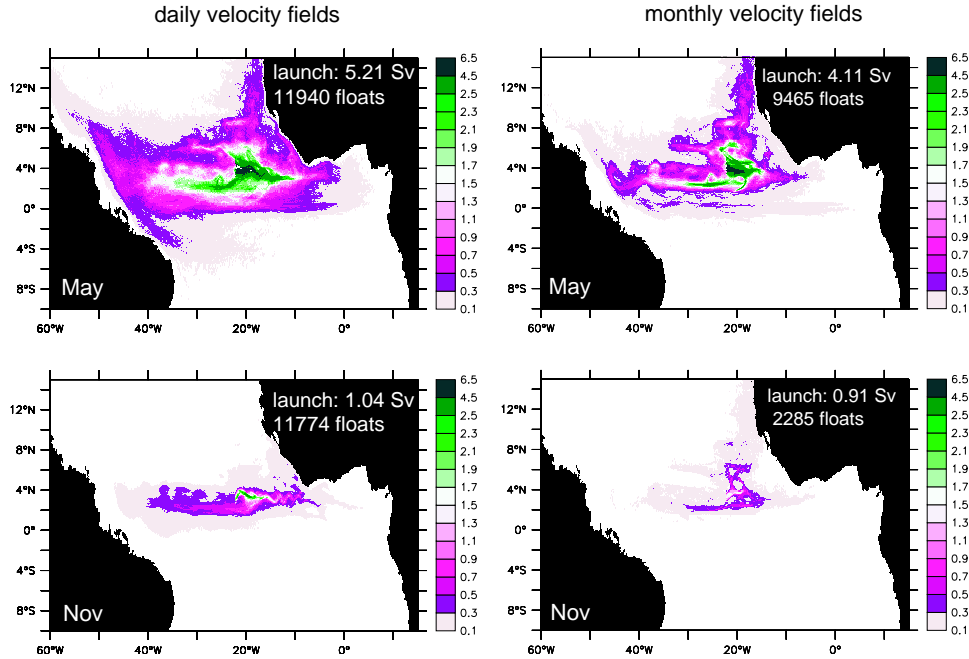Figure 3.25: Fate of the NEUC for May and November launches at 23°W. Left panel: pathways including wave effects, right panel: pathways using monthly mean velocity data. Obviously, the waves cause the recirculation inside the zonal current system and thus helps to minimize the export of NEUC waters to the off-equatorial upwelling regions.

After four years all launches also show a conversion of denser waters to less denser ones: in all runs, the transport in the lowest σ_θ-layer is significantly increased (black bars) to about one third or fourth of the total transport. Interestingly, in the range σ_θ=25.5-26.4 kg/m^3 no strong variations occur during the four years of integration, hence the upwelling seems to originate from the waters in the density classes below, i.e. from σ_θ=26.2-26.6 kg/m^3 (cyan and blue bars). Also, all experiments show an increase of waters below σ_θ=26.8 kg/m^3 (magenta) which is fed mostly by the σ_θ=26.4-26.8 kg/m^3 waters, thus by downwelling processes. The transformation between the density classes does not seem to be influenced quite strong by the seasonal cycle, even if the differences in the density classes show such a behavior: at the end of an 4-year time range the amount of σ_θ=26.4-26.6 kg/m^3-water has been reduced to the half and has been introduced mainly into lower and to a small part also into higher density classes.

Consequently, the effect of the multiple recirculation of the trajectories in the tropical current system leads to a transformation of the southern hemispheric waters to lower densities by gradually upwelling.

SEUC In the discussion of Fig. 3.8 the SEUC was found to end up between 0°W and 5°E. The question now is, on which pathways the waters from the SEUC continue. This is illustrated by Fig. 3.28 for the launches in February and August.
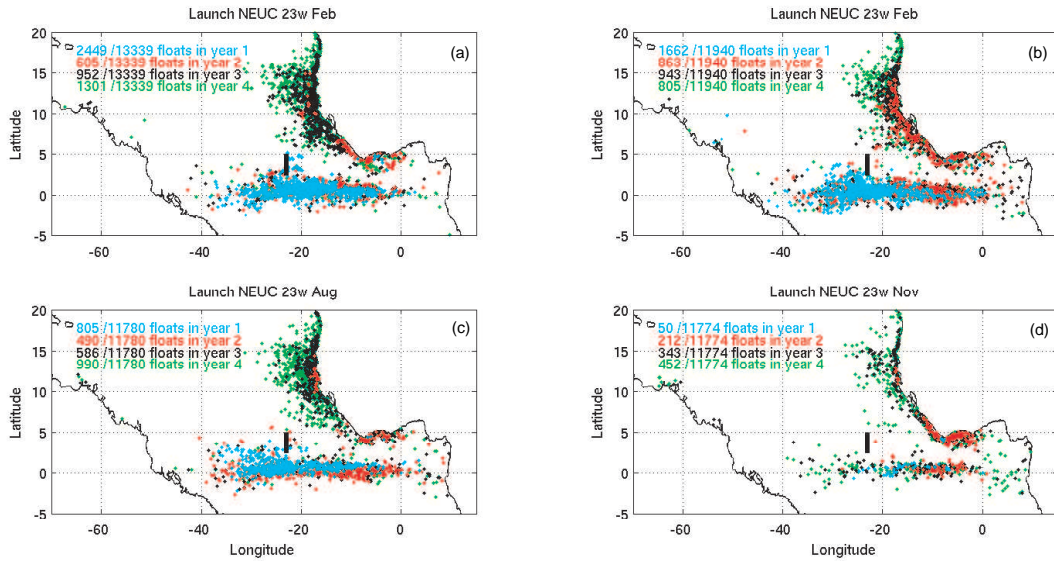
Figure 3.26: Upwelling sites of the NEUC 23°W launches. The points indicate the positions and year where the trajectory enters the mixed layer (defined as 0-30m). The results show trajectories upwell along the equator within 1 year time mostly or along the African coast after 3 to 4 years. The upwelling off the coast occurs mainly during year 4 and is small compared to the coastal upwelling.

Similar to the NEUCs fate, about half of the SEUC launch recirculates into the sSEC and EUC due to wave processes while the remainder is distributed into direction of the Angola dome without showing a prevailing pathway. Excluding the waves leads to a preferred southward export of the SEUC waters.

The upwelling of the SEUC transport in the east is small and ranges between 20% (February) and 10% (August) of the SEUC at 10°W. In contrast to findings for the NEUC, the upwelling is nearly totally confined to the region south of 3°S and has vanishing values along the southern flank of the EUC (see Fig. 3.29). Interestingly, the upwelling latitude shows a linear relationship to the time span in which the trajectory is introduced into the mixed layer: this indicates a weak, but continuous south-eastward current that might forms the inflow into the Angola Dome. Such an interior eastward current has not been observed yet. But as indicated from the depth of the σ_θ=26.5 kg/m^3 isopycnal (see Fig. 3.4), the Angola Dome and the corresponding gyre circulation is badly represented in the model. Thus, the sources of the Angola Dome and its corresponding upwelling can not be trusted in too much detail. However, the fate of the SEUC will be described further, because the current might be independent of the right position of the Angola Dome. As visible from Fig. 3.29 the upwelling rate along the southeastward extension of the SEUC is nearly constant during the 4 years of integration which is contrasting the clear 3 to 4 year time span of the NEUC waters to get upwelled in off-equatorial regions.

Similar to the results shown for the NEUC the largest part of the SEUC water does not upwell in the time span of the four years of integration. Fig. 3.27 shows the
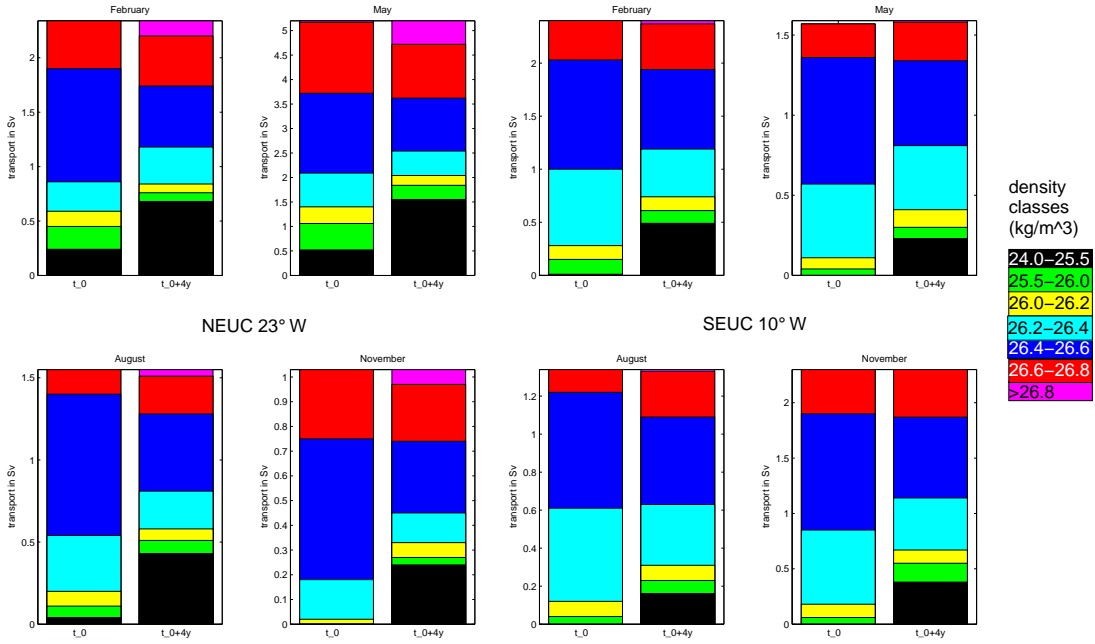
Figure 3.27: Transports splitted into density classes at launch and after 4 years forward integration. Left: transports of the NEUC launches, right: transports for the SEUC launches.

NEUC	total	equator	coast	SEUC	total	equator	>3°S
Feb	0.93	0.53	0.4		0.48	0.13	0.35
May	1.87	1.23	0.64		0.2	0.03	0.17
Aug	0.38	0.19	0.19		0.16	0.02	0.14
Nov	0.08	0.03	0.05		0.39	0.06	0.33

Table 3.3: NEUC and SEUC upwelling in Sv. Values give the summed transport of the trajectories entering the 0-30m layer.

distribution of the float trajectories into density classes analogous to the NEUC. The SEUC is also mainly formed by waters of the density classes between σ_θ=26.2 and 26.8 kg/m^3 but with a higher percentage of waters in the density class σ_θ=26.2 to 26.4 kg/m^3 and only 10-15% of waters above σ_θ=26.2 kg/m^3. Similar to what was found for the NEUC, after 4 years a noteable part of the dense waters has upwelled into the range σ_θ=24.0 to 25.5 kg/m^3. However, the total upward transport is of lesser amplitude for the SEUC. A downwelling of the SEUC waters is less obvious than for the NEUC.

A general impression when comparing NEUC and SEUC contributions in Fig. 3.27 is, that the southern current shows a more homogeneous distribution of waters in the different density classes: after the 4 years of trajectory calculation more than 2/3 of the trajectories belong to only 3 density classes and most trajectories do not
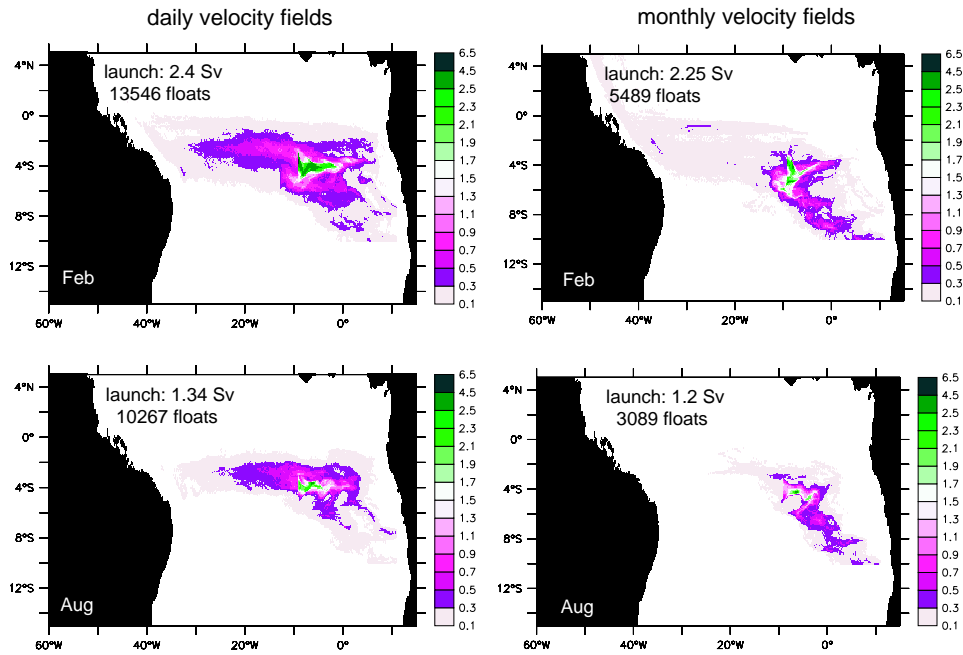
daily velocity fields   monthly velocity fields

Figure 3.28: Fate of the SEUC for February and August launches at 10°W. Left panel: pathways including wave effects, right panel: pathways using monthly mean velocity data. A clear pathway to the south is not recognizable. The effect of waves is the same as described for the NEUC.

show strong diapycnal movements during their way. The weak upwelling is fed by the density layers σ_θ=26.2 to 26.6 kg/m^3.

The slowly varying properties of the SEUC underline the finding, that the SEUC is not fed directly by the western boundary system but is a result of the well mixed waters from different zonal current bands. The small upwelling rates and the strong subseasonal eddy-variability associated with the tropical instability waves cause a larger part of recirculating waters on the southern hemisphere.

3.4.3   Doming circulations

Both, the NEUC and the SEUC showed weak connections to the upwelling regions off the equator. But, as deduced from the Lagrangian analysis in the last sections, it is not clear if they provide all the waters upwelling along the doming circulations. Thus, there might exist other pathways reaching into that regions. In this section the pathways of watermasses reaching the Guinea Dome will be studied, the Angola Gyre is omitted because of its poor representation in the model. The total upwelling rates along the both doming circulations will be discussed and related to estimates from Ekman divergence and other model results.
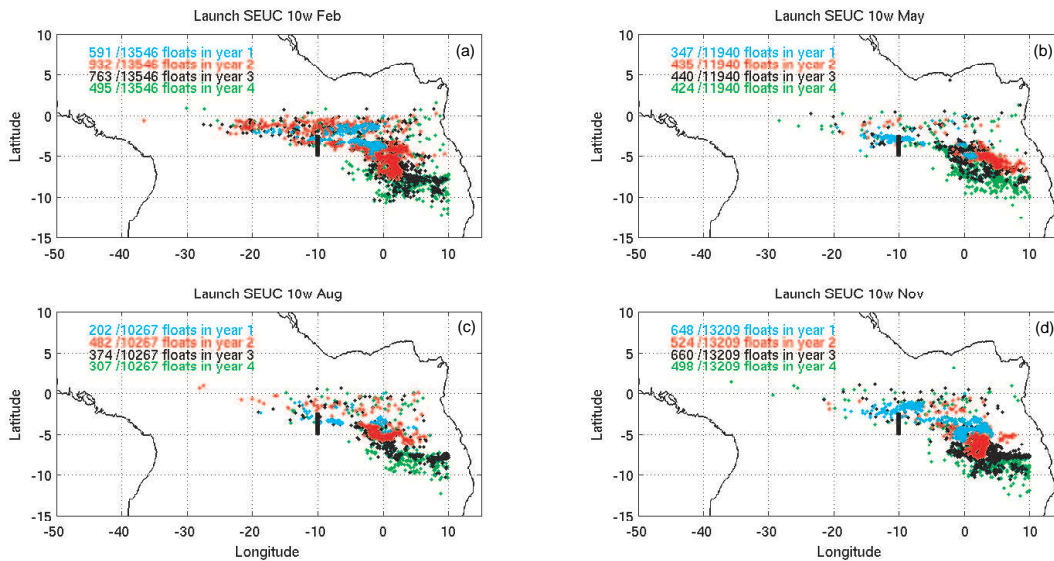
Figure 3.29: Upwelling sites of the SEUC. The points indicate the positions and year where the trajectory enters the mixed layer (defined as 0-30m). The results show trajectories upwell mainly south of 3°S and not along the equator as found for the NEUC.

Guinea Dome

As visible in Fig. 3.4 and described by SIEDLER ET AL. (1992) the Guinea Dome appears as a top along the zonal ridge of high density waters between 10°N and 20°N. The zonal ridge is formed by the Ekman divergence related to the ITCZ (ZHANG ET AL. (2003)) which leads to a strong stratification of the waters in this region. This creates a (potential vorticity) barrier for water masses from the south to flow further northward. Thus, the ridge visible in Fig. 3.4 separates the central water masses from the northern and southern hemisphere, forming the Cape Verde front.

The Guinea Dome was shown to exist throughout the year both in subthermocline and thermocline layers (SIEDLER ET AL. (1992)) and corresponds to a cyclonic geostrophic flow of typically order 5 cm/s. The doming shows seasonal variability and reaches to the surface in boreal summer. The vertical structure of the dome shows an inclination of 10m/(degree longitude) of the dome axis to the west with increasing depth (SIEDLER ET AL. (1992), see also Fig. 3.32).

STRAMMA ET AL. (2005a) showed the connection of the Guinea Dome to the eastward flows of the NECC, NEUC and EUC by the trajectory of an APEX float deployed at the equator at 35°W at 200m as well as by trajectory analysis of FLAME HIGH-RES. They find complicated recirculation pathways through the zonal current bands (as discussed for the sources of the off-equatorial undercurrents) and a trapping of the APEX float trajectory in the Guinea Dome region for more than 3 years. The investigation of the origins of the Guinea Dome waters at 13°N revealed a connection to the NECC/NEUC regime which is fed by the NBC. They found the seasonally existing northward branch of the NECC seems to be fed by shifted waters

from the NEUC between 22°W and 32°W which is therefore suspected to feed the western part of the Guinea Dome. The possible mechanism determining the shift is again related to the TIWs as indicated by the westward detour of the observed trajectory as well as by the model floats which are mainly shifted northward in boreal summer.

Sources of the Guinea Dome According to the results of STRAMMA ET AL. (2005a) the watermasses of the Guinea Dome have to depend strongly on the strength of the northward shift of southern hemispheric waters through the various zonal current bands. If one of the currents is abnormally weak, or in extreme cases absent, the contribution of the southern currents has to decrease or vanish too. The same effect is possible to occur if wave activity is different from year to year. It is not obvious if this influences the Guinea Dome remarkably because the currents are that weak in this region and the trapping of waters in this region is found to occur for more than 3 years. However, the Guinea Dome maybe has also northern hemispheric sources as discussed by STRAMMA ET AL. (2005b). These waters can be carried eastward by the upper NECC.

The overriding importance of the NEUC for the waters found in the Guinea Dome is evident when comparing the Lagrangian trajectories from FLAME HIGH-RES and the correspondent 1/3° run from FLAME REF (see Fig. 3.30). As shown in Fig. 3.5 FLAME REF does not resolve the NEUC but only the NECC. This allows for a conclusion of the role of the NEUC in transferring waters to the Guinea Dome.

Both trajectory launches start at 13°N, 20°-25°W in depths between 50 and 150m and were tracked backward for four years. While FLAME HIGH-RES shows meandering pathways from the NECC to the NEUC which is fed mainly by the NBC, the FLAME REF gives a straight connection to the NECC which is made up mostly of NEC water with an admixture of NBC waters (which form the deepest parts of the NECC in this model). Thus, the southern hemispheric waters carried eastward by the NEUC seem to play an important role for maintaining the density ridge shown in Fig. 3.4 especially in the western tropical Atlantic where the inflow from the NBC into the NEUC/NECC occurs. If more southern hemispheric water flows into the eastward current system this strengthens the density ridge towards the boundary and blocks the inflow of northern waters.

The influence of the different zonal currents on the sources of the Guinea Dome is also visible when tracking back trajectories from the Dome launched in different seasons (see Fig. 3.31). While the launches in boreal summer and fall show strong connections to eastward NEUC and NECC the pathways during rest of the year remain much more blurred. Interestingly, the November launch of the Guinea Dome shows some connection of the waters across the Cape Verde front to the northern hemisphere (between 40°W and 30°W north of 12°N), a similar behavior can be found for the August launch, although weaker. This inflow is on the order of 0.1 of totally 5.33 (Aug)/4.08 (Nov) Sv and hence of minor importance for the watermass characteristics of the Guinea Dome.

All launches reveal 1.5 Sv to 2 Sv of NEUC waters from which 0.5Sv to 1Sv originate directly from the NBC. However, even in the launches where the eastward currents are detectable as maxima in the trajectory concentration, there are no dis-
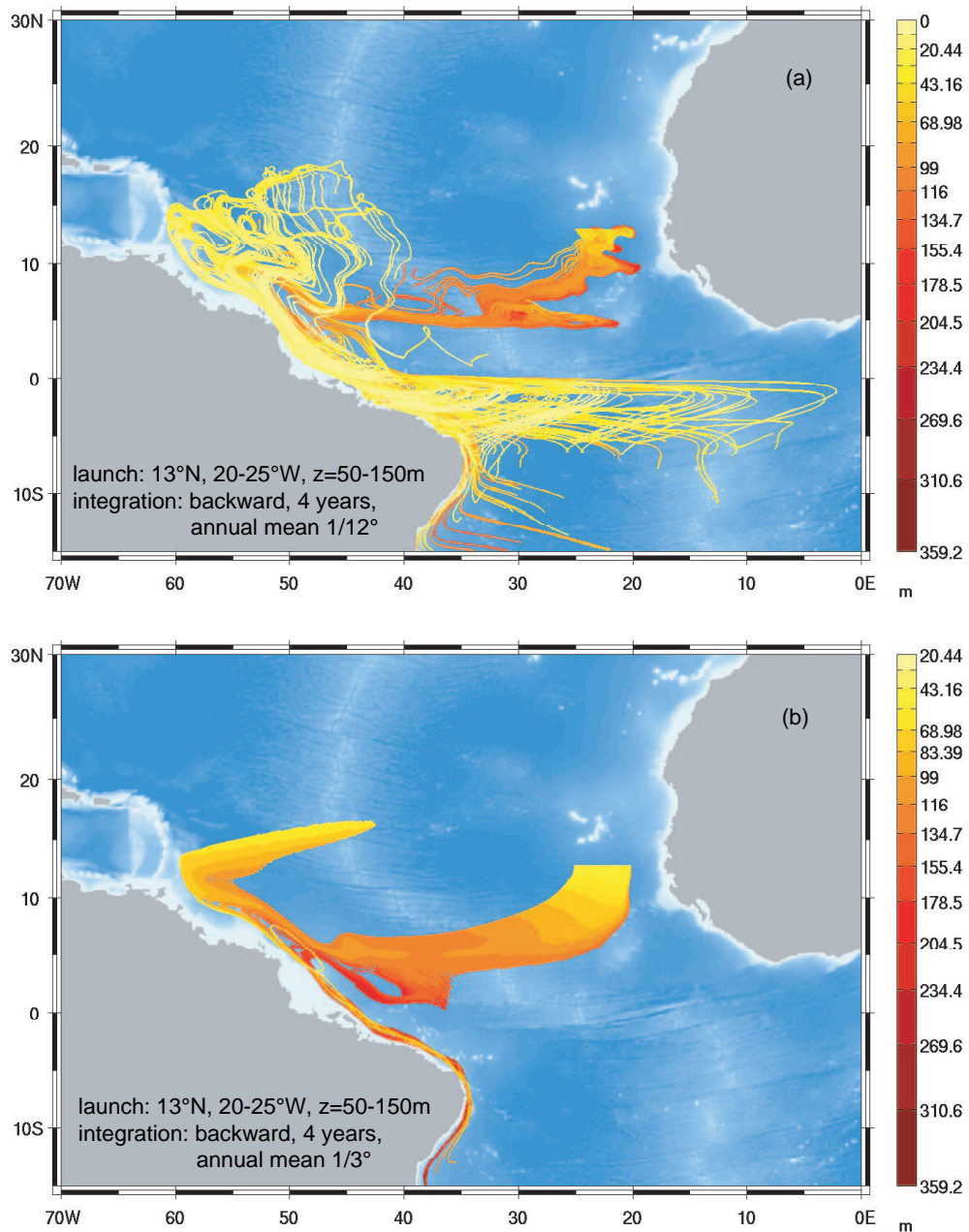
Figure 3.30: Sources of the Guinea Dome obtained from a 4 year backward integration of FLAME HIGH-RES (a) and a corresponding setup of FLAME REF (b).
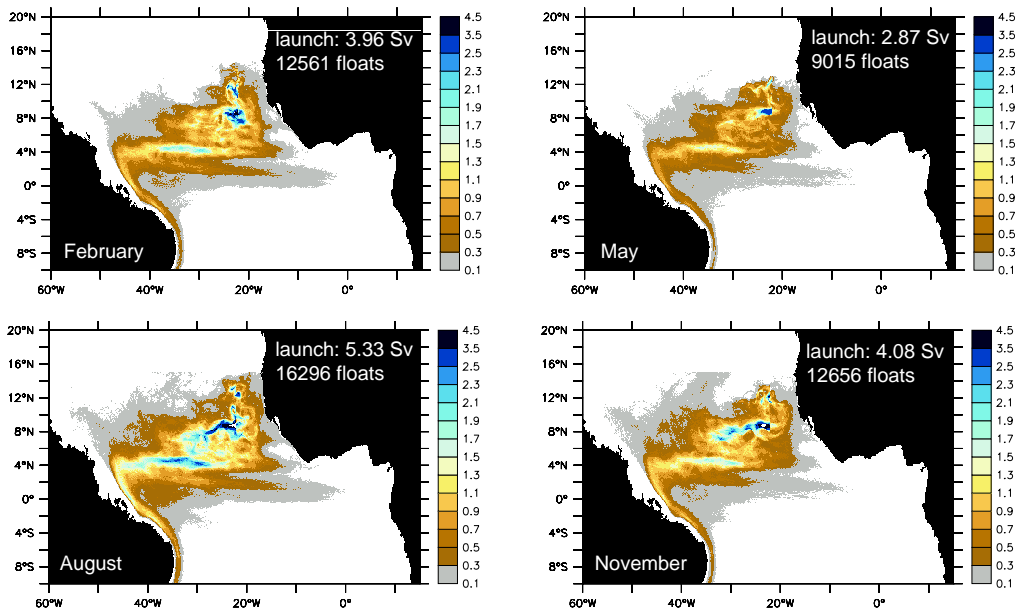
Figure 3.31: Sources of the Guinea Dome obtained from a 4 year backward integration of FLAME HIGH-RES with trajectory launches in different seasons.

tinct pathways visible. This coincides well with the weak currents in this region and the behavior of an APEX float trajectory described by STRAMMA ET AL. (2005a).

So far, as a conclusion from this analysis, the Guinea Dome is supported from southern hemisphere waters which enter the region mainly through the eastward flowing NEUC interacting by wave processes with the deeper, seasonally occurring parts of the NECC. Thus, the waters upwelling in the Guinea Dome are mainly of southern hemispheric origin too. The transition from the NEUC to the NECC has to occur west of 23°W because most of the NEUC launch at 23°W does not reach the Guinea Dome upwelling but the coastal upwelling along Africa and the equatorial upwelling by recirculation into the EUC.

Thus, the western NEUC plays an important role for the ventilation of the Guinea Dome, not the eastern or mid-basin part of the current (as discussed for the NEUC launches at 23°W). This is in contrast to the schematic view shown in the introduction (Fig. 3.1) which is based on the ideas of VOITURIEZ (1981). The northward shift of the NEUC into the Guinea Dome, shown in the FLAME HIGH-RES analyses here and in STRAMMA ET AL. (2005a), are visible too in the analysis of ELMOUSSAOUI ET AL. (2005) (see their Fig.s 5c and 13) showing the inflow into the dome for the upper central water masses from the CLIPPER 1/6° model run.

Upwelling in the Guinea Dome Area   The vertical transports in the Guinea Dome region are calculated from the horizontal transport divergence for 5x5° boxes and the upper 50 meters and shown in Fig. 3.32. The upwelling into layers shallower than 50m is indicated by negative sign. Obviously, there is upwelling along the coast and south of 15°N as far west as 35°W. The upwelling into the 0-50m layer off the coast is 0.85 Sv, along Africa 0.64 Sv, both values together are less than half as

large as the Ekman divergence of 4.4 Sv between 30°W and the eastern boundary, within 5-22°N, given by SCHOTT ET AL. (2004). But the upwelling is not due to Ekman divergence alone, as confirmed by regarding the vertical transports in the layer 50-150m. South of 15°N there is upwelling into this layer too and the coastal upwelling along the box from 15°N to 20°N is sustained by waters from these depths alone. Thus, the upwelling associated with the Guinea Dome reaches down to layers deeper than 150m.
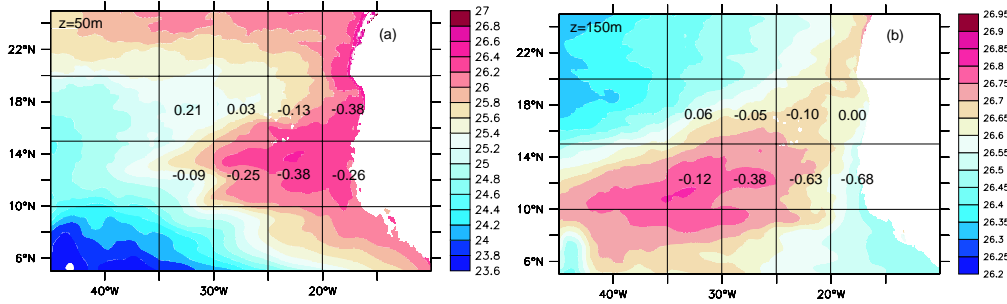

Figure 3.32: Vertical transports in the Guinea Dome region. Negative numbers indicate transport out of the layer (i.e. upwelling). The color indicates the density at the depth of 50m (a) and 150m (b). Figure (a) gives the transport in the layer 0-50m, (b) shows the values for the layer 50-100m. The upwelling associated with the Guinea Dome reaches to depths below 150m.

The Guinea Dome was found to have a sea-surface signature only in summer. In this season Ekman pumping forces an upwelling of subsurface isopycnals, which form the permanent dome in layers between 50 and 300m depth, into the mixed layer. This implies a stronger upwelling into the shallower layer. This effect can be seen in Fig. 3.33. The upwelling in the four boxes between 30°W and 20°W and 10°N to 20°N is enhanced significantly during boreal spring and summer reaching values of 1.56 Sv (spring) and 1.74 Sv (summer). The only regions where upwelling occurs year-round is between 25°W and 20°W, 10°N to 15°N and along the African coast north of 15°N. In the summer months the coastal upwelling is weakest (0.23 Sv), strongest values can be found in winter (0.95 Sv). During all seasons the northwestern most box belongs to the subduction regime. This regime is broadest in autumn (where it covers five boxes, see Fig. 3.33d and weakens from winter (2 northwestern boxes, see Fig. 3.33a) and is smallest during summer. This findings indicate a permanent upwelling in the Guinea Dome region with small values (0.32 Sv in winter) and an intensification during spring and summer with values of 1.74 Sv. The time series of the box-transports (not shown) indicate interannual variability which is mainly a modulation of the annual cycle. Only the southern boxes east of 25°W show some irregular behavior. What the reasons for this irregularity may are is behind the scope of this work.

Angola Dome

As indicated in Fig. 3.4 the Angola dome was found to have no clear signature in the used model. This view was completed by studying the fate of the SEUC
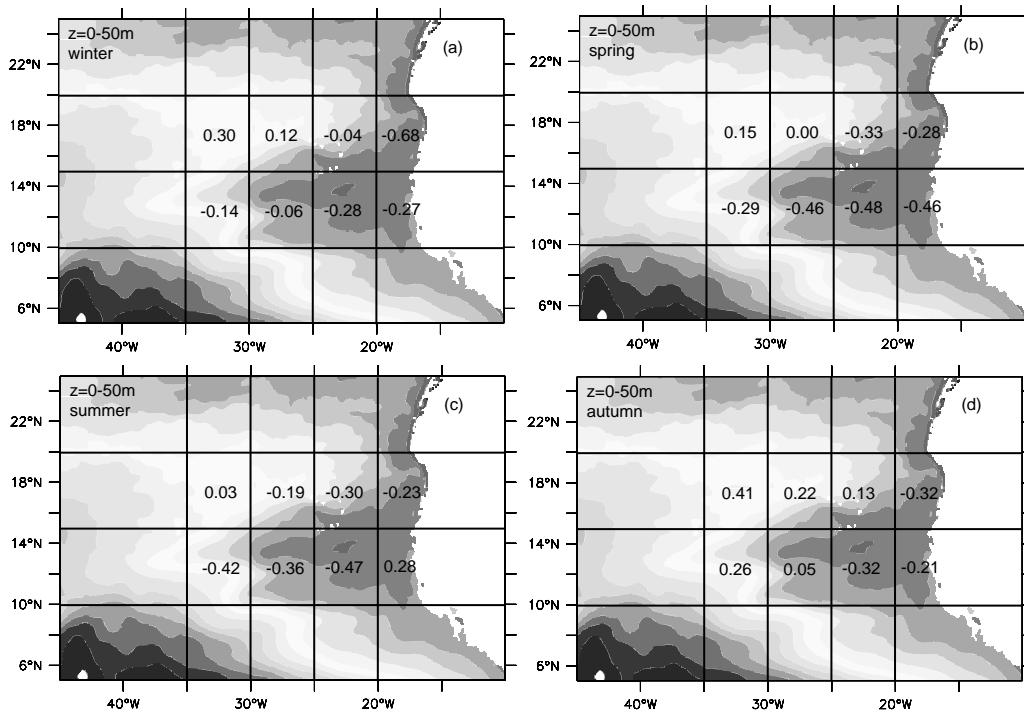
Figure 3.33: Seasonal cycle of vertical transports in the Guinea Dome region. Negative numbers indicate transport out of the layer (i.e. upwelling).

which partly feeds a broad upwelling patch after turning southward at about 0°E. The density structure at 50m depth (see Fig. 3.34) reveals different centers for a possible dome: around 6°S, 6°E and also near the eastern boundary south of 13°S, 10°E. A similar structure has been found in the 1/10° model of DOI ET AL. (2006). They relate the two centers of the Angola Dome to a decreased Ekman upwelling in the region between the two centers. However, in our case it is difficult to determine if there are really two centers or if it is an artifact due to an unrealistic circulation near the models southern boundary. None of the isopycnal domings coincides with the observed position of the dome near 5-10°E, 8-12°S. The inflow of lighter waters along 12°S in Fig. 3.34 is due to a eastward recirculation of the Benguela current near 0°W, 14°S, which separates the high salinity waters near the eastern boundary. The recirculation of the Benguela current in the model occurs too far north and east, what partly explains the missing representation of the Angola Dome.

The mean vertical transports in the Angola Dome regions from Fig. 3.34 confirm the results obtained from the trajectory runs: along the southward extention of the SEUC, upwelling occurs. This is in contrast to observations which indicate a connection of the SEUC to the northern flank of the Angola Dome, then entering the Angola Current, flowing southward and around the center of the dome and upwell in this region (MERCIER ET AL. (2003), STRAMMA ET AL. (2004)). The model shows inflow into the Angola Current only on isopycnals above 26.0 kg/m^3, i.e. above the core of the models SEUC (see Fig. 3.27). Thus, no significant amount of trajectories launched in the undercurrent reaches the eastern boundary current.

Thus, the trajectories drift in the interior to the south, maybe shifted meridionally by wave processes. Along the coast there is upward motion too, which is not fed by the SEUC but by the EUC which feeds an poleward undercurrent along the African coast, called the Gabon-Congo-Undercurrent and described by Stramma & Schott (1999).
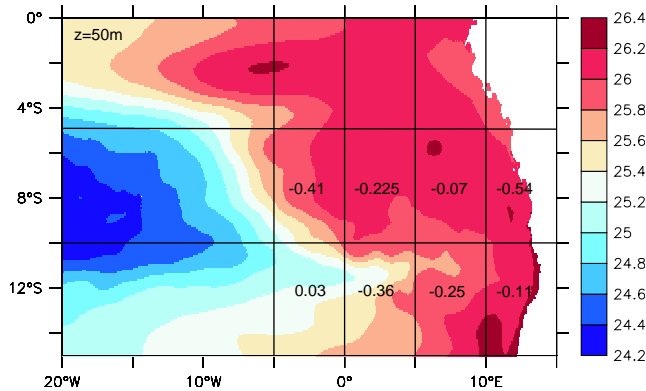

Figure 3.34: Seasonal cycle of vertical transports in the Angola Dome region. Negative numbers indicate transport out of the layer (i.e. upwelling).

The seasonal cycle of the vertical transports shown in Fig. 3.35 reveals the upwelling around a possible center of the Angola Dome at 6° as a seasonal artifact while the upwelling along the southward SEUC extension appears as a year-round feature. The coastal upwelling shows some interesting behavior: while the vertical transports in boreal summer and winter are on the same order north and south of 10°S, in spring and autumn, the upwelling south of 10°S has vanished and the northern part is strengthened remarkably. Yamagata & Iizuka (1995) and Doi et al. (2006) refer this behavior to the seasonally existing Gabon-Congo-Undercurrent along the west coast of Africa which they find to be established by a semi-annual downwelling coastal Kelvin wave. The current then transports waters from the EUC southward along the coast, feeding the upwelling in these region.

3.5   Conclusions and discussion

The investigation of the pathways inside the tropical current system revealed a strong dependence of the mean currents and their supply from the seasonal cycle and high-frequency variability. Especially the various near-equatorial (under)currents depend on this short time fluctuations induced directly by wind or by wind-induced wave processes. This fast reaction of the oceanic circulation to atmospheric changes is a special feature of the equatorial circulation because the equator acts as a waveguide. In contrast to most studies describing the equatorial currents separately from each other, but the results from this section indicate a strong interaction between the different east- and westward current bands which is triggered by TIW-induced eddy processes.
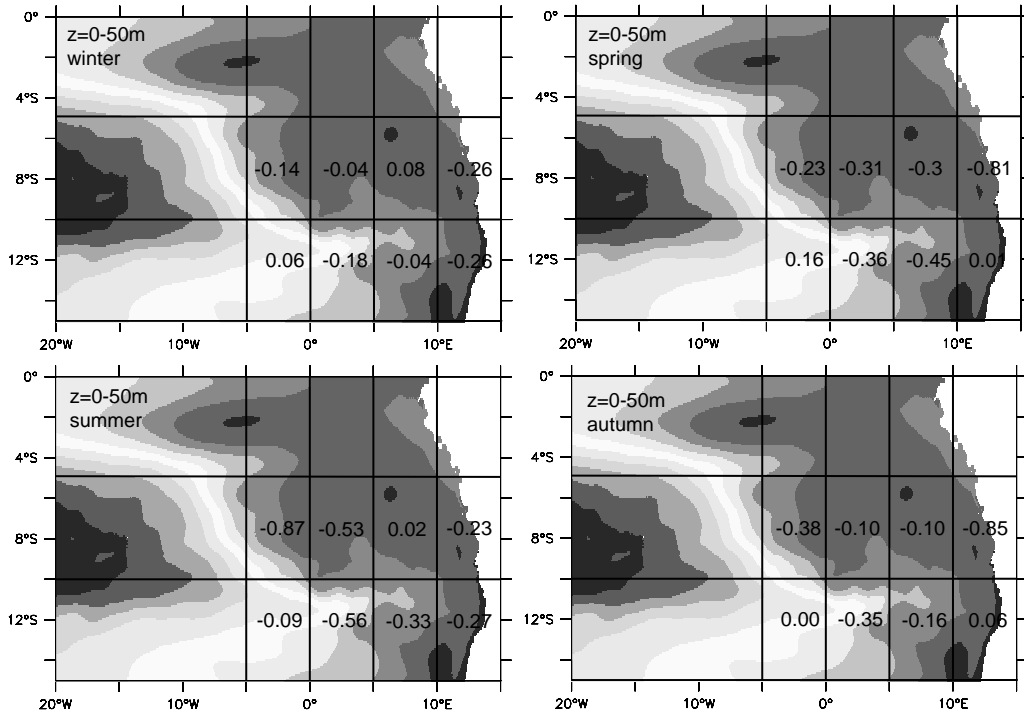
Figure 3.35: Seasonal cycle of vertical transports in the Angola Dome region. Negative numbers indicate transport out of the layer (i.e. upwelling).

The time-mean structure of the models used here reproduces the observed near-surface currents at several sections (35°W, 23°W, 5°S) but always shows some differences dependend on the number of observational casts or the resolution of the model. Strong differences occur regarding the annual cycle. This is quite apparent for the annual signal of the EUC in the different models (see Fig. 3.9) and is related to the different ability of the models to resolve intraseasonal processes like instability waves. The scatter in the observed EUC transport values (SCHOTT ET AL. (2003)) supports this finding. By intercomparision between different FLAME configurations it turned out that the yearly Rossby wave signal discussed by BRANDT & EDEN (2005) for mid-depth layers and by BÖNING & KRÖGER (2005) for the deep western boundary circulation, is masked in the surface near layers by the instability wave variability. In contrast, the directly wind-driven variability, as for example the annual cycle of the NECC (see Fig. 3.9) is simulated in a very similar manner in the different FLAME configurations and in the ORCA model.

The various off-equatorial current bands are only represented in FLAME HIGH-RES and the discussion of the pathways into this currents and their connections to the upwelling regions therefore bases on this model experiment. Eulerian analysis of the seasonality of the off-equatorial currents revealed a strong seasonal behavior but an especially strong variability was visible for the occurrence of the SEUC (see Fig. 3.8). The onset of the current was found to migrate between 30°W in autumn and 20°W in summer. Interestingly, the current never showed a direct link to the western boundary. This behavior of the SEUC is in contrast to observations by

BOURLES ET AL. (1999), BOURLES ET AL. (2002) and SCHOTT ET AL. (2003) who found the SEUC at 35°W near the western boundary. In the model the eastward flow at 35°W around 3°S is connected to the recirculation of the NBC which is well separated from the interior eastward flow associated with the SEUC. The question, what sustains the SEUC in the model could not be clarified from this Eulerian view of the currents but with the aid of Lagrangian floats a connection of the SEUC to the eastward flow of the EUC was detected.

The mechanism providing a connection between the EUC and the SEUC is based on tropical instability waves. These were found to influence significantly the spreading of southern hemispheric water masses by creating vortices in the mid and western basin. These eddies shift waters from the zonal currents north- or southward into the next zonal current band. Such a behavior has also been evident in the trajectories of various APEX floats (STRAMMA ET AL. (2004)) and it has been shown by the trajectory computations in FLAME HIGH-RES, that the shift occurs mainly at the poleward edges of the EUC (see Figure 3.36). Thus, the EUC, which is the only permanently ventilated of the eastward currents, shows connections to the NEUC and SEUC, as well as to the different branches of the westward flowing SEC.

Similar eddy-driven transports have been described for nutrients and oxygen-rich waters by MENKES ET AL. (2002) in the context of ecosystem variability and several other authors (see FOLTZ & CARTON (2004) and references therein) revealed a temperature advection going along with the instability waves. Additionally, the dynamics of the southern off-equatorial undercurrent were shown to be dependend on the energy of the tropical instability waves (JOCHUM ET AL. (2004b)). Here, the results from the Lagrangian analysis indicates that both phenomena belong to the same mechanism and visualize how the eddy-kinetic energy associated with the tropical instability waves is transferred into the mean kinetic energy of the off-equatorial undercurrents.

The analysis of the sources of the NEUC and the SEUC revealed that both currents are strongly affected by the eddy-transports and the SEUC has been found to be totally determined by them. Both currents were shown to consist of major fractions of recirculating tropical water, which originates from the EUC and afterwards flows around multiple times in different zonal currents before entering the NEUC or SEUC. These recirculations occur mainly between the equator and about 4°N/S. Particles north or south of that latitude usually do not recirculate back to the equator. Thus, the surface-near part of the waters can be understood to form the so-called "tropical cell" (LU ET AL. (1998)) which was shown to be cancelled by high-frequency variability (HAZELEGER ET AL. (2003)) and not ventilating the equatorial thermocline (HAZELEGER ET AL. (2001), HAZELEGER ET AL. (2003)). However, the results from the trajectories also admits the idea that the TCs are forced and formed by the wave-induced transports and thus vanish in the longterm mean. If this is the case their downwelling branch has some influence on the ventilation of the off-equatorial currents. However, the multiple wave-induced recirculations in the tropical current system explain the weak connections of the NEUC and SEUC to the off-equatorial upwelling areas and why the undercurrents go along with oxygen minima.

A feature not detectable in the present model analysis concerns the poleward divergence of the off-equatorial undercurrents on their way eastward. But the poleward shift of the undercurrents core as observed by BOURLES ET AL. (2002) can easily
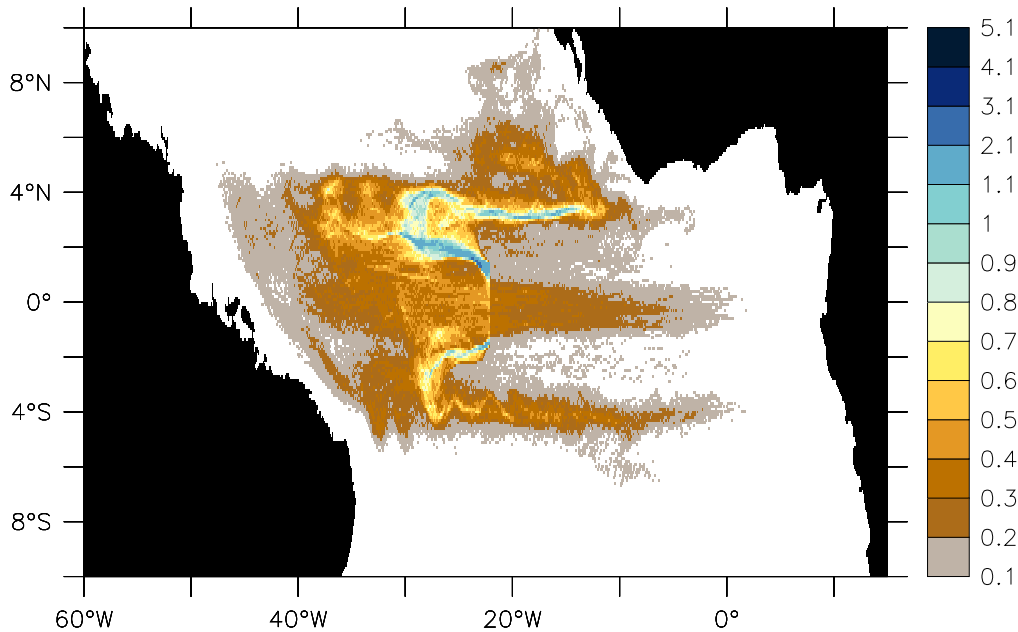
Figure 3.36: Fate of the waters along the flanks of the EUC at 23°W after 4 years. The shown trajectories were started in February and confirm the existence of winter TIWs and the connection of the EUC to the NEUC and SEUC. The numbers indicate transport in Sv, transport associated with the launch was 1.34 Sv.

be related to the wave-induced meandering of the undercurrents. In the present model none of the currents connects directly to the upwelling regions of the doming circulations and hence can not be driven by the upwelling in the doming areas as proposed by McCreary et al. (2002) and Furue et al. (2006).

The meridional shifts caused by the instability waves might be also the reason for the seasonal occurring northern deep NECC branch which has been reported by Richardson & Reverdin (1987), Stramma et al. (2005a) and Urbano et al. (2006). By transferring mass from the NEUC to this northern branch, the instability processes were found to also play a role for the waters in the Guinea Dome region.

An investigation of the upwelling in the domes indicates only weaker upwelling in these regions than estimated by Ekman divergence (Schott et al. (2004)). The transport of the NEUC into the mixed layer occurs mainly along the African coast and the EUC on the northern hemisphere, while the SEUC upwelling happens along the southward extension of the SEUC. This last feature is highly unrealistic and results from a blurred circulation near the southern model boundary at 18°S. Thus, only the sources of the Guinea Dome were studied in more detail.

The sources of the Guinea Dome waters were found to be on the southern hemisphere. The major source for the dome waters is the NEUC. The eastward flow of this current is shifted by TIW-induced processes into the eastern part of the NECC and forms a seasonally occurring northern NECC band around 8°N that feeds into the Guinea Dome circulation. However, the inflow into the dome can not be characterized by a particular pathway but is blurred over a region between 35°W and the

eastern boundary. If the NEUC is missing (like in FLAME REF) the Guinea Dome is found to be fed by waters from the NEC and hence shows different characteristics.

4 STC & MOC variability

4.1 Introduction

Variability on interannual to decadal timescales is influenced by changes in the wind fields as well as by fluctuations concerning the thermohaline circulation. The major importance of the wind variability and wave processes for the annual cycle and the mean state of the equatorial currents has been discussed in the last chapter but these modulations project onto the interannual variability, too. Hence, a large part of the interannual variability should be related to anomalies of the wind-driven circulation.

On the other hand, as described in section 3.1, the tropical meridional and zonal currents are connected to each other and can be imagined as a shallow meridional overturning cell, the STC (MCCREARY & LU (1994)), which overlays the deep meridional overturning cell (MOC).

Conceptionally, the STC exists on both hemispheres and is forced either by the subduction in the subtropics, the strength of the zonal wind field or the upwelling at the equator. The last two mechanisms were found to be the most plausible as the oceans show a fast response of the STC circulation to the prevailing wind fluctuations.

Introduced by the idea of the STC, a possible longer-term variability mechanism for equatorial variability came into play because the waters subducted in the subtropics need some time to spread into the equatorial region. Idealized tracer studies in ocean models (LAZAR ET AL. (2000)) indicated a timescale of about 6 years for subducted anomalies to propagate into the inner tropics. Thus, variations on time-scales of 5-10 years might be linked to variability in the equatorward branch of the STCs.

However, such a spreading of temperature or salinity anomalies, originally proposed by GU & PHILANDER (1997) as a modulation mechanism for the ENSO signal and referred as the $\bar{v}T'$-mechanism, is not observed in the oceans. Rather, tracer fluctuations linked to a variation of the transport are observed, which are referred as the $v'\bar{T}$-mechanism. The remaining question about the STC transport variability is: is it a locally forced variability connected to the divergence at the equator or are the STC variations a result of the zonally integrated wind-induced circulation changes i.e., a coherent variability of the tropical gyre? This question will be studied here

by using results from various ORCA and FLAME runs, which differ in the choice of
the surface forcing.

Another remote effect influencing the equatorial current variability is connected to
the variations of the deep circulation. The main effect of an increase/decrease of
the equator-crossing transport in depth is a strengthening/reduction of the return
flow in the upper 1000m which overlays the wind-driven STC variations. Apart from
some idealized studies by FRATANTONI ET AL. (2000) and JOCHUM & MALANOTTE-
RIZZOLI (2001) the influence of the MOC on the equatorial currents has not been
studied very much. The results from these studies indicate a coupling of STC and
MOC strengths: in presence of a realistic MOC of O(15Sv) they find the northern
hemispheric STC blocked by the MOC return flow and in idealized experiments
without the return flow, the Atlantic STCs occur on both sides of the equator with
comparable strengths. A conclusion from this findings is that the northern STC
(nSTC) might occurs in phases with considerable decreased MOC. Indeed, the nSTC
is found to appear temporarily in ocean models: KRÖGER ET AL. (2005) revealed
the nSTC existing as an anomaly pattern during the early to mid-eighties. However,
the possible mechanism leading to this anomaly pattern could not be investigated
because of the regional model setup by KRÖGER ET AL. (2005). If the occurrence of
the nSTC is a consequence of a decreased MOC will be investigated in this chapter.

The mechanism leading to changes of the MOC transport is linked mainly to vari-
ability in the subpolar North Atlantic, especially in the formation of Labrador Sea
Water. As studied in many idealized ocean models (for instance by: KAWASE (1987),
YANG (1999), JOHNSON & MARSHALL (2002)) the anomalies of the deep water for-
mation create fast boundary wave signals transferring the anomalies to the regions
more south and lead to an adjustment there. At the equator the wave signals are
captured by the equatorial waveguide, propagate eastward and adjust the basin from
the eastern boundary. Thus, variability introduced in the North Atlantic should be
felt rather fast at the equator and the longer term wave adjustment might influ-
ences significantly the return flow variability on decadal to interdecadal timescales.
If such a mechanism and the corresponding variability can also be found in realistic
models and if there is a significant influence of this remote variability process will
be investigated here by the aid of a host of sensitivity experiments.

4.2   Subtropical-tropical transport patterns

4.2.1   Zonally integrated transports

Since the structure of the STCs and, accordingly, the intensity of the tropical cur-
rent system in the Atlantic is strongly affected by the cross-equatorial transports
associated with the southward export of NADW, it is useful to begin with an exam-
ination of the zonally-integrated transports for both the upper- and deep-layers of
the tropical Atlantic. Figure 4.1 depicts the meridional overturning streamfunction
for the reference experiments of both ocean models: Fig. 4.1a for FLAME REF and
Fig. 4.1b for ORCA REF. FLAME REF shows a net southward flow of 16 Sv in
the subpolar North Atlantic which is in accordance with recent inversions of hy-
drographic section data by LUMPKIN & SPEER (2003). The deep water export in
ORCA REF is significantly lower (10 Sv). The deep southward transport across

the equator is 15 Sv in FLAME REF and 8 Sv in ORCA REF. This influences also the transports in the upper 300m: FLAME REF reveals a shallower southern STC cell which is much more surface intensified than the corresponding cell in ORCA. Nevertheless, both southern STCs reveal a similar transport of 6 Sv.

Even if there are strong differences in the southward deep flow none of the models reveals a mean northern STC, although in ORCA REF a shallow recirculation cell between 10°N and 18°N exists which might forms the northern STC in cases of even weaker northward return flow or strengthened surface transport on the northern hemisphere in direction to the equator.
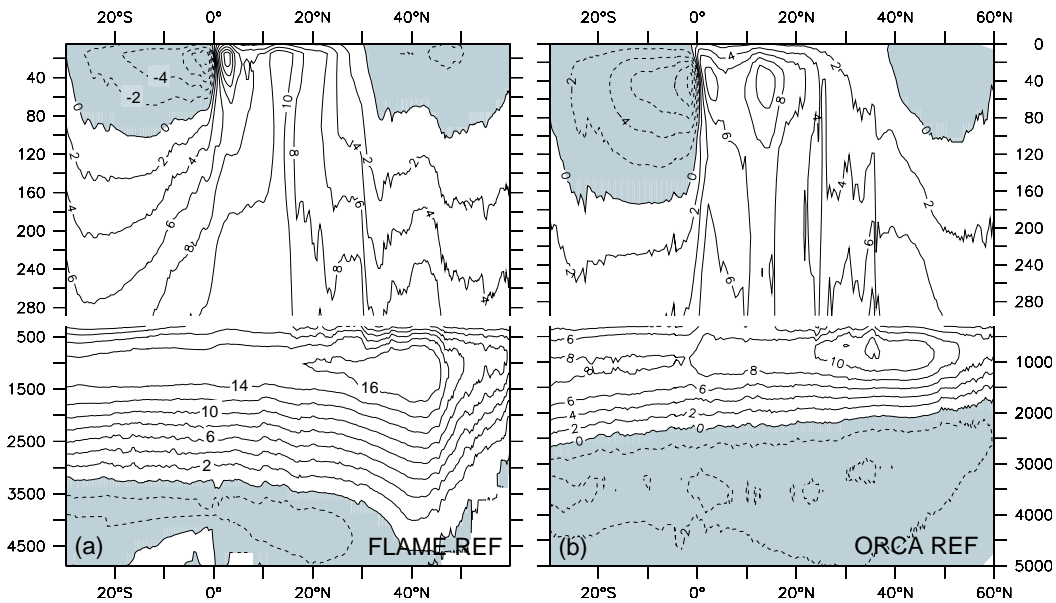

Figure 4.1: Meridional overturning streamfunction from (a) FLAME REF and (b) ORCA REF. For details see text.

The strong tropical cells, between 4°S/N and the equator, found in FLAME REF in the upper 40m are shifted downward in ORCA REF to the range 40-80m and have weaker transports. This feature might be related to the differences in surface forcing between the NCEP/NCAR and the CORE fields but can also be attributed to the different mixed-layer schemes used by the models. While the Kraus-Turner-scheme in FLAME mixes only the upper 10m of the tropical oceans, the TKE scheme used by the ORCA models creates a mixed layer of about 20-25m and thus transports the wind energy deeper into the ocean.

For both models the upwelling transport into the surface layer (above 40m) between 10°S and 10°N, associated with the wind-driven Ekman-divergence, is about 14 Sv. These values appear very close to the estimate of the Ekman divergence between 35°W and 4°W (15 Sv) by GOURIOU & REVERDIN (1992), but are significantly lower than values inferred from NCEP reanalysis stresses (26 Sv) by SCHOTT ET AL. (2004); higher values (21±2.1 Sv) are also reported by ZHANG ET AL. (2003) based on surface drifter data between 6°S and 10°N. It should be noted, that values for the equatorial upwelling/divergence are very sensitive to the latitudinal range

considered: e.g. in the narrow band of 2°S to 2°N, there is an upwelling of 23 Sv (FLAME REF) or 20 Sv (ORCA REF), similar to that found by HAZELEGER ET AL. (2003) for the OCCAM model in this area. Thus, the wind-driven part of the shallow overturning is quite robust feature in both models, even if the differences between NCEP/NCAR and CORE forcing are strongest in the tropics.

A significant part of the equatorial upwelling is associated with recirculating water in the tropical cells (TCs, LU ET AL. (1998), MOLINARI ET AL. (2004)). As shown in previous studies (HAZELEGER ET AL. (2003)), the TCs are not associated with significant mean diapycnal transports and tend to disappear when considering eddy activity and integrating the flow in density instead of z-coordinates, thus eliminating isopycnic recirculation water (KRÖGER (2001)).

As the northern hemisphere circulation shows no mean contribution to the equatorial upwelling and the TCs have a vanishing transport, the equatorward flow can be understood to consist of two components: an upper part associated with the wind-driven southern STC (negative values of the streamfunction in Fig. 4.1a and b, upper 100m for FLAME REF/180m for ORCA REF) and a part of the MOC return flow, below ≈ 100m/180m and above 300m. Note, that the northward transport associated with the NBC reaches down to about 1000m, but the deeper parts do not contribute to the upwelling into the surface layer (roughly defined here as the upper 20m) at the equator. Hence, in the discussion of the variability of the STC or the NBC, transports will be calculated above 300m depth. Specifically, the transport of the NBC will be calculated as the northward flow between the western boundary and 33°W, from 20m to 300m depth, thereby excluding the surface (Ekman) flow to the south. The EUC is calculated in the same depth range and is defined as the eastward flow between 3°S and 3°N.

Before a discussion of the manifestation of variability in the different currents, it is useful to look at the variability of the zonally integrated transports. Figure 4.2 shows the Hovmoeller diagrams of the different models and experiments for the surface near layer between 0 and 80m. The anomalies of the meridional overturning in these depths are averaged by a three year running mean and reveal similar structures regarding the wind-driven variability. In all experiments with interannual wind variability (FLAME REF, ORCA REF, ORCA WIND, ORCA EQ) anomalies of comparable amplitude are found on the northern and southern hemisphere. The signals show different signs on both sides of the equator and are strongest close to the equator. This is indicative of a pronounced variability of the tropical cells. Note that positive (negative) anomalies in the northern (southern) hemisphere correspond to enhanced cell strengths, with maxima from the seventies to mid-eighties. The northern and southern maxima are slightly out of phase.

Interestingly, the ORCA REF experiment shows the northern maximum in the mid-seventies, while the experiments FLAME REF, ORCA WIND and ORCA EQ all show a northern hemisphere mid-eighties maximum. Thus, the conclusion is that the wind-forced interannual to decadal variability is partly counteracted in ORCA REF by other processes. Also, the wind-driven variability pattern visible for the experiments FLAME REF, ORCA WIND, and partly ORCA REF too, is generated by variability in the inner tropics as the strong similarity of the different runs with the results form ORCA EQ (where interannual forcing is applied only in the tropics between 5°S and 5°N) indicates.
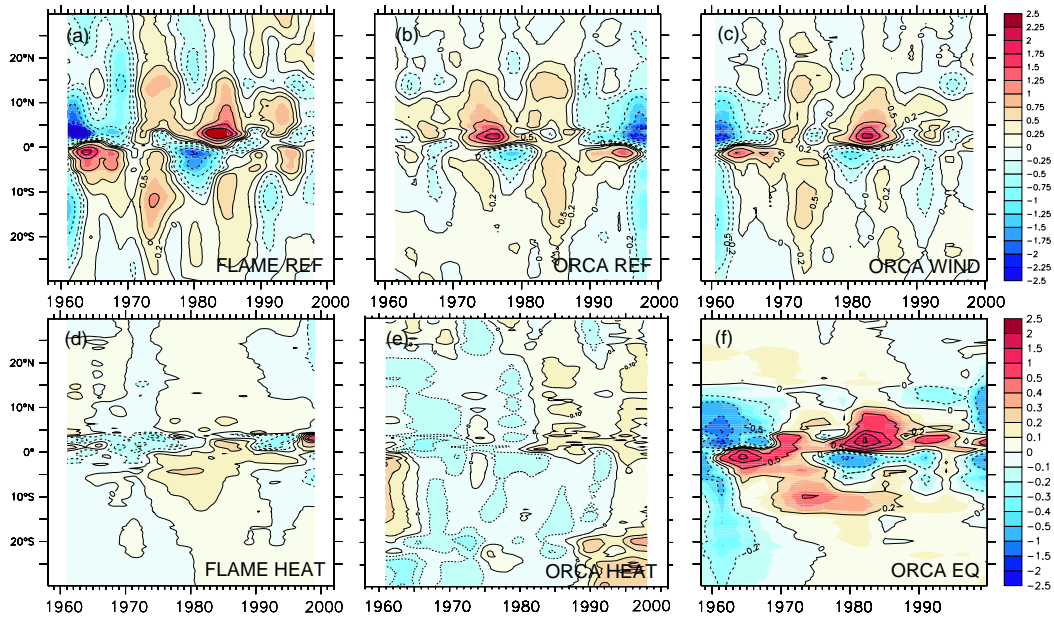
Figure 4.2: Zonally integrated meridional transport anomalies in Sv. Hovmoeller diagrams of the transport in the upper 80m of (a) FLAME REF, (b) ORCA REF, (c) ORCA WIND, (d) FLAME HEAT, (e) ORCA HEAT and (f) ORCA EQ.

The strongest variability signal is related to the wind fluctuations as a comparison to the anomalies from the experiments FLAME HEAT and ORCA HEAT indicates. However, for the experiments forced only with thermohaline forcing even the sign of the near-surface anomalies is unclear. While FLAME HEAT shows a kind of decadal variability with stronger than normal northward transports from the sixties to mid-seventies and after the eighties, ORCA HEAT shows weaker transports at the beginning and end of the run and strengthened transports during the 1965-1995.

In contrast to the bipolar STC variability pattern the HEAT runs show a cross-equatorial structure. The weakening of the zonally integrated flow in FLAME HEAT during the seventies to nineties can be found in FLAME REF and ORCA REF too, if one imagine the increased transports during the late seventies and early eighties to vanish. Thus, there might be an interaction between the wind-driven interannual signals most dominant in the experiments FLAME REF, ORCA REF, ORCA WIND and ORCA EQ and a longer term thermohaline modulation as indicated by the runs FLAME HEAT and ORCA HEAT.

The vertical structure of the wind-driven signal is shown for the period 1980-1985 (for ORCA REF 1978-1982) in Fig. 4.3 and appears to be a robust feature, too: for all runs with interannual wind-variability there is a significantly enhanced tropical cell on both hemispheres. Additionally, on the northern hemisphere the northern STC can be found as an anomaly pattern, reaching as far north as 15°N, although with small amplitudes. Thus, the conclusion from this zonally integrated view is that a dominating wind-driven anomaly signal influences the interannual variability not only in the inner tropics but also reaches more poleward. The STC variability appears thus "pulled" by the equatorial wind-stress.
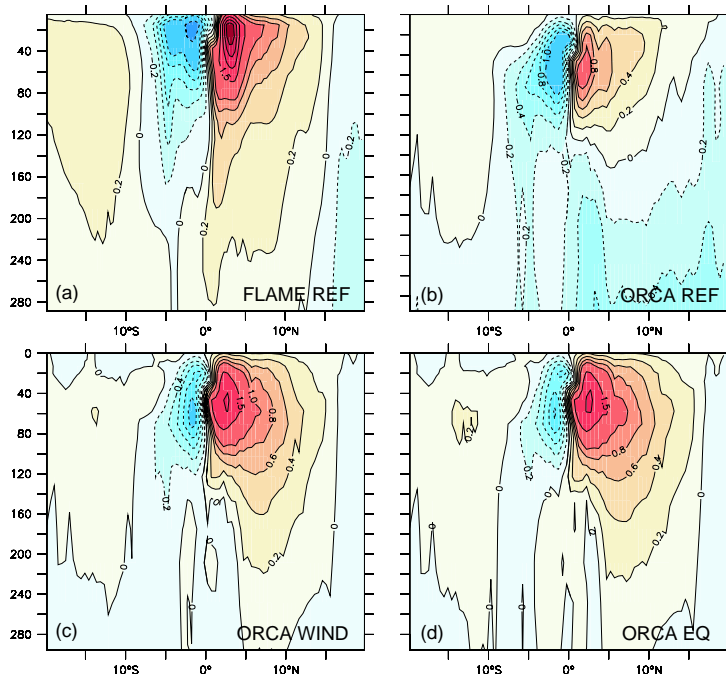
Figure 4.3: Vertical structure of the 1980-1985 streamfunction anomaly of 4.2 for the experiments (a) FLAME REF, (b) ORCA REF(1978-1982), (c) ORCA WIND and (d) ORCA EQ.

The wind stress variability in the subtropics seems to play a minor role for the variability of the zonally integrated flow equatorward of 15°latitude. This is an interesting finding because the major supply of the inner tropics is via the North Brazil Current (NBC) which is bifurcating around this latitude on the southern hemisphere and the possible supply of water masses from the northern STC is blocked slightly south of this latitude on the northern hemisphere. Thus, the NBC variability south of 15°S is no more forced by the equatorial winds and possible anomalies originating from further south will be overlaid by local variations on their way equatorward. For the northern hemisphere Fig. 4.3 shows strong indications for a possible inflow of northern hemisphere waters into the tropical Atlantic via strengthening of the equatorward convergence forced by an equatorial wind anomaly.

The close correspondence between the solutions of two different models and confirmed also by results from a reduced gravity model by KRÖGER ET AL. (2005)), with different basin configurations (Atlantic basin, global solution, subtropical-tropical domain), and different atmospheric forcing concepts (linearized bulk formula, full bulk formulation or atmospheric mixed layer model) emphasizes the overriding importance of the wind stress in the simulation of the zonally integrated variability.

4.2.2 Manifestation of transport anomalies in equatorial currents

The last section provided a view on the zonally integrated variability. As the STC is formed by equatorward flow, upwelling in the east along the equator and poleward

surface flow, it is interesting to see how the variability is distributed in the various currents. Of particular interest for the variations of the equatorial upwelling are the anomalies in the upper thermocline (50-100m). These are illustrated in Fig. 4.4 for the phase of intensified STC/TC cells during 1980-1985 for FLAME REF and ORCA EQ and from 1978-1982 for ORCA REF. The color indicates northward (yellow) or southward (blue) anomalies exceeding 5cm/s (FLAME REF) e.g. 2cm/s (ORCA REF, ORCA EQ). The figures show the current anomaly relative to the long-year mean.

In all experiments the enhanced northern transport in the southern STC appears clearly associated with a stronger north-westward SEC in the region from 0° to 6°S. Differences between the ORCA and FLAME experiments occur for the variability patterns along the EUC and on the northern hemisphere. While FLAME REF shows a strengthened EUC from about 35°W to 5°W, ORCA REF and ORCA EQ reveal an increased eastward EUC from 25°W (ORCA REF) e.g. 20°W (ORCA EQ) and even show a westward anomaly near the western boundary. The EUC in ORCA REF shows strong anomalies between 15°W and the eastern boundary resulting from a strong recirculation in the interior between 4°N/S and the equator. This recirculation is indicated by the FLAME REF-solution too, but much weaker in amplitude. Thus, the tropical cell visible in the meridional overturning streamfunction (see Fig. 4.1) is located mostly in the west for FLAME REF, but has a significant eastern contribution by recirculation in the ORCA experiments. A consequence of the deeper TC recirculation in the ORCA experiments could be a stronger damping of the interannual current variability in these runs and might lead to a different interannual wind response of the zonal currents in both models. For the meridional structure strong similarity between the models was found in the analysis of the zonally integrated transports.

Another interesting difference concerns the anomaly patterns on the northern hemisphere. While FLAME REF indicates a complicated variability pattern with anomalies along the NBC retroflection and along the NECC, the ORCA experiments reveal more clearly a northern hemispheric contribution to the EUC via a zig-zag-pathway through NEC, NECC and nSEC (shaded arrows in Fig. 4.4). This pathway compares well to the interior zig-zag pathways between the northern subtropics and the tropics suggested by Jochum & Malanotte-Rizzoli (2001) and Kröger (2001). Thus, temporarily there is a northern STC contribution to the EUC also in the models used here. Going along with the northern anomaly signal, the westward anomaly of the nSEC weakens the EUC in ORCA REF and ORCA EQ in the west and partly counteracts the variability of the southern inflow. Interestingly, in both models the NBC and the southern tropical gyre are weakened but this is visible much stronger in the ORCA runs. The comparison between the ORCA experiments allows for the conclusion that this kind of variability mechanism is introduced by the tropical wind variability. The assumption, introduced in the discussion of the mean meridional overturning, that the weaker MOC in ORCA might permit a northern hemisphere EUC contribution, is supported by the current anomaly plots from ORCA REF and ORCA EQ and suggest a possibility of MOC-driven variability in the Tropical Atlantic.
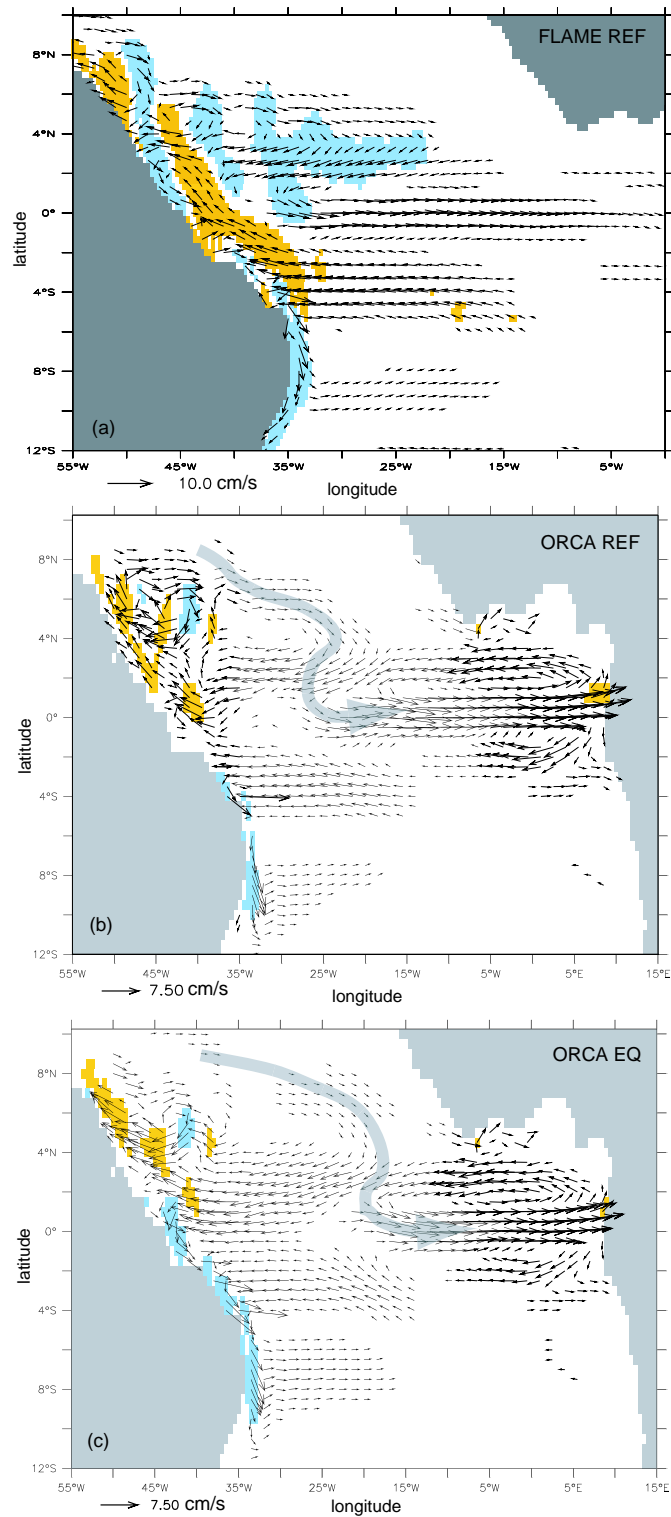
Figure 4.4: Horizontal velocity anomalies averaged between 50-100m for the period of enhanced equatorward transports (1980-1985) for a) FLAME REF, b) ORCA REF and c) ORCA EQ. Yellow: areas of positive northward flow anomalies > 5cm/s (FLAME REF) or 2cm/s (ORCA REF, ORCA EQ), blue areas of corresponding southward anomalies.

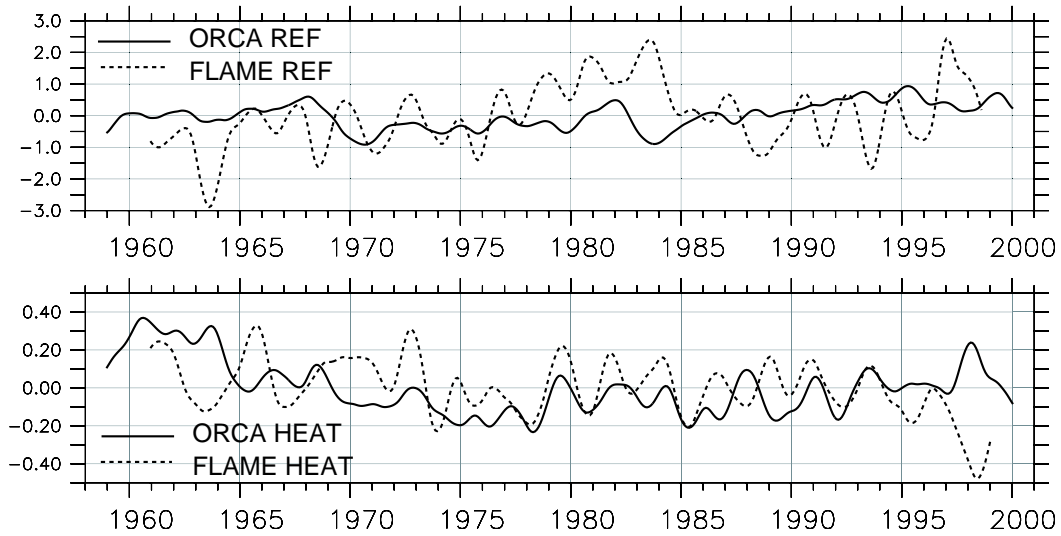Figure 4.5: Time series of EUC transport anomalies at 23°W in correspond-ing ORCA and FLAME experiments. Upper: interannual variability in FLAME REF and ORCA REF, lower: FLAME HEAT and ORCA HEAT.

EUC variability

In the discussion of Fig. 4.4 it appeared, that there might be significant differences in the temporal and spatial variability of the EUC between the reference experiments FLAME REF and ORCA REF. These difference arise particular in mid and eastern basin. This was hypothesized because the deeper reaching recirculation of the tropical cells in ORCA REF might influence the variations there additionally and possibly counteract the variability originating from the NBC and feeding into the EUC (as visible in the FLAME REF-anomaly pattern). This is indeed the case, when comparing the time series of EUC anomalies of the corresponding experiments in FLAME and ORCA in mid-basin at 23°W (see Fig. 4.5). In the runs the EUC interannual amplitudes range between 1 Sv for FLAME REF and less than 0.5 Sv for ORCA REF. In the experiments FLAME HEAT and ORCA HEAT the amplitudes are of the same order around 0.2 Sv. However, the time series of the both models do not show a closer similarity concerning the temporal evolution. This is linked to the strong differences of the annual cycle of the EUC as discussed in chapter 3.

 The EUC variability of the ORCA experiments including interannual wind-forcing show marked similarities (see Fig. 4.6) in the phases and amplitudes of the EUC anomalies. The comparison between ORCA WIND, ORCA REF and ORCA EQ al-lows the conclusion that nearly all EUC variability is forced locally by the equatorial winds. As found for the anomalies in Fig. 4.4 the EUC variability is not zonally co-herent: the 23°W variability sometimes shows the same temporal variability as more west at 35°W (for example in the late sixties or at the beginning of the eighties), in other years it does not resemble the western variations. The EUC variability at 10°W shows a completely different behavior from the fluctuations in the west, mainly due to the recirculations visible in Fig. 4.4b/c. Thus, a longitudinally coher-
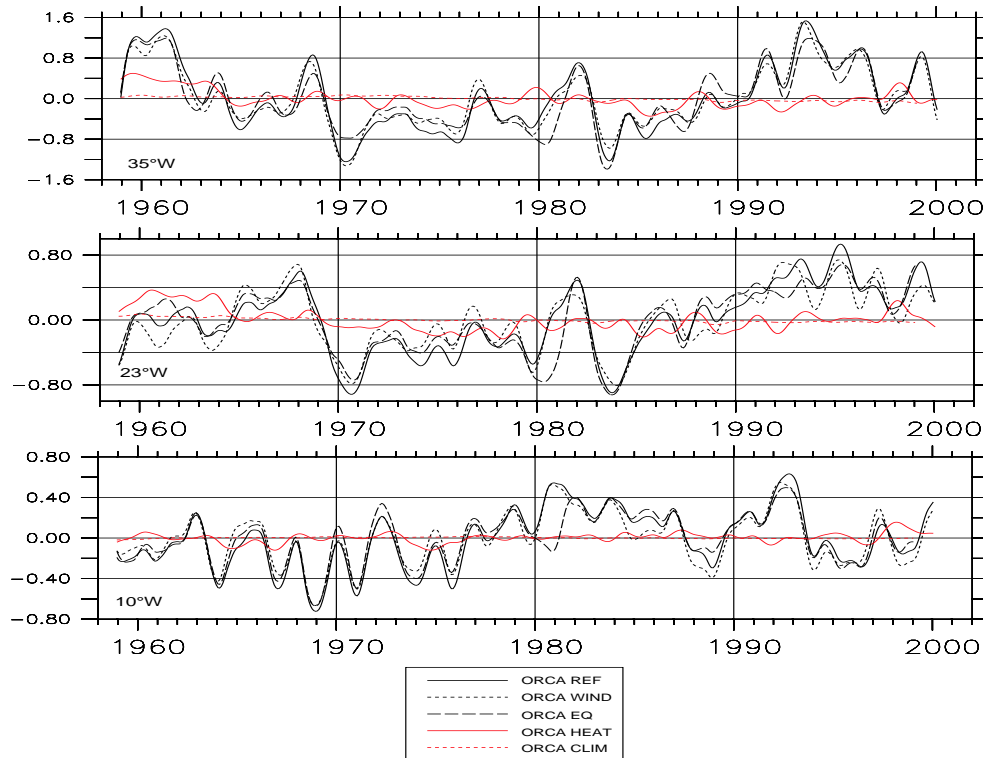
Figure 4.6: Time series of EUC transport anomalies in corresponding different ORCA runs. Interannual variability at 35°W (upper), 23°W (middle) and 10°W (lower).

ent variation of the upwelling branch of the STC can not be found on interannual timescales.

Interestingly, the fluctuations of the EUC at 35°W and 23°W also show some decadal anomaly pattern. During the sixties and nineties the EUC transport is mostly stronger than normal, during the seventies and eighties mostly below the longterm mean. This longterm modulation has also to be linked to equatorial, wind-driven processes due to the strong similarity between the experiments ORCA REF, ORCA WIND and ORCA EQ. However, this finding is contrasted by the presence of this decadal modulation pattern in the western EUC of FLAME HEAT (not shown, see Fig. 11c of HÜTTL & BÖNING (2006)) and the meridional transport anomalies in Fig. 4.2d between the years 1973-1989.

The apparent presence of the decadal variability signal also in the NCEP-wind anomalies indicate towards a coupled mechanism which links the thermohaline forced variability to corresponding fluctuations of the wind field patterns. This might work by an influence of the MOC variations to the upwelling along the EUC, leading to a meridional shift of the ITCZ. This link and a discussion how and if the MOC anomalies influence the tropical currents and upwelling will be given in a separate section. But before drawing the attention to this, the discussion of the interannual and directly wind-driven processes will be continued.
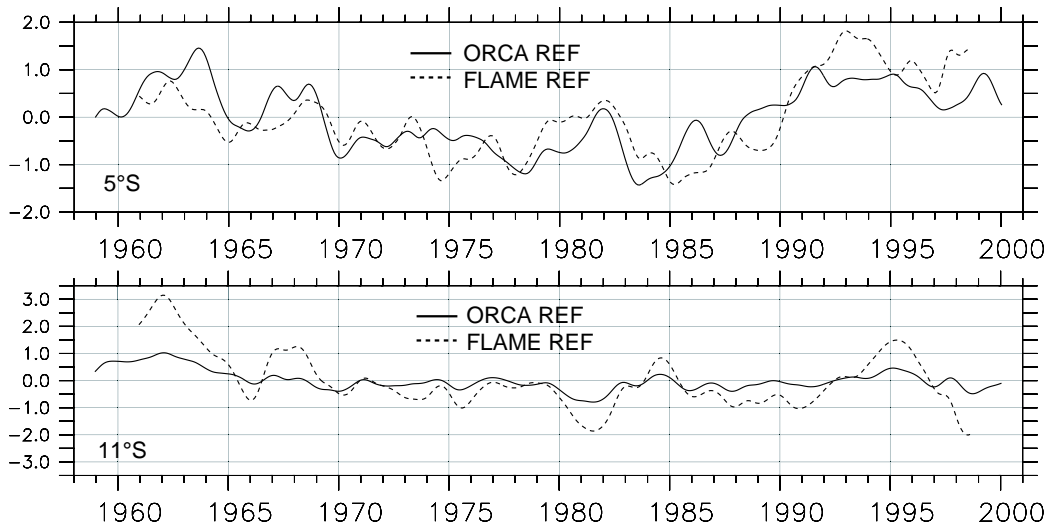
Figure 4.7: Time series of NBC transport anomalies in corresponding ORCA and FLAME experiments. Upper: interannual variability at 5°S in FLAME REF and ORCA REF, lower: for 11°S.

NBC variability

In contrast to the zonal current fluctuations the variability of the meridional transport anomalies reveal strong similarity for the reference runs of the different ocean models concerning amplitudes and phases at least for the zonally integrated transports. This is confirmed by the time series of the NBC transport anomalies at 5°S, shown in Fig. 4.7, too. Especially the longterm trend, showing enhanced equatorward transports during the sixties and in the nineties, and weakened transport during the seventies and eighties, is robust in both models. In some years the amplitudes of the anomalies differ, indicating the influence of a slightly different response to the wind-forcing in the two models at the equator. For 11°S the amplitudes of the interannual signal differ between FLAME REF and ORCA REF, but the phase and sign of both anomalies is still the same. This corroborates the idea of the same variability mechanism in both models as discussed for the zonally integrated transports.

The horizontal current patterns in Fig. 4.4 show some corresponding features concerning the variability of the southern hemispheric equatorward flow. Both models indicate for the phase of strengthened equatorward flow also a strengthened interior flow (associated with the SEC) to the western boundary which adds up to the NBC and partly compensates fluctuations carried by the NBC along the western boundary from further south. This compensating tendency between western boundary current and interior ocean flow appears analogous to the behavior observed in the Pacific Ocean at interannual to decadal timescales (LEE & FUKUMORI (2003), CAPOTONDI ET AL. (2005)). The mechanism of this anti-phase relation remains unclear. LEE & FUKUMORI (2003) explain the compensation of interior and boundary current transports due to the presence of two different mechanisms: while the boundary current variability results from the adjustment of the gyre circulation to changes
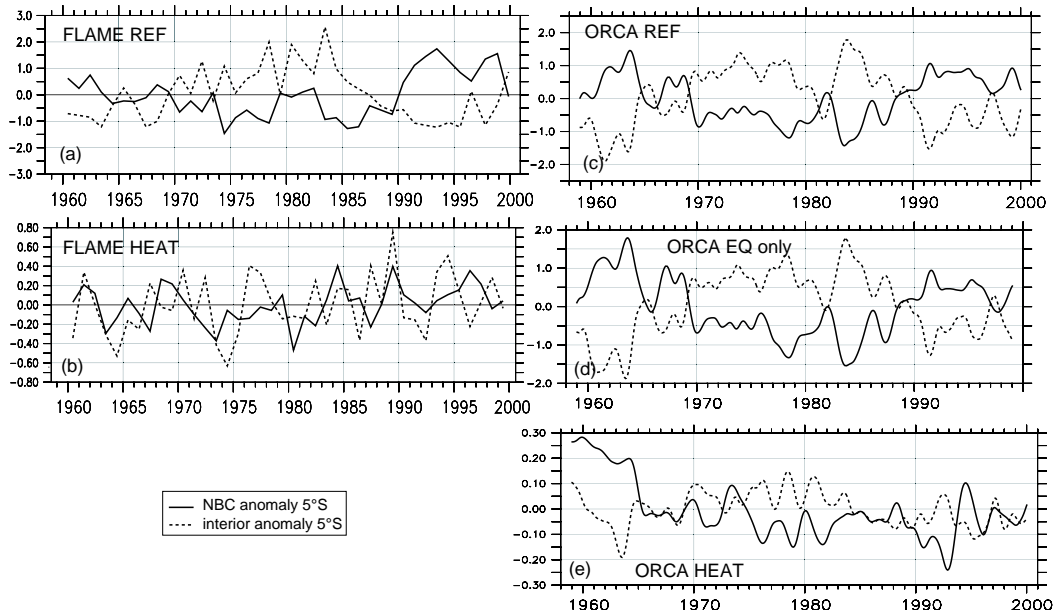
Figure 4.8: Time series of NBC transport and interior transport anomalies at 5°S in different ORCA and FLAME experiments.

in the Ekman pumping, the interior transport may also result from changes in the near-equatorial variations of surface wind stress. The results of CAPOTONDI ET AL. (2005) suggest that both the western boundary and the interior transport are adjusted through baroclinic Rossby waves. Recent analysis of the ORCA REF experiment in the tropical Pacific (LÜBBECKE ET AL. (2006)) indicate that both processes act together.

  The compensational behavior in the Tropical Atlantic can be found in nearly all experiments analyzed here. Fig. 4.8 shows the NBC (western boundary to 33°W) and interior transport (eastward of 33°W) transports at 5°S. With the exception of FLAME HEAT all experiments show the anti-phases of both anomalies, with the interior transport having a slightly higher amplitude. Thus, changes in meridional transport are influenced stronger by the interior flow than by the western boundary current. This is the case for thermohaline driven anomalies in ORCA HEAT too, while in FLAME HEAT there is no clear connection between the interior transport variability and the NBC transport at 5°S. However, for FLAME HEAT the zonally integrated transport variability is mainly given by the NBC variability, both variables show a correlation of ≈0.8 in the region between 2°S and 15°S (see HÜTTL & BÖNING (2006), Fig. 10d). For all other runs discussed here, the zonally integrated transport is determined by the sum of NBC and interior variability and resembles the stronger of the two anomaly signals.

  The zonally integrated meridional transport anomalies show a meridionally coherent variability structure reaching to approximate 10°N/S (Fig. 4.2). The velocity anomalies for the phase of enhanced equatorward transport phase (1978/80-1982/85) confirm this finding by revealing a meridionally incoherent NBC variability caused by additional SEC inflow from the interior. Thus, anomaly signals advected by
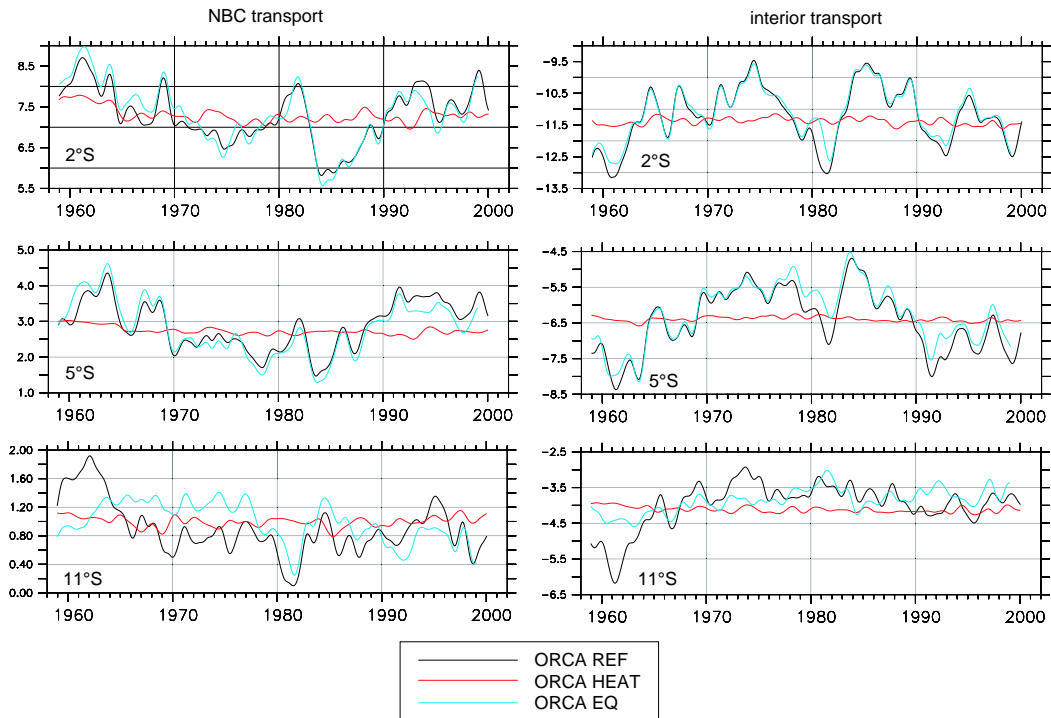
Figure 4.9: Time series of NBC transport and interior transport anomalies at 2°S, 5°S and 11°S in different ORCA experiments (ORCA REF, ORCA HEAT and ORCA EQ).

the NBC from further south than about 6°S can be canceled or even reverse sign. This behavior is illustrated by the time series of the NBC and interior transport in Fig. 4.9. The variability patterns at 2°S and 5°S reveal the same structure while the fluctuations at 11°S do not show any similarity with the fluctuations more north. However, it can be noted, that even at 11°S the NBC and interior transports in ORCA REF counteract.

Another interesting point is, that the NBC variability is resembled pretty well by using only equatorial forcing. Equatorward of 5°S the variations of the NBC in ORCA REF are fully reproduced by ORCA EQ and at 11°S the fluctuations have still the same phases like in the reference run, but much weaker amplitudes. This goes along with the findings from the integrated transports and the horizontal velocity patterns discussed in Fig. 4.4. The interior variability at this latitude shows more differences and seems to originate also from subtropical or basin wide subtropical wind-driven processes.

Thus, the conclusion is, that wind-driven variability at the equator explains almost all NBC variations between the equator and the NBC bifurcation around 11°S. This includes the decadal trend, found in both, the western EUC and the NBC in runs with interannual wind-forcing, and hence questions the influence of any thermohaline driven variability at the equator. However, there are studies which propose interactions with the thermohaline circulation at the equator and thus, in the next section the effects of MOC variability will be studied.

4.3   Effects of MOC variability

In some contrast to the overriding importance of the wind-induced variability found
for the variability of the shallow overturning, the EUC and the NBC, in the Hov-
moeller diagrams of Fig. 4.2 variability related to thermohaline variability can be
found, too, although with small amplitudes. The possible effect of MOC changes on
the equatorial circulation is via influencing the strength of the STCs: a strengthened
deep flow should force also strengthened northward return flow. If the northward
return flow in the upper approximate 300m is influenced, this might have conse-
quences for the equatorial upwelling rates and for the meridional heat transport.
An increased southward flow at depth is related to a strengthened northward heat
transport in the return flow and thus linked to a warming of the northern and a
cooling of the southern hemisphere. Such a dipole pattern has been found in the
observed SSTs (NOBRE & SHUKLA (1996), RIUZ-BARRADAS ET AL. (2000)) and
in coupled ocean-atmosphere models (DONG & SUTTON (2003), ZHANG & DEL-
WORTH (2005)) and is related to a shift in the wind-stress patterns, because the
ITCZ is found over the regions of warmest SSTs. An idealized model experiment
by YANG (1999) revealed a lag-correlation of 5 years between the variability of the
Labrador Sea Water formation and the SST dipole in the tropics. Model results
by BENTSEN ET AL. (2004) using the Bergen Climate Model confirm such a link
with a slightly longer time lag, if the ocean model is uncoupled to the atmosphere.
Thus, the decadal anomaly signals reproduced in the ORCA EQ run are locally
forced by wind in the equatorial region, but the question what causes the decadal
wind variability manifested in the NBC transports can not be clarified by this kind
of model experiment. So, the decadal wind-driven variability might results from a
change in the thermohaline circulation which forces or reduces upwelling and hence
ITCZ variability. From the viewpoint of coupled ocean-atmosphere reactions it is
thus worth to study the possible influence of the MOC on the equatorial circulation
in more detail. However, it is not possible to confirm, with the ocean-only models
used here, the possible link between MOC variability, SST and wind-fields due to
the restoring of the model SSTs to observed values and the wind-fields which are
prescribed as the surface boundary condition.

  Variability of the deep MOC is given by fluctuations of the NADW water formation.
The main sources for a renewal of NADW are the very localized convection sites in
the North Atlantic: the Greenland Sea north of Iceland, the Irminger Sea and the
Labrador Sea. While the convection north of Iceland gives the densest parts of the
NADW and the mid-depth water masses originate primarily from recirculation along
the fracture zones of the Mid-Atlantic-Ridge, the Labrador Sea Water (LSW) forms
the upper part of the deep water. Only a small amount of the dense waters formed
in the Arctic Seas leave this region through the narrow straits over relatively high
sills into the North Atlantic. Downstream the passages on their way southward these
waters are mixed with warmer and saltier waters from the North Atlantic Current
along the mid-Atlantic ridge. Estimates by LATIF ET AL. (2006) show that the
observed density fluctuations at the sills on the order of 0.02 kg/m^3 might lead to a
MOC change in the North Atlantic on the order of 1 Sv.

  Stronger variability is thought to be associated with the response of the ocean to a
varying NAO which triggers water mass formation in the Labrador Sea via heat loss

(EDEN & WILLEBRAND (2001), CURRY ET AL. (1998)). The variation of the LSW formation is on the order 10 Sv, based on observational data by MARSH (2000) and RHEIN ET AL. (2002). However, little is known about the dynamical response of the MOC transport apart from model studies. Ocean models forced by reanalysis fluxes (HÄKKINEN (1999), EDEN & WILLEBRAND (2001), BEISMANN & BARNIER (2004), BENTSEN ET AL. (2004)) consistently show an increase of the MOC at mid-latitudes by about 20% of its mean, from lowest values during the 1960s or early 1970s, to a maximum in the mid-1990s.

While transport anomalies of subarctic origin extend quite rapidly, albeit attenuated, to the equator by fast wave processes along the western boundary (GETZLAFF ET AL. (2005)), the effect of the ensuing, relatively small, changes in the equatorial MOC transport on the upper-layer tropical variability has remained controversial.

According to the previous findings, a sudden shut-down of the LSW formation should lead to a strong anomaly signal in the North Atlantic. In the experiment FLAME NOLAB such a shut-down is simulated by preventing Sea Surface Temperatures below 5°C in the region of the Labrador Sea, thus effectively eliminating deep winter convection and the renewal of LSW. This model setup differs from the more idealized configurations used e.g. by YANG (1999) and include a realistic topography which influences the wave propagation to the equator and hence the response timescale there. As the northern boundary of FLAME NOLAB does not permit for any variability from the regions north of the overflows, the effects of LSW variability can be studied in isolation.

4.3.1   Response to MOC changes in an idealized configuration

The adjustment to a new equilibrium state after a perturbation of the basin-scale circulation and the role of oceanic waves for this process have been investigated both in idealized models (KAWASE (1987), JOHNSON & MARSHALL (2002)) and in models with realistic geometry (DÖSCHER ET AL. (1994), CAPOTONDI (2000)). The discussion here will focus on the effect of the adjustment process on the decadal variability in the equatorial current regime, i.e. the process of wave propagation itself is not the interesting point here.

The temporal characteristics and spatial patterns of the zonally-integrated transports in the Atlantic are provided in Figs. 4.10 and 4.11. In both figures the resulting MOC anomalies relative to the climatological initial conditions from FLAME NO-LAB are shown. Fig. 4.10 shows the anomaly signals in the meridional-vertical plane and Fig. 4.11 gives the anomaly signal at 1000m depth as a function of time.

Figure 4.11 indicates a very fast response to the step-function change in the subpolar buoyancy forcing: after 2-3 years the anomaly signal has reached 40°N (a result also found in previous studies e.g. by EDEN & WILLEBRAND (2001)) and is after that communicated more rapidly towards the tropics by coastally-trapped waves (see e.g. GETZLAFF ET AL. (2005), their Fig. 3). In the fourth year after the cessation of convection, a peak signal of 1 Sv reduction of the southward transport arrives and crosses the equator at depth. The corresponding MOC transport anomalies in the meridional-vertical plane (Fig. 4.10a) reveal a basin-scale pattern, with a reduction of cross-equatorial transports of about half the reduction in the meridional transports at 40°N. This initial, fast pulse in the MOC gives way to a relaxation phase
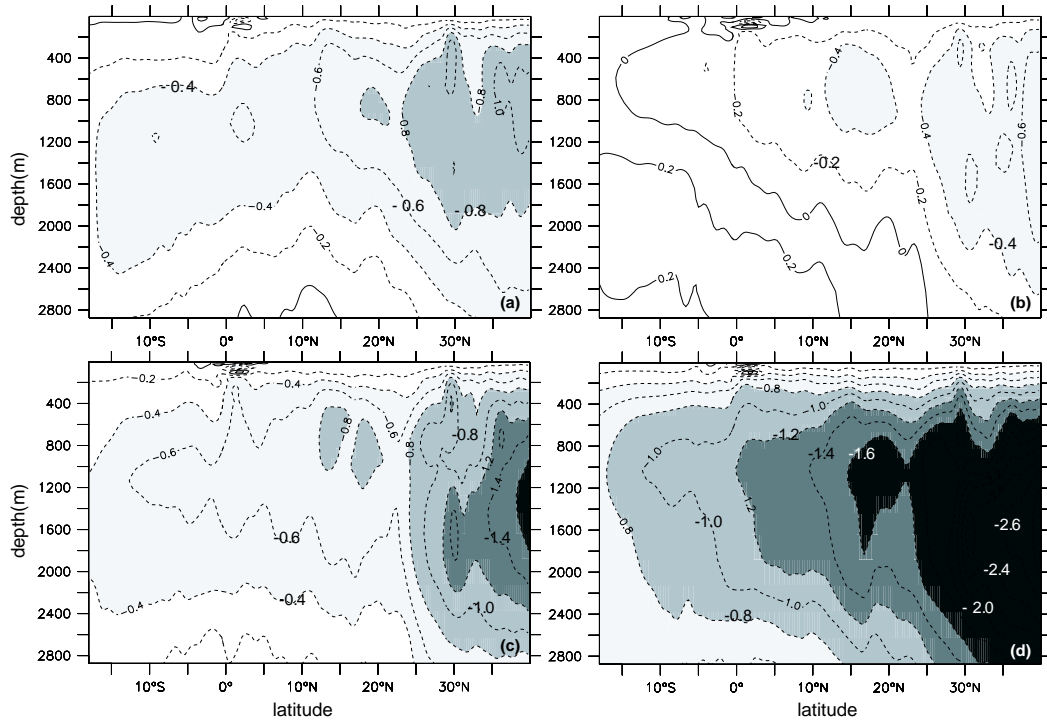
Figure 4.10: Reaction of the MOC in the tropical Atlantic to a cessation of Labrador Sea Water formation as simulated in FLAME NOLAB after: a) 3 years, b) 5 years, c) 9 years and d) 15 years. Negative values indicate a weakening of the deep south-ward transport of NADW and a concomitant weakening of the zonally integrated northward transport in the upper 1000m.

in the tropics, with a drop in the transport anomalies most strongly in the southern hemisphere (Fig. 4.10b), followed by a more gradual increase on a decadal time scale (Figs. 4.10c, d).

Comparison of these results with the complementary experiments (RESP 1/3) of GETZLAFF ET AL. (2005), indicates a rather robust temporal behavior in the main characteristics of the tropical MOC response, i.e., an initial peak after 3-4 years followed by a O(5 year)-relaxation phase. It should be noted, that their individual realizations demonstrate that the details of transport time series are affected by the superimposed internal variability. This also includes the phase of the signal: an initial, significant change in transport may already be felt in the tropics after 2 or only after 5 years. However, the signal's amplitude during the first response in year 3 (Fig. 4.10a) is of small amplitude near the surface, the main signal is around 1200m depth. During the long term response also the change in the upper surface layer becomes stronger, even if the main reduction of the MOC is around 1000m. Thus, the MOC effect on the equatorial circulation might be visible on decadal to inter-decadal timescales and acts as a small modulating effect.
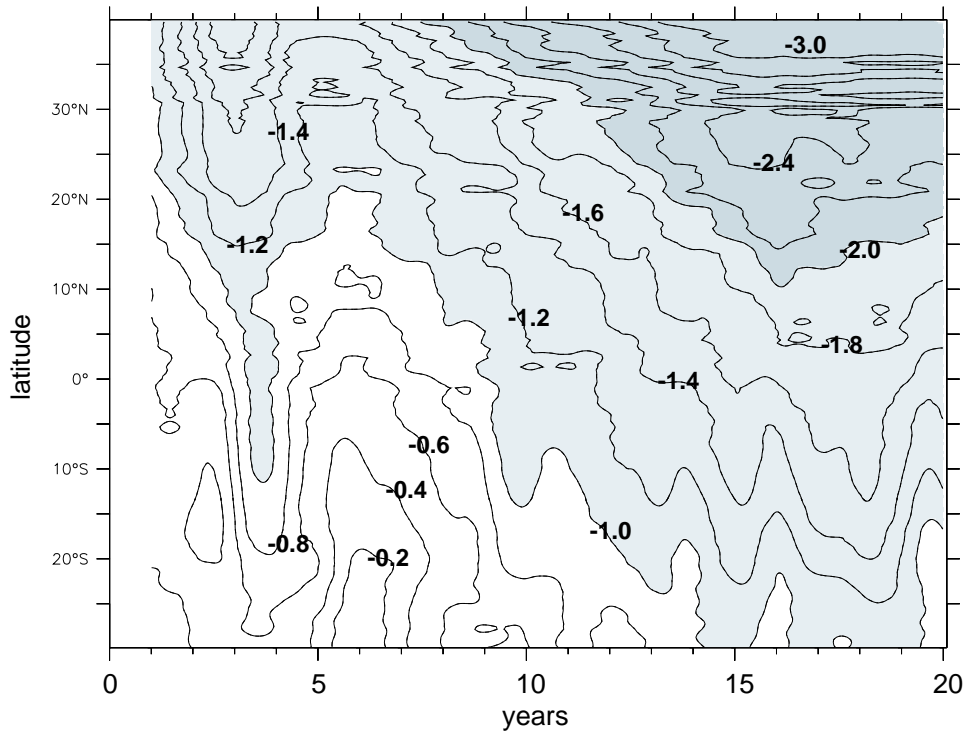
Figure 4.11: Meridional propagation of the MOC signal in 1000m following a cessation of LSW formation (FLAME NOLAB).

4.3.2 Patterns of MOC variability in more realistic configurations

The effect of the Labrador Sea variability on the MOC fluctuations can also be studied in the sensitivity experiment ORCA LS where interannual forcing is used over a meridional strip covering the Labrador Sea and the corresponding latitudes of the North Atlantic while the rest of the ocean is forced climatological. This allows for a determination of the influence radius of the variability generated in the Labrador Sea. If all variability is generated in this region, there should be no strong MOC anomaly differences between the amplitudes of ORCA HEAT and ORCA LS. If the variability of the Labrador Sea Water formation rate has an influence on the MOC return flow at the equator and in consequence influences the upwelling and SST, this should be visible in the ORCA LS experiment, too.

The LSW variations and the corresponding MOC anomalies (in 1000m depth) for ORCA HEAT and ORCA LS are shown in Fig. 4.12. The connection between LSW formation, deep MOC changes an their possible links to the equatorial circulation are represented in a similar manner in these experiments. A comparison of the Labrador Sea Water formation rates (Fig. 4.12a) reveals a quite similar phase and amplitude behavior between ORCA REF, ORCA HEAT and ORCA LS. The amplitudes of ORCA HEAT in most cases are stronger, those in ORCA LS mostly are somewhat weaker than the corresponding values of the ORCA REF-run. Stronger differences between the runs only occur at the beginning of the nineties, where ORCA REF shows strong LSW variability which is only partly reproduced by ORCA

HEAT and ORCA LS. These differences are linked to the enhanced variability in the freshwater fluxes from the Arctic during this time span, but the overall temporal behavior indicates only a modulating influence of the forcing north and south of the Labrador Sea onto the LSW formation rates. However, the triggering effect for the MOC-changes, as shown in FLAME NOLAB as well as notable in FLAME HEAT (see GETZLAFF ET AL. (2005), their Fig. 3), is clearly visible in the Hovmoeller diagrams in Fig. 4.12b and c.

The amplitudes of the MOC variability show an interhemispheric structure very similar to the patterns found for the idealized FLAME NOLAB-experiment (Fig. 4.11): the anomalies have the same sign in each hemisphere and reach the equatorial region after 3-5 years. The signals amplitude weakens equatorward and the strongest amplitudes are confined to the subpolar gyre. The reaction south of the equator shows some lag to the variability on the northern hemisphere, a phenomenon referred as the "equatorial buffer" and discussed for example in KAWASE (1987) or JOHNSON & MARSHALL (2002).

The buffer effect is linked to the fact that the equator is acting as waveguide, so no wave signal form the north (i.e. the first, fast response found in FLAME NOLAB) is able to cross the equator but is carried eastward along the equator as an equatorial Kelvin wave. This wave reflects at the eastern boundary into boundary Kelvin waves and westward propagating Rossby waves which adjust the ocean interior from the east. Thus, the first signal arriving on the southern hemisphere off the equator is linked to the fastest equatorial Rossby wave modes. The higher wave modes in initiated by the MOC signal create the decadal variability signal visible in Fig. 4.12b and c. The wave propagation mechanism and the effect of the equatorial buffer (which leads to a lag of 2-3 years between northern (10°N) and southern (10°S) anomalies) is more clearly visible in ORCA LS, but the Rossby wave response at the equator is strong in both experiments. Thus, directly at the equator the decadal variability introduced by the MOC leads to variations on short timescales of 1-2 years.

The amplitudes of the signals in Fig. 4.12b and c do not differ strongly in the North Atlantic north of 40°N but south of this latitude the amplitudes in ORCA LS are diminished by about half of the values from ORCA HEAT. This indicates the LSW variability to be the main generation mechanism for the decadal MOC variability in the ORCA experiments, too. For the amplitude of the signal propagating to the equator also interannual variability off the Labrador Sea region is important. It is also interesting to note, that in ORCA HEAT the interannual and fast signals are emphasized and in ORCA LS the decadal modulation is more obvious.

4.3.3   Influences on the tropical circulation

Up to this point the discussion focused on the connection between MOC variability, its origins and the propagation of MOC anomaly signals. However, as discussed for Fig. 4.10 and from the viewpoint of mass conservation, the variations are not confined to a certain depth and the variability of the deep southern export forces a reaction of the northward return flow, too. This is illustrated in Fig. 4.13a and b for ORCA LS. The return flow reacts with a time lag of approximately 6 years to the variations in the North Atlantic. The response time scale is somewhat longer than
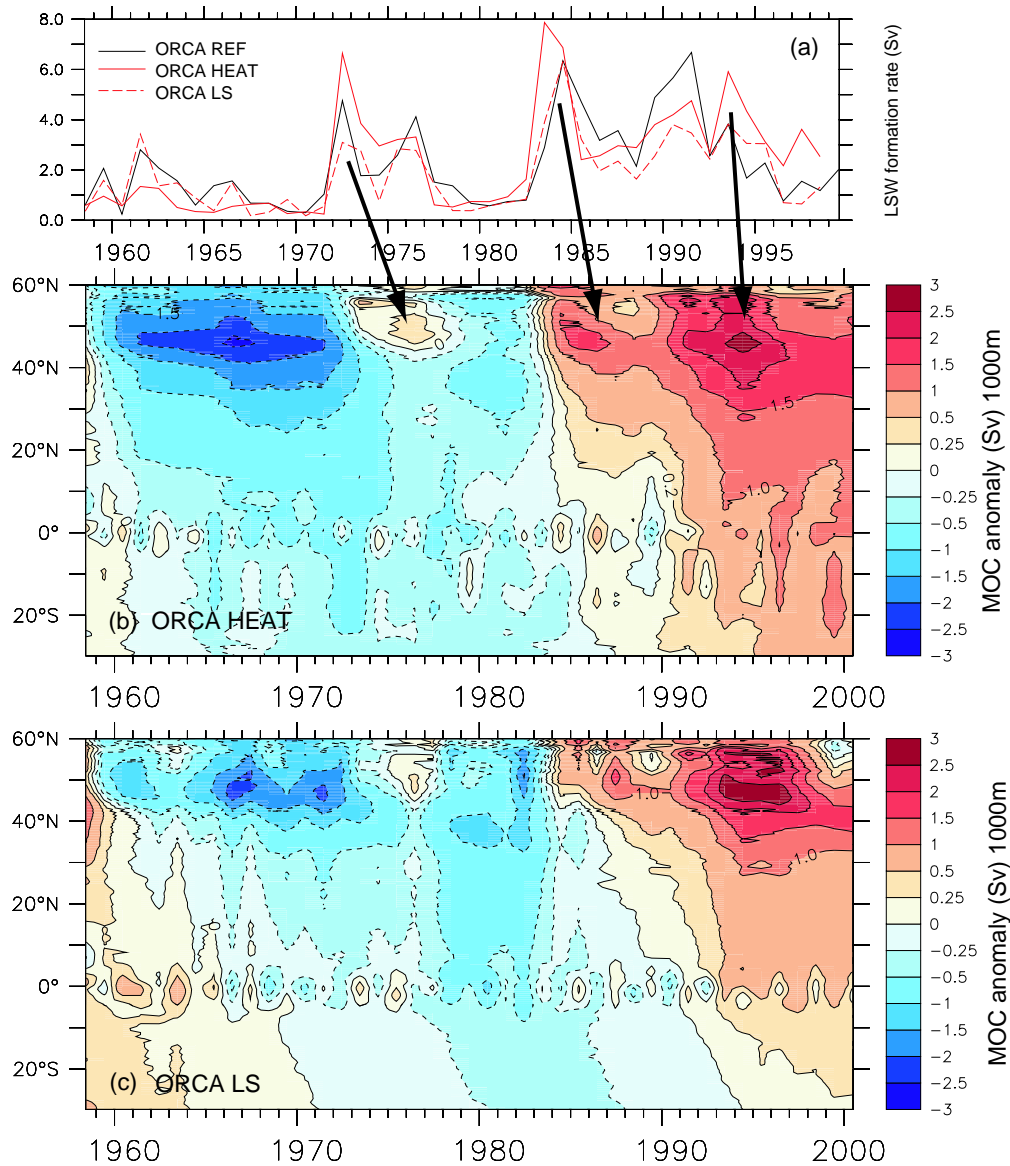
Figure 4.12: Interaction of LSW variability (a), deep MOC variations in 1000m and their propagating structure in ORCA HEAT (b) and ORCA LS(c). The peaks of LSW variability are similar when comparing ORCA REF, ORCA HEAT and ORCA LS. Larger differences occur only in the late nineties. Each LSW peak can be associated with an MOC variation further south with a lag of about 2 years. Enhanced variability at the equator is visible both in ORCA HEAT and ORCA LS.

indicated by the idealized FLAME NOLAB-experiment. This can be attributed to the differences in the forcing of both experiments or to the different horizontal discretization used in the two models: while ORCA is implemented on a Arakawa C-grid, FLAME uses a B-grid where boundary waves are simulated insufficiently well. However, the decadal variability found for the deep fluctuations is visible in shallower depths to and has a peak-to-peak amplitude of 0.5 Sv over the top 300m layer. That, the longer time scales are influenced by MOC behavior, in some contrast to what has been found from the analyses of the wind-driven fluctuations.

Interestingly, the NBC in ORCA LS (see Fig. 4.13c) also shows the decadal modulation signal found for the MOC and the return flow. This is surprising because compensational behavior between interior transport variability and boundary current transports has been found also in ORCA HEAT when discussing the influence of the wind-driven variability. But this coherent behavior in ORCA LS clearly shows a limitation of the MOC-related anomaly signal to the western boundary current as found in the FLAME HEAT experiments (see Fig. 4.8b). When comparing the decadal variability of the MOC signal to the NBC time series discussed in Fig. 4.9 it obviously covers the same time-span like the transport minimum phase found in ORCA REF , ORCA EQ and ORCA WIND. This corroborates the idea, that the shallow variability found in Fig. 4.2 has something to do with the decadal variability found in ORCA LS.

Especially the NBC minimum phase during the years 1978-1985 and the corresponding northern STC strengthening during these years go along with this idea: the weak thermohaline signal connected to the LSW formation and found to be confined to the western boundary weakens the northward NBC transport while the interior transport is strengthened. The latter signal is stronger than the NBC anomaly and a consequence of the Rossby wave adjustment process introduced by the MOC signal (CAPOTONDI ET AL. (2005)). This leads to the strengthening signal of the zonally integrated transport visible in Fig. 4.2a,b,c and f.

Thus, the decadal STC fluctuations discussed at the beginning of this chapter can not be explained by wind-forcing only. There must be an interaction between the wind-driven and the thermohaline induced circulation changes which can not be separated in detail in the used configuration of the model. This is because the interannual forcing at the equator, which clearly pulls the STCs as revealed by the ORCA sensitivity studies, already includes the effects of the MOC signal which has some influence on the longterm variability at the equator.
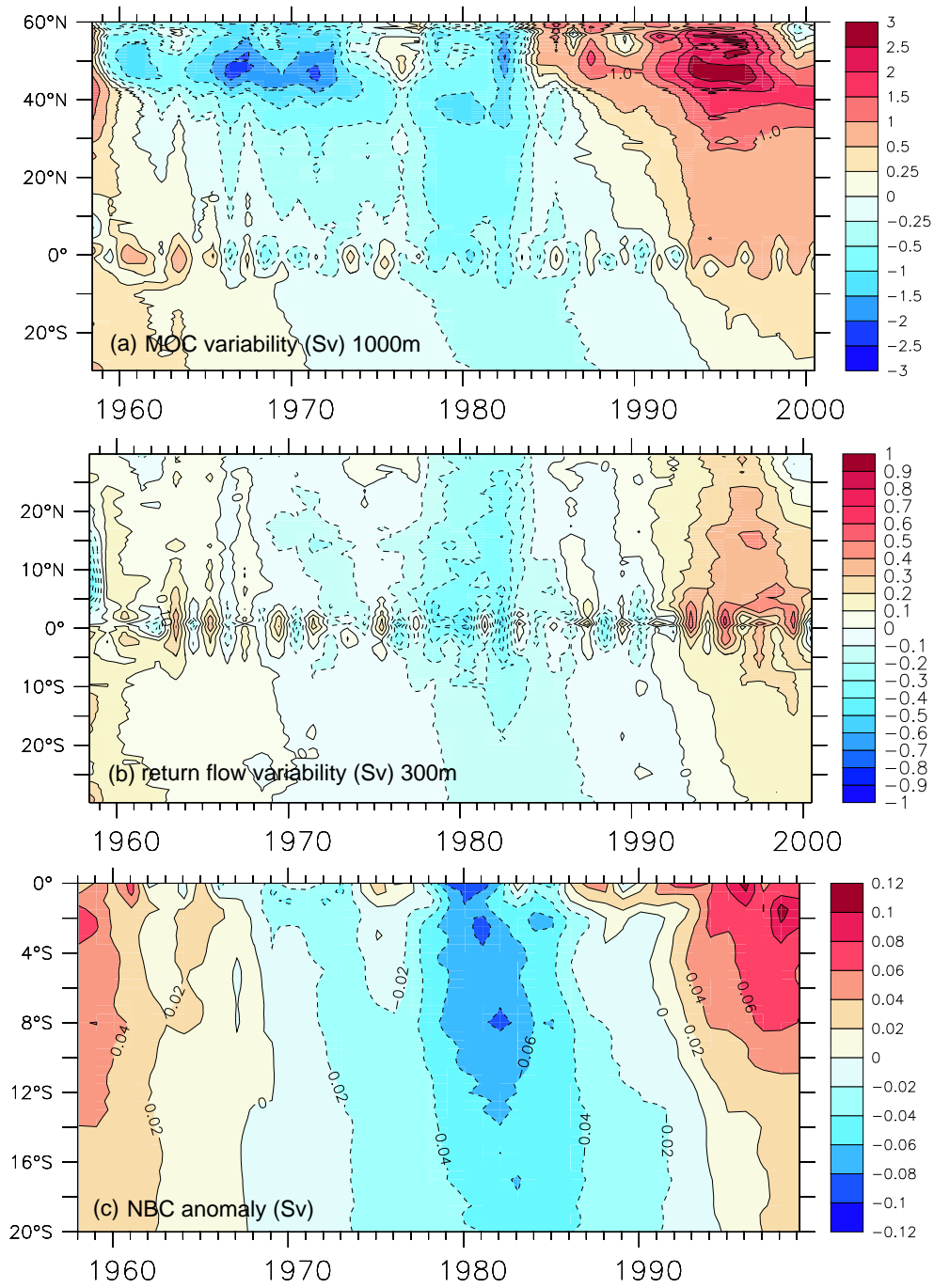
Figure 4.13: Interaction of deep MOC, return flow and NBC: a) MOC variability in Sv from ORCA LS in 1000m depth, b) variability of the return flow in Sv in ORCA LS in 300m depth and c) transport anomaly of the NBC along the western boundary in Sv. The temporal coherence between response of the return flow and the NBC is obvious. Comparison between deep MOC and return flow anomaly shows a lag of about 5 years between anomalies north of 40°N and corresponding anomalies at the equator.

4.4   Conclusions and discussion

In this chapter the interannual and decadal variability which is linked to the STCs and the MOC in the tropical Atlantic was studied. The use of two different ocean models and a host of sensitivity experiments allowed for insight into the wind driven and thermohaline forced mechanisms leading to longer term variability at the equator. As a main result it turned out, that interannual variability is primarily forced by wind variations in the equatorial region between 5°N and 5°S. The decadal modulation of the STC transports was found to be an effect of the MOC and can be related to the variability of the meridional overturning which is triggered in both models by the formation of Labrador Sea Water.

The wind-forced variability patterns (Fig. 4.4) revealed the importance of the interior pathway variations for the equatorial current variability on interannual timescales. For both models the reference runs showed compensation tendencies for the transport anomalies of the shallow western boundary current (the NBC) and the transports fluctuations in the ocean interior. This finding is equivalent to what is observed for the STC variability in the tropical Pacific (Lee & Fukumori (2003), Capotondi et al. (2005)) but has not been discussed as a mechanism acting also in the Tropical Atlantic.

As the ORCA sensitivity runs indicate, the interannual STC variability can be reproduced by using only interannual forcing in a small equatorial band or interannual wind forcing only. The response to the wind changes is a basinwide process and it is thus not remarkable to find the strongest variations to be manifested in the interior transports. These anomalies have the potential to change or fully reverse the variations which are carried by the boundary current transport. This has some consequences on the idea of STC variability: at least at interannual timescales one can not imagine the STC as a consistently varying cell. Every STC branch underlies different variability mechanisms which add up and form no coherent pattern.

The MOC is found to modulate the interannual variability on decadal time scales in the tropical Atlantic. The variability of the deep water export is determined mainly by the Labrador Sea Water formation rate and is represented in a variation of the return flow at the equator about 5 years later. This effect has been found in many idealized studies (Yang (1999), Johnson & Marshall (2002)) and was confirmed by analyzing a climatological FLAME sensitivity experiment where the Labrador Sea Water formation was prevented. The anomaly signal associated with the MOC fluctuations showed a coherent behavior through the whole Atlantic basin south of 50°N and leads to a decrease in the return flow from the seventies to nineties and a strengthening of it during the nineties, as another sensitivity experiment (ORCA LS) revealed. The anomaly structures between the idealized FLAME case and the MOC anomalies in more realistic configurations of both models showed similar temporal and basin wide structures, so the conclusion was that in both models the same mechanism is apparent. The decadal modulation was overlaid also on the variability of the NBC from the wind driven experiments in ORCA and FLAME.

Interestingly, the same decadal modulation patterns as discussed here can also be found in the regional model study of Kröger et al. (2005). They used the same heat flux and wind stress fields as the FLAME model but the surface boundary conditions are calculated by an advective atmosphere mixed layer model (Seager

ET AL. (1995)) allowing for some interaction between the ocean and the overlying atmosphere. Their results for experiments without equatorial forcing reveal decadal scale SST anomalies of O(0.1°C) with strongest amplitudes occurring in mid-basin around 20°W during the seventies to nineties even without interannual wind forcing. Combing these findings to the results of the ORCA and FLAME runs of this work, it can be concluded that, the MOC variability seems to influence also the wind variability via changing the meridional heat transfer rates and causing a shift of the ITCZ. However, the signal of the MOC variability near the surface is too small in the uncoupled ocean models investigated here, to be visible in the near-surface transports, the upwelling rate or in the SSTs. In consequence, there was no evidence found for a SST-dipole mode which is directly driven by the oceanic variability as suggested by YANG (1999). Such a pattern may arise from changes in the atmospheric circulation due to the oceanic heat transport changes but this aspect can not be studied using an ocean-only model. Coupled simulations of the tropical ocean are needed to fully resolve and understand the interactions between the ocean and atmosphere.

As a second consequence of the MOC variability for the tropical current system evidence for a temporarily existing northern STC cell has been found. In the long-term mean this circulation cell does not exist but during the years 1980-1985 all ORCA and FLAME runs with interannual wind forcing reveal such a northern STC cell (nSTC). When comparing this finding to the ORCA sensitivity run ORCA LS (Fig. 4.12) the nSTC occurs during the phase of minimum MOC transport and hence minimum cross-equatorial return flow transport. From studies by FRATANTONI ET AL. (2000) and JOCHUM & MALANOTTE-RIZZOLI (2001) it turned out, that the asymmetry of the Atlantic STCs occurs only due to the presence of the MOC return flow; if the return flow is weakened strong enough (what seems to be the case during 1980-1985), the nSTC develops and enables a zig-zag pathway between the northern subtropics and the equator as visible in Fig. 4.4. How strong influence of this additional northern flow for the variability at the equator is and how this compares to the variations introduced by the southern hemispheric STC has not been investigated here but is an issue for further Lagrangian studies.

5   Summary

The goal of this work was to contribute to the understanding of the mechanisms influencing the upwelling regions and variability in the tropical Atlantic. The study focused on the analysis of pathways into the tropical upwelling regions and on mechanisms influencing the upwelling on interannual to decadal timescales by changing the transport of the equatorial currents. The complex current system in the vicinity of the equator is overlaid by the meridional overturning cells of the STCs and the MOC introduces fluctuations on several timescales reaching from the subseasonal fluctuations associated with the instability processes to (mulit)decadal variability introduced by changes in the deep water export across the equator. With the help of two ocean models the different variability processes were studied. A high-resolution version (1/12°) of the FLAME Atlantic model enabled the investigation of short temporal and small spatial structures of the tropical instability waves, while a host of lower resolution experiments based on FLAME 1/3° and the global ORCA05-configuration (1/2° resolution at the equator) allowed for several sensitivity studies.

  Comparison of both models and observational data showed that only the high-resolution FLAME 1/12°-model was able to reproduce the details of the zonal current system like the off-equatorial undercurrents NEUC and SEUC. The 1/3°-FLAME-version and the ORCA experiments reproduced the main features of the circulation like the boundary current system and the EUC in sufficient detail to study longer term variability of the STCs.

Mean pathways and mesoscale variability

The analysis of the annual cycles in both models indicated a large range of seasonal to annual variability which depended not only on the model but also on the horizontal resolution. Comparisons between the different models and data from observations by SCHOTT ET AL. (2003) at 35°W hint at an important role of instability processes for the representation of the annual cycle by adding some statistical variability to the mean annual cycle. For the EUC in the models this effect was suggested to lead to a modulation of the annual cycle but also to an incoherent behavior between the western and mid- to eastern-basin EUC. Using results from the 1/12°-run the NEUC was found to be modulated significantly by the instability processes during its annual

cycle and the SEUC was found to be dominated by the influence of the instabilities by showing irregular temporal behavior overlaid on a weak mean current.

The investigation of the sources and sinks of the mean current system was carried out mainly by the use of Lagrangian analysis allowing the tracking of the pathways of watermasses instead of describing them along sections. The method was first applied to the Equatorial Undercurrent (EUC) which was studied also by other authors (Blanke et al. (1999), Hazeleger et al. (2003), Hazeleger & de Vries (2004)), but in all cases in models with rather low horizontal resolution and a less detailed zonal current system. The analysis demonstrated the importance of small-scale features and the need for high resolution models for the seasonally varying supply to the EUC: while the 1/3°-version of FLAME showed a small but clear exchange window between subtropics and tropics between 10°W and 20°W this connection is disturbed in the 1/12°-model by the eastward SEUC flow. The trajectories were found to make several zonal excursions through the different branches of the SEC and the SEUC until ending up in the EUC. The upwelling of the EUC ranges seasonally between 50% to 70% of the total EUC transport and was found to occur mainly in the southern hemisphere and seasonally along the African coast. The remaining part of the waters was found to recirculate into the SEC and from there into other equatorial zonal currents. Part this water was found to be trapped longer than four years in the tropics without getting upwelled.

Upwelling along the doming circulations of the Guinea Dome and the Angola Gyre was thought to be supplied by the waters of the NEUC and SEUC flowing eastward off the equator around 4°N/S (Voituriez (1981), Tsuchiya (1986)) and feeding into the domes near the eastern boundary. Both regions show low subsurface oxygen contents indicating waters which were not recently ventilated. The sources of the NEUC and SEUC and their connection to the off-equatorial upwelling has been studied here by Lagrangian analysis as well. Complicated zig-zag pathways of the waters forming the off-equatorial undercurrents have been found: the NEUC is fed seasonally by the NBC retroflection and throughout the year by recirculating EUC and nSEC waters. The SEUC never showed a connection to the western boundary current and is maintained only by recirculating EUC and sSEC waters. This indicated that the equatorial zonal currents show strong interactions which allow for a mass exchange between them.

The mechanism generating a connection between the EUC and the off-equatorial undercurrents is related to the occurrence of tropical instability waves. In mid-basin the waves lead to the formation of vortices (Menkes et al. (2002), Foltz & Carton (2004)) which propagate, intensify westward, and enable a mass transport from the EUC into the different SEC bands and from there towards the NEUC and SEUC. The model trajectories show such zig-zag pathways clearly and reveal seasonally dependent transition zones between the several zonal current bands. To confirm this hypothesis for a transport mechanism, most of the wave signal was averaged out by calculating monthly means and the trajectory calculation was re-done with these input fields. This led to a significant change in the supply pathways of the undercurrents: while the NEUC was found to be fed now only by the NBC, the SEUC waters recirculated mainly around their launch positions and showed strongly reduced input from the EUC. The inflow from the EUC was likely due to wave residuals in the monthly mean velocities.

In studying the connections between the NEUC/SEUC and the off-equatorial up-welling regions, different pathways than those suggested by VOITURIEZ (1981) and refined by STRAMMA ET AL. (2004) have been found: for the Guinea Dome the western NEUC west of 23°W plays a major role in watermass supply. The trajectory calculations revealed a meridional transfer of waters by instability vortices (as found for the sources of the NEUC and SEUC) from the western NEUC into a seasonally occurring deep northern NECC branch which transfers the water into the dome region. This pathway of supplying the Guinea Dome is important for the watermass characteristics in the dome region: a comparison between 1/3°-FLAME (which does not resolve the NEUC) and 1/12°-FLAME points out that if the NEUC is missing, the waters found in the Guinea Dome originate mainly from the northern (instead of the southern) hemisphere. With respect to the unrealistic representation of the Angola Gyre at the models' southern boundary the connection between the southern dome and the SEUC could not be fully explored.

The upwelling patterns of the NEUC also shows connections to the equatorial upwelling and the coastal upwelling along Africa. The SEUC waters mainly upwell along their way southward to the Angola Gyre. However, the total upwelling rates are low: 20-35% of the total eastward transports of the NEUC and only 10-20% of the SEUC transports reach the surface layers. The remaining waters recirculate in the inner tropics between the different zonal currents for longer than four years similar to what was found for the EUC waters. This long subsurface recirculation explains the low oxygen contents along the currents and in the thermal domes.

Summarizing the findings from the analysis of the mean circulation it was shown by the help of Lagrangian analysis in the 1/12°-model that instability waves and vortices in the inner tropics are of strong importance in both sustaining the mean and variability of the NEUC, SEUC and the westward SEC bands in between. The results from an energy cycle study by JOCHUM ET AL. (2004a), indicating towards a role of the eddy kinetic energy of the waves in sustaining the off-equatorial currents, was confirmed in this work by the finding that the tropical instability waves generate eddies which account for a mass transfer between the different zonal currents. This zig-zag pathway through the zonal currents was found to be the only source of the SEUC and also to contribute to the sources of the NEUC which is fed seasonally from the western boundary current.

Effects of thermohaline and wind-driven variability

The variability of the shallow tropical currents on interannual and decadal timescales is driven both by thermohaline and wind-driven fluctuations. Both mechanisms possibly interact but are studied first in separation. Wind variability was found to be the major driving mechanism of current fluctuations in the tropics also on interannual and decadal time scales as experiments with different forcing setups both in the FLAME models and the ORCA runs suggest. The fluctuations of the two ocean models resemble each other concerning the variability of the tropical gyre and the structures of the shallow overturning circulation.

The strongest wind-driven circulation changes was found in the vicinity of the equator, a result in accordance with other modeling studies like KRÖGER ET AL. (2005). The wind changes cause a variation of the so-called tropical cells (TCs)

which are directly forced by the Ekman divergence at the equator. These cells were shown to have a minor influence on the ventilation of the equatorial thermocline (HAZELEGER ET AL. (2001)). The TCs were found to exist mostly in the western basin in the FLAME models and more in the mid and eastern basin in ORCA. This incoherent behavior led to differences in the EUC interannual and decadal variability between both models which are manifested in different recirculation pathways and different eddy-driven flow components. A comparison of various ORCA experiments revealed the EUC changes to be forced directly by the tropical winds.

In contrast to the model-to-model differences concerning the zonal current system, the variability of the meridional current variability has been found to be similar in both models. The changes of the western boundary current are found to be incoherent between the tropics and the subtropics and dominated by the wind-driven variability. This is due to a partial counteracting behavior between the boundary flow and the interior transports in the tropical Atlantic. Such a partial compensation has been described only for the Pacific Ocean (LEE & FUKUMORI (2003), CAPOTONDI ET AL. (2005)). The major consequence of this finding is that the STC can not be imagined as a coherently varying cell on interannual time scales.

The interannual time series of nearly all experiments from ORCA and FLAME showed a decadal modulation of the EUC and NBC. With the help of two different sensitivity runs it was possible to link this modulation to deep water export variations triggered by the Labrador Sea Water (LSW) formation rate. Such a link was proposed by YANG (1999) and discussed as a possible long term variability mode of the tropical SSTs. The results from the sensitivity runs revealed the LSW anomaly signal propagating towards the equator as a boundary wave. At the equator it triggers different Rossby wave modes adjusting the circulation on very short (about 3-5 years) and decadal to multi-decadal timescales (more than 15 years). However, only the latter signal was found to have some minor influence on the near-surface: this modulating effect was found to be small: a MOC signal of O(1Sv) led to an equatorial signal of only 0.2 Sv amplitude with negligible effects on the SSTs. Interestingly, the MOC-related weak decadal variability was found to be limited to the western and mid basin tropical Atlantic. This implies, that the thermohaline signal does not influence the current variability in the eastern basin and the corresponding upwelling processes.

A major limitation of the current model setup concerns the effect of the different variability mechanisms on the SST. Using a thermal boundary condition based on a bulk formulation (as in the ORCA runs) or a linearized form (as in FLAME) involves an interaction between SST anomalies and the air-sea heat flux. With a prescribed atmospheric state as given reanalysis products, this implies an effective damping of SST anomalies evolving through changes in the oceanic circulation. On the other hand, if there is an effect of the oceanic variability on the atmospheric circulation this effect is represented by the reanalysis product used for the surface boundary condition. To fully understand the effects of oceanic anomalies on the atmospheric circulation coupled models are needed.

Bibliography

ADCROFT, A., HILL. C & MARSHALL J., 1997. Representation of topography by shaved cells in a height coordinate ocean model. *Mon. Weather Rev.*, **125**, 2293–2315.

ARAKAWA, A., 1966. Computational design for long-term numerical integration of the equations of fluid motion: Two-dimensional incompressible flow. Part I. *J. Computational Physics*, **1**, 119–43.

BARNIER, B., SIEFRIDT L. & MARCHESIELLO P., 1995. Thermal forcing for a global ocean circulation model using a three-year climatology of ECMWF analysis. *J. Mar. Systems*, **6**, 363–380.

BECKMANN, A. & R. DÖSCHER, 1997. A method for improved representation of dense water spreading over topography in geopotential-coordinate models. *J. Phys. Oceanogr.*, **29**(11), 581–591.

BEISMANN, J. O. & B. BARNIER, 2004. Variability fo the meridional overturning circulation of the North Atlantic: sensitivity to the overflow of dense water masses. *Ocean Dyn.*, **54**(1), 701–720.

BENTSEN, M., H. DRANGE, T. FUREVIK & T. ZHOU, 2004. Simulated variability of the Atlantic meridional overturning circulation. *Clim. Dyn.*, **22**, 701–720.

BLANKE, B., M. ARHAN, G. MADEC & S. ROCHE, 1999. Warm water pathways in the Equatorial Atlantic as diagnosed with a general circulation model. *J. Phys. Oceanogr.*, **29**, 2753–2768.

BLANKE, B. & S. RAYNAUD, 1997. Kinematics of the Pacific Equatorial Undercurrent: An Eulerian and Lagrangian approach from GCM results. *J. Phys. Oceanogr.*, **27**, 1038–1053.

BÖNING, C. W. & M. D. COX, 1988. Particle dispersion and mixing of conservative properties in an eddy-resolving model. *J. Phys. Oceanogr.*, **18**(2), 320–338.

BÖNING, C. W. & J. KRÖGER, 2005. Seasonal variability of deep currents in the equatorial Atlantic: a model study. *Deep–Sea Res.*, **52**(1), 99–121.

BÖNING, C. W., M. RHEIN, J. DENGG & C. DOROW, 2003. Modeling CFC inventories and formation rates of Labrador Sea Water. *Geophys. Res. Letters*, **30**(2), 1050.

BOURLES, B., M. D'ORGEVILLE, G. ELDIN, Y. GOURIOU, R. CHUCHLA, Y. D. PENHOAT & S. ARNAULT, 2002. On the evolution of the thermocline and sub-thermocline eastward currents in the equatorial Atlantic. *Geophys. Res. Letters*, **29**(16), 1785, doi:10.1029/2002GL015098.

BOURLES, B., R. L. MOLINARI, E. JOHNS, W. D. WILSON & K. D. LEAMAN, 1999. Upper layer currents in the western tropical Atlantic (1989-1991). *J. Geophys. Res.*, **104**(C1), 1361–1375.

BOYER, T. P. & S. LEVITUS, 1997. Objective analyses of temperature and salinity for the world ocean on a 1/4 degree grid. *Technical Report*, NOAA Atlas NESDIS 11, U.S. Gov. Printing Office, Washington, D.C.

BRANDT, P. & C. EDEN, 2005. Annual cycle and interannual variability of the mid-depth tropical Atlantic ocean. *Deep–Sea Res.*, **52**(2), 199–219.

BRANDT, P., F. A. SCHOTT, C. PROVOST, A. KARTAVTSEFF, V. HORMANN, B. BOURLES & J. FISCHER, 2006. Circulation in the central equatorial Atlantic: mean and intraseasonal variability. *Geophys. Res. Letters*, **33**(L07609), doi:10.1029/2005GL025498.

BRAUCH, J. P. & R. GERDES, 2005. Response of the northern North Atlantic and Arctic oceans to a sudden changes of the North Atlantic Oscillation. *J. Geophys. Res.*, **110**(C11), doi:10.1029/2004JC002436.

CAPOTONDI, A., 2000. Oceanic wave dynamics and interdecadal variability in a climate system model. *J. Geophys. Res.*, **195**(C1), 1017–1036.

CAPOTONDI, A., M. A. ALEXANDER, C. DESER & M. J. McPHADEN, 2005. Anatomy and decadal evolution of the Pacific Subtropical-Tropical Cells (STCs). *J. Climate*, **18**(9), 3739–3758.

COX, M. D., 1980. Generation and propagation of 30-day waves in a numerical model of the Pacific ocean. *J. Phys. Oceanogr.*, **10**, 1168–1186.

CUMMINS, P. F., G. HOLLOWAY & A. E. GARGETT, 1990. Sensitivity of the GFDL ocean general circulation model to a parameterization of vertical diffusion. *J. Phys. Oceanogr.*, **20**, 817–830.

CURRY, R. G., M. S. McCARTNEY & T.M. JOYCE, 1998. Oceanic transport of subpolar climate signals to mid-depth subtropical waters. *Nature*, **291**, 575–577.

CZESCHEL, L., 2004. *The role of eddies fo the deep water formation in the Labrador Sea*. PhD thesis, Christian-Albrechts-Universität zu Kiel.

DOI, T., T. TOZUKA, H. SASAKI, Y. MASUMOTO & T. YAMAGATA, 2006. Seasonal and interannual variations of oceanic conditions in the Angola Dome. In revision.

DOMMENGET, D. & M. LATIF, 2000. Interannual to Decadal variability in the Tropical Atlantic. *J. Climate*, **13**(4), 777–792.

DONG, B. W. & R. T. SUTTON, 2003. Variability of Atlantic Ocean heat transport and its effects on the atmosphere. *Ann. Geophysics*, **46**(1), 87–97.

DÖSCHER, R., C. W. BÖNING & P. HERMANN, 1994. Response of the circulation and heat transport in the North Atlantic to changes in thermohaline forcing in northern latitudes: A model study. *J. Phys. Oceanogr.*, **24**, 2306–2320.

DYNAMO GROUP, 1997. Dynamo Scientific Report. No. 3, Kiel.

EDEN, C. & J. WILLEBRAND, 2001. Mechanism of interannual to decadal variability of the North Atlantic circulation. *J. Climate*, **14**, 2266–2280.

ELMOUSSAOUI, A., M. ARHAN & A. M. TREGUIER, 2005. Model-inferred upper ocean circulation in the eastern tropics of the North Atlantic. *Deep–Sea Res.*, **52**, 1083–1120.

ENFIELD, D. B. & D. A. MAYER, 1997. Tropical SST variability and its relation to El Nino-Southern Oscillation. *J. Geophys. Res.*, **102**, 929–945.

FICHEFET, T. & M. A. MORALES-MARQUEDA, 1997. Sensitivity of a global sea ice model to the treatment of ice thermodynamics and dynamics. *J. Geophys. Res.*, **102**, 12609–12646.

FOLTZ, G. R. & J. A. CARTON, 2004. Tropical instability vortices in the Atlantic Ocean. *J. Geophys. Res.*, **109**(C03029), doi:10.1029/2003JC001942.

FONSECA, C. A., G. J. GONI, W. E. JOHNS & E. J. D. CAMPOS, 2004. Investigation of the North Brazil Current retroflection and North Equatorial Countercurrent variability. *Geophys. Res. Letters*, **31**, doi:10.1029/2004GL020054.

FRATANTONI, D., W. E. JOHNS, T. L. TOWNSEND & H. E. HURLBURT, 2000. Low-latitude circulation and mass transport pathways in a model of the tropical Atlantic Ocean. *J. Phys. Oceanogr.*, **30**(8), 1944–1966.

FURUE, R., J. P. MCCREARY, Z. YU & D. WANG, 2006. Dynamics of the Southern Tsuchiya Jet. In press.

GANACHAUD, A. & C. WUNSCH, 2001. Improved estimates of global ocean circulation, heat transport and mixing from hydrographical data. *Nature*, **408**, 453–457.

GARZOLI, S. L. & E. J. KATZ, 1983. The forced annual reversal of the Atlantic North Equatorial Countercurrent. *J. Phys. Oceanogr.*, **13**, 2082–2090.

GARZOLI, S. L. & P. L. RICHARDSON, 1989. Low-frequency meandering of the North Equatorial Countercurrent. *J. Geophys. Res.*, **94**, 2079–2090.

GENT, P. R. & J. C. MCWILLIAMS, 1990. Isopycnal mixing in ocean circulation models. *J. Phys. Oceanogr.*, **20**, 150–155.

GETZLAFF, J., C. W. BÖNING, C. EDEN & A. BIASTOCH, 2005. Signal Propagation related to the North Atlantic Overturning. *Geophys. Res. Letters*, **32**(L09602), doi:10.1029/2004GL021002.

GILL, A. E., 1982. *Atmosphere-Ocean Dynamics*, Vol. 30 of *International Geophysics Series*. Academic Press.

GOURIOU, Y. & G. REVERDIN, 1992. Isopycnal and diapycnal ciruclation of the upper equatorial Atlantic Ocean in 1983-1984. *J. Geophys. Res.*, **97**(C3), 3543–3572.

GRODSKY, S. A., J. A. CARTON, C. PROVOST, J. SERVAIN, J. A. LORENZZETTI & M. J. MCPHADEN, 2005. Tropical instability waves at 0°N, 23°W in the Atlantic: a case study using Pilot Research Moored Array in the Tropical Atlantic (PIRATA) mooring data. *J. Geophys. Res.*, **110**(C08010), doi:10.1029/2005JC002941.

GU, D. & S. G. H. PHILANDER, 1997. Interdecadal climate fluctuations that depend on exchanges between the tropics and the subtropics. *Science*, **275**, 805–807.

HAGEN, E. & R. SCHEMEINDA, 1984. Der Guineadom im ostatlantischen Stromsystem. *Beiträge zur Meereskunde*, **51**, 5–27.

HÄKKINEN, S., 1999. A simulation of thermohaline effects of a Great Salinity Anomaly. *J. Climate*, **12**(6), 1781–1795.

HANEY, L. R., 1971. Surface thermal boundary conditions for ocean circulation models. *J. Phys. Oceanogr.*, **1**, 241–248.

HAZELEGER, W. & P. DE VRIES, 2004. *Fate of the equatorial undercurrent in the Atlantic*, Chapt. 6, pp. 175–192. Elsevier Oceanographic Series.

HAZELEGER, W., P. DE VRIES & Y. FRIOCOURT, 2003. Sources of the equatorial undercurrent in the Atlantic in a high resolution ocean model. *J. Phys. Oceanogr.*, **33**, 677–693.

HAZELEGER, W., P. DE VRIES & G. J. VAN OLDENBORGH, 2001. Do tropical cells ventilate the Indo-Pacific equatorial thermocline? *Geophys. Res. Letters*, **28**, 2763–1766.

HENIN, C. & P. HISARD, 1987. The North Equatorial Countercurrent observed during FOCAL. *J. Geophys. Res.*, **92**, 3751–5758.

HOURDIN, F. & A. ARMENGAUD, 1999. The use of Finite-Volume Methods for atmospheric advection of trace species: part I: test of various formulationons in a general circulation model. *Mon. Weather Rev.*, **127**, 822–837.

HUA, B. L., F. MARIN & R. SCHOPP, 2003. Three-dimensional dynamics of the subsurface countercurrents and equatorial thermostad. Part I: Formulation of the problem abd generic properties. *J. Phys. Oceanogr.*, **33**, 2588–2609.

HÜTTL, S. & C. W. BÖNING, 2006. Mechanisms of decadal variability in the shallow subtropical-tropical circulation of the Atlantic Ocean: A model study. *J. Geophys. Res.*, **111**, doi:10.1029/2005JC003414.

INUI, T., A. LAZAR, P. MALANOTTE-RIZZOLI & A. BUSALACCHI, 2002. Wind stress effects on subsurface pathways from the subtropical to tropical Atlantic. *J. Phys. Oceanogr.*, **32**(10), 2257–2276.

ISHIDA, A., H. MITSUDERA, Y. KASHINO & T. KADOKURA, 2005. Equatorial Pacific subsurface countercurrents in a high-resolution global ocean circulation model. *J. Geophys. Res.*, **110**(C07014), doi:10.1029/2003JC002210.

JOCHUM, M. & P. MALANOTTE-RIZZOLI, 2001. Influence of the meridional overturning circulation on tropical–subtropical pathways. *J. Phys. Oceanogr.*, **31**(5), 1313–1323.

JOCHUM, M., P. MALANOTTE-RIZZOLI & A. BUSALACCHI, 2004a. A new theory for the generation of the equatorial subsurface undercurrents. *J. Phys. Oceanogr.*, **34**, 755–771.

JOCHUM, M., P. MALANOTTE-RIZZOLI & A. BUSALACCHI, 2004b. Tropical instability waves in the Atlantic ocean. *Ocean Mod.*, **7**, 146–163.

JOHNSON, E. S. & J. A. PROEHL, 2004. Tropical instability wave variability in the Pacific and its relation to large-scale currents. *J. Phys. Oceanogr.*, **34**, 2121–2147.

JOHNSON, G. C. & M.J. MCPHADEN, 1999. Interior pycnocline flow from the subtropical to the Equatorial Pacific ocean. *J. Phys. Oceanogr.*, **29**, 3073–3089.

JOHNSON, G. C. & D. W. MOORE, 1997. The Pacific Subsurface countercurrents and an inertial model. *J. Phys. Oceanogr.*, **27**(11), 2448–2459.

JOHNSON, H. J. & D. P. MARSHALL, 2002. A theory for the surface Atlantic response to thermohaline variability. *J. Phys. Oceanogr.*, **32**(4), 1121–1132.

KALNAY, E., M. KANAMITSU, R. KISTLER ET AL., 1996. The NCEP 40-year reanalysis project. *Bull. Am. Met. Soc.*, **77**, 437–471.

KARA, A. B. & H. E. HURLBURT, 2004. A note on the stability-dependent exchange coefficients of air-sea fluxes for use in gerneral circulation models. *J. Atmospheric and Oceanic Technolgy*.

KAWASE, M., 1987. Establishment of deep ocean circulation driven by deep-water production. *J. Phys. Oceanogr.*, **17**, 2294–2317.

KRAUS, E. B. & J. S. TURNER, 1967. A one–dimensional model of the seasonal thermocline I. A laboratory experiment and its interpretation. *Tellus*, **19**, 88–97.

KRÖGER, J., 2001. *Mechanismen meridionaler Transportprozesse im tropischen Atlantik*. PhD thesis, Christian-Albrechts-Universität zu Kiel.

KRÖGER, J., A. BUSALACCHI & J. BALLABRERA-POY, 2005. Decadal variability of shallow cells and equatorial SST in a numerical model of the Atlantic. *J. Geophys. Res.*. Doi:10.1029/2004JC002703.

LARGE, W. & S. YEAGER, 2004. Diurnal to decadal global forcing for ocean and sea-ice models: the data sets and flux climatologies. *Technical Report*, CGD Division of the National Center for Atmospheric Research. NCAR Technical Note.

LATIF, M., C. W. BÖNING, J. WILLEBRAND, A. BIASTOCH, J. DENGG, N. KEENLYSIDE, G. MADEC & U. SCHWECKENDIEK, 2006. Is the thermohaline circulation changing? *J. Climate*, **19**(18), 4631–4637.

LAZAR, A., T. INUI, P. MALANOTTE-RIZZOLI, A. J. BUSALACCHI, L. WANG & R. MURTUGUDDE, 2002. Seasonality of the ventilation of the tropical Atlantic thermocline in an ocean general circulation model. *J. Geophys. Res.*, **107**(C8), doi:10.1029/2000JC000667.

LAZAR, A., R. MURTUGUDDE & A. J. BUSALACCHI, 2000. A model study of temperature anomaly propagation from the subtropics to tropics within the south Atlantic thermocline. *Geophys. Res. Letters*, **28**(7), 1271–1274.

LEE, T. & I. FUKUMORI, 2003. Interannual-to-decadal variations of tropical-subtropical exchange in the Pacific ocean: boundary versus interior pycnocline transports. *J. Climate*, **16**, 4022–4042.

LEVITUS, S. & T. P. BOYER, 1994. World Ocean Atlas 1994. *NOAA Atlas NESDIS*, NOAA, Washington D.C.

LU, P. & J. P. MCCREARY, 1995. Influence of the ITCZ flow of the thermocline water from the subtropical to the equatorial Pacific Ocean. *J. Phys. Oceanogr.*, **25**, 3076–3088.

LU, P., J. P. MCCREARY & B. A. KLINGER, 1998. Meridional circulation cells and the source waters of the Pacific equatorial undercurrent. *J. Phys. Oceanogr.*, **28**(1), 62–84.

LÜBBECKE, J. F., A. BIASTOCH & C. W. BÖNING, 2006. Interannual to decadal variability of the STCs in the tropical Pacific. *Geophys. Res. Letters*. In prep.

LUMPKIN, R. & K. SPEER, 2003. Large-scale vertical and horizontal circulation in the North Atlantic Ocean. *J. Phys. Oceanogr.*, **33**(9), 1902–1920.

LUYTEN, J. R., J. PEDLOSKY & H. STOMMEL, 1982. The ventilated thermocline. *J. Phys. Oceanogr.*, **13**(2), 292–309.

MADEC, G., P. DELECLUSE, M. IMBARD & C. LEVY, 1998. OPA 8.1 general circulaton model reference manual. *Technical Report*, Notes de l'IPSL, Université P. et M. Curie, Paris.

MADEC, G. & M. IMBARD, 1996. A global ocean mesh to overcome the North Pole singularity. *Clim. Dyn.*, **12**, 381–388.

MALANOTTE-RIZZOLI, P., K. HEDSTROM, H. ARANGO & D. B. HAIDVOGEL, 2000. Water mass pathways between the subtropical and tropical ocean in a climatological simulation of the North Atlantic ocean circulation. *Dyn. Atm. Oc.*, **32**, 331–371.

MARIN, F., B. L. HUA & S. WACONGNE, 2000. The equatorial thermostad and subsurface countercurrents in the light of the dynamics of atmospheric Hadley cells. *J. Mar. Res.*, **58**(3), 405–437.

MARIN, F., F. SCHOPP & B. L. HUA, 2003. Three-dimensional dynamics of the subsurface countercurrents and equatorial thermostad. Part II: Influence of the large-scale ventilation and equatorial winds. *J. Phys. Oceanogr.*, **33**, 2610–2626.

MARSH, R., 2000. Recent variability of the North Atlantic thermohaline circulation inferred from surface heat and freshwater fluxes. *J. Climate*, **13**(18), 3239–3260.

MASINA, S., S.G.H. PHILANDER & A.B.G. BUSH, 1999. An analysis of tropical instability waves in a numerical model of the Pacific Ocean 2. Generation and energetics of the waves. *J. Geophys. Res.*, **104**(C12), 29637–29661.

MAZEIKA, P.A., 1967. Thermal domes in the eastern tropical Atlantic ocean. *Limnol. Oceanogr.*, **12**(3), 537–539.

MCCREARY, J. P., 1981. A linear stratified ocean model of the equatorial undercurrent. *Phil. Trans. Roy. Soc. Lond.*, **298**(A), 603–635.

MCCREARY, J. P. & P. LU, 1994. Interaction between the subtropical and equatorial ocean circulations: the subtropical cell. *J. Phys. Oceanogr.*, **24**(2), 466–497.

MCCREARY, J. P., P. LU & Z. YU, 2002. Dynamics of the Pacific subsurface countercurrents. *J. Phys. Oceanogr.*, **32**, 2379–2404.

MCPHADEN, M. J., 1984. On the dynamics of equatorial subsurface countercurrents. *J. Phys. Oceanogr.*, **14**, 1216–1225.

MENKES, C. E., S.C. KENNAN, P. FLAMENT et al., 2002. A whirling ecosystem in the equatorial Atlantic. *Geophys. Res. Letters*, **29**(11), doi:10.1029/2001GL014576.

MERCIER, H., M ARHAN & J.R.E. LUTJEHARMS, 2003. Upper layer circulation in the eastern equatorial and south Atlantic oceans in January-March 1995. *Deep–Sea Res.*, **50**, 863–887.

METCALF, W. & M. C. STALCUP, 1967. Origin of the Atlantic equatorial undercurrent. *J. Geophys. Res.*, **72**(20), 4959–4975.

MOLINARI, R. L., S. BAUER, D. P. SNOWDEN, G. C. JOHNSON, B. BOURLES, Y. GOURIOU & H. MERCIER, 2004. *Interhemispheric Water Exchanges in the Atlantic Ocean*, Chapt. A comparision of kinematic evidence for tropical cells in the Atlantic and Pacific oceans. Elsevier Oceanographic Series.

NOBRE, P. & J. SHUKLA, 1996. Variations of Sea Surface Temperature, wind stress and rainfall over the tropical Atlantic and South America. *J. Climate*, **9**, 2464–2479.

OORT, A. H., S. C. ASCHER, S. LEVITUS & J. P. PEIXOTO, 1989. New estimates of the available potential energy in the world ocean. *J. Geophys. Res.*, **94**, 3187–3200.

OSCHLIES, A. & V. GARCON, 1999. An eddy-permitting coupled physical-biological model of the North Atlantic Part I: Sensitivity to advection numerics and mixed layer physics. *Glob. Biogeoch. Cycl.*, **13**, 135–160.

PACANOWSKI, R. C., 1995. MOM 2 Documentation, User's Guide and Reference Manual. *Technical Report 3*, GFDL Ocean Group.

PHILANDER, S. G. H., 1976. Instabilities of zonal equatorial currents - Part I. *J. Geophys. Res.*, **81**, 3725–3735.

PHILANDER, S. G. H. & R. C. PACANOWSKI, 1986. A model of the seasonal cycle in the tropical Atlantic ocean. *J. Geophys. Res.*, **91**(C12), 14192–14206.

QIAO, L. & R. H. WEISBERG, 1998. Tropical instability wave dynamics: observations from the Tropical Instability Wave Experiment. *J. Phys. Oceanogr.*, **28**(2), 345–360.

RAHMSTORF, S., 1993. A fast and complete convection scheme for ocean models. *Ocean Mod.*, **101**, 9–11.

REDI, M. H., 1982. Oceanic isopycnal mixing by coordinate rotation. *J. Phys. Oceanogr.*, **12**(10), 1154–1158.

RHEIN, M., J. FISCHER, W. M. SMETHIE, D. SMYTHE-WRIGHT, R. F. WEISS, C. MERTENS, D.-H. MIN, U. FLEISCHMANN & A. PUTZKA, 2002. Labrador Sea Water: Pathways, CFC Inventory and Formation Rates. *J. Phys. Oceanogr.*, **32**(2), 648–665.

RICHARDSON, P. L. & G. REVERDIN, 1987. Seasonal cycle of velocity in the Atlantic North Equatorial Countercurrent as measured by surface drifters, current meteres and ship drifts. *J. Geophys. Res.*, **92**, 3691–3708.

RIUZ-BARRADAS, A., J. CARTON & S. NIGAM, 2000. Structure of interannual-to-decadal climate variability in the tropical Atlantic sector. *J. Climate*, **13**, 3285–3297.

ROWE, G. D., E. FIRING & G. C. JOHNSON, 2000. Pacific equatorial subsurface countercurrent velocity, transport and potential vorticity. *J. Phys. Oceanogr.*, **30**, 1172–1187.

SCHOTT, F., M. DENGLER, P. BRANDT, K. AFFLER, J. FISCHER, B. BOURLES, Y. GOURIOU, R. L. MOLINARI & M. RHEIN, 2003. The zonal currents and transports at 35°W in the tropical Atlantic. *Geophys. Res. Letters*, **30**(7), doi:10.1029/2002GL016849.

SCHOTT, F., M. DENGLER, R. J. ZANTOPP, L. STRAMMA, J. FISCHER & P. BRANDT, 2005. The shallow and deep western boundary circulation of the South Atlantic at 5-11S. *J. Phys. Oceanogr.*, **35**, 2031–2053.

SCHOTT, F. A., P. BRANDT, M. HAMANN, J. FISCHER & L. STRAMMA, 2002. On the boundary flow off Brazil at 5-10°S and its connection to the interior tropical Atlantic. *Geophys. Res. Letters*, **29**(17).

SCHOTT, F. A., J. FISCHER & STRAMMA, 1998. Transports and pathways of the upper–layer circulation in the Western Tropical Atlantic. *J. Phys. Oceanogr.*, **28**, 1904–1928.

SCHOTT, F. A., J. P. MCCREARY & G.C. JOHNSON, 2004. *Earth Climate: The ocean-atmosphere interactions*, Chapt. Shallow overturning circulations of the tropical-subtropical oceans, pp. 261–304. Geophysical Monograph Series 147. American Geophysical Union.

SEAGER, R., M. B. BLUMENTHAL & Y. KUSHNIR, 1995. An advective atmospheric mixed layer model for ocean modeling purposes: Global simulation of surface heat fluxes. *J. Climate*, **8**(8), 1951–1964.

SIEDLER, G., N. ZANGENBERG, R. ONKEN & A. MOLIERE, 1992. Seasonal changes in the tropical Atlantic Circulation: observation and simulation of the Guinea Dome. *J. Geophys. Res.*, **18**(6), 1853–1860.

STEELE, M., R. MORLEY & W. ERMOLD, 2001. PHC: A global ocean hydrography with a high-quality Arctic Ocean. *J. Climate*, **14**(9), 2079–2087.

STRAMMA, L., J. FISCHER, P. BRANDT & F. SCHOTT, 2004. *Circulation, variability and near-equatorial meridional flow in the central tropical Atlantic*, Chapt. 1, pp. 1–22. Elsevier Oceanographic Series.

STRAMMA, L., S. HÜTTL & J. SCHAFSTALL, 2005a. Water masses and currents in the upper tropical Northeast Atlantic off northwest Africa. *J. Geophys. Res.*, **110**(C12), doi:10.1029/2005JC002939.

STRAMMA, L., M. RHEIN, P. BRANDT, M. DENGLER, C. BÖNING & M. WALTER, 2005b. Upper ocean circulation in the western tropical Atlantic in boreal fall 2000. *Deep–Sea Res.*, **52**(1), 221–240.

STRAMMA, L. & F. SCHOTT, 1999. The mean flow field of the tropical Atlantic ocean. *Deep–Sea Res. II*, **46**, 279–303.

SUTTON, R. T., S. P. JEWSON & D. P. ROWELL, 2000. The elements of climate variability in the tropical Atlantic region. *J. Climate*, **13**(18), 3261–3284.

THIERRY, V., A. M. TREGUIER & H. MERCIER, 2004. Numerical study of the annual and semi-annual fluctuations in the deep equatorial Atlantic ocean. *Ocean Modelling*, **6**, 1–30.

TSUCHIYA, M., 1975. Subsurface countercurrents in the eastern equatorial Pacific Ocean. *J. Mar. Res.*, **33**, 145–175.

TSUCHIYA, M., 1986. Thermostads and circulation in the upper layer of the Atlantic ocean. *Prog. Oceanogr.*, **16**, 235–267.

URBANO, D. F., M. JOCHUM & I. C. A. DA SILVEIRA, 2006. Rediscovering the second core of the Atlantic NECC. *Ocean modelling*, **12**(1–2), 1–15.

VERDY, A. & M. JOCHUM, 2005. A note on the validity of the Sverdrup balance in the Atlantic North Equatorial Countercurrent. *Deep–Sea Res.*, **52**, 179–188.

VOITURIEZ, B., 1981. Northern and southern equatorial undercurrents and the formation of tropical thermal domes. *Oc. Acta*, **4**(4), 497–506.

WEIDMAN, P. D., D. L. MICKLER, B. DAYYANI & G. H. BORN, 1999. Analysis of Legeckis eddies in the near-equatorial Pacific. *J. Geophys. Res.*, **104**(C4), 7865–7887.

WEISBERG, R. & T. WEINGARTNER, 1988. Instability waves in the equatorial Atlantic ocean. *J. Phys. Oceanogr.*, **18**, 1641–1657.

WILSON, W. D., E. JOHNS & R. L. MOLINARI, 1994. Upper layer circulation in the western tropical North Atlantic ocean during August 1989. *J. Geophys. Res.*, **99**(C11), 22513–22523.

XIE, S. P. & Y. TANIMOTO, 1998. A pan-Atlantic decadal climate oscillation. *Geophys. Res. Letters*, **25**, 2185–2188.

YAMAGATA, T. & S. IIZUKA, 1995. Simulation of the tropical thermal domes in the Atlantic: a seasonal cycle. *J. Phys. Oceanogr.*, **25**(9), 2129–2140.

YANG, J., 1999. A linkage between decadal climate variations in the Labrador Sea and the Tropical Atlantic Ocean. *Geophys. Res. Letters*, **26**(8), 1023–1026.

ZHANG, D., M. J. MCPHADEN & W. E. JOHNS, 2003. Observational evidence for flow between the subtropical and tropical Atlantic: the Atlantic subtropical cells. *J. Phys. Oceanogr.*, **33**(8), 1783–1797.

ZHANG, R. & T. L. DELWORTH, 2005. Simulated tropical response to a substantial weakening of the Atlantic thermohaline circulation. *J. Climate*, **18**(6), 1853–1860.

Abbreviations

Currents

EUC	Equatorial Undercurrent
NBC	North Brazil Current
NEC	North Equatorial Current
NECC	North Equatorial Countercurrent
NEUC	North Equatorial Undercurrent
SEC	South Equatorial Current
SEUC	South Equatorial Undercurrent

Others

ENSO	El Nino-Southern Oscillation
ITCZ	Innertropical Convergence Zone
LSW	Labrador Sea Water
MOC	Meridional Overturning Circulation
NADW	North Atlantic Deep Water
NAO	North Atlantic Oscillation
SST	Sea Surface Temperature
STC	Subtropical-Tropical-Cell
TC	Tropical Cell

Danksagung

Erklärung

Hiermit erkläre ich, dass ich die vorliegende Dissertation, abgesehen durch die Beratung meiner akademischen Lehrer, selbstständig verfasst habe und keine weiteren Quellen und Hilfsmittel, als die hier angegebenen verwendet habe.
Diese Arbeit hat weder ganz, noch in Teilen, bereits an anderer Stelle einer Prüfungskommission zur Erlangung des Doktorgrades vorgelegen.
Ich erkläre, dass die vorliegende Arbeit gemäß der Grundsätze zur Sicherung guter wissenschaftlicher Praxis der Deutschen Forschungsgemeinschaft erstellt wurde.

Kiel, den 26. Oktober 2006

Sabine Hüttl

Lebenslauf

Persönliche Daten

Vor- und Zuname	Sabine Hüttl
Geburtsdatum	26. Juni 1979
Geburtsort	Jena
Anschrift	Mühlenstraße 56
Ort	23552 Lübeck
Telefon	0451-3973848
E-mail	shuettl@ifm-geomar.de
Staatsangehörigkeit	deutsch

Ausbildung

07/1998	Abitur am Adolf-Reichwein-Gymnasium Jena
09/1998 – 08/2000	Grundstudium Meteorologie an der CAU Kiel
09/2000 – 03/2002	Hauptstudium Meteorologie an der CAU Kiel
04/2002 – 10/2003	Hauptstudium Ozeanographie an der CAU Kiel, Abschluß mit Diplom 10/2003
seit 11/2003	Doktorandin am IfM-GEOMAR Kiel